



Search for pair production of third-generation leptoquarks decaying into a bottom quark and a τ -lepton with the ATLAS detector

ATLAS Collaboration*

CERN, 1211 Geneva 23, Switzerland

Received: 3 March 2023 / Accepted: 2 October 2023 / Published online: 24 November 2023
© CERN for the benefit of The ATLAS Collaboration 2023

Abstract A search for pair-produced scalar or vector leptoquarks decaying into a b -quark and a τ -lepton is presented using the full LHC Run 2 (2015–2018) data sample of 139 fb^{-1} collected with the ATLAS detector in proton-proton collisions at a centre-of-mass energy of $\sqrt{s} = 13\text{ TeV}$. Events in which at least one τ -lepton decays hadronically are considered, and multivariate discriminants are used to extract the signals. No significant deviations from the Standard Model expectation are observed and 95% confidence-level upper limits on the production cross-section are derived as a function of leptoquark mass and branching ratio \mathcal{B} into a τ -lepton and b -quark. For scalar leptoquarks, masses below 1460 GeV are excluded assuming $\mathcal{B} = 100\%$, while for vector leptoquarks the corresponding limit is 1650 GeV (1910 GeV) in the minimal-coupling (Yang–Mills) scenario.

1 Introduction

Many extensions of the Standard Model (SM) of particle physics predict particles known as leptoquarks (LQs) [1–7]. These particles provide a connection between the lepton and quark sectors, which are similar in structure in the SM. LQs can be scalar (spin-0) or vector (spin-1) bosons, and they carry colour and a fractional electric charge. They also have non-zero lepton and baryon numbers, and decay into quark-lepton pairs. They can mediate neutral and charge currents, and therefore can potentially provide an explanation for hints of violations of lepton universality observed in flavour experiments [8–14].

This analysis searches for the pair-production of LQs that couple strongly to the third generation of quarks and leptons in proton–proton (pp) collisions at the LHC. Within the Buchmüller–Rückl–Wyler (BRW) model [15], which is the benchmark for scalar LQs in this analysis, it is assumed that these LQs can only interact within the same family via

a Yukawa interaction. This interaction is described by two parameters, a model parameter β and a coupling parameter λ . In the BRW model, the pair-production cross-section is independent of λ . This analysis also considers pair-production of vector LQs [16,17] corresponding to the U_1 state in the BRW classification [15]. The scenarios considered in this model differ by a dimensionless coupling constant k , which is zero for the minimal-coupling scenario and one for the Yang–Mills scenario. For both scalar and vector LQs, the parameter β controls the coupling to charged leptons. For third generation LQs, results are generally given in terms of the mass of the LQ (m_{LQ}) and its branching ratio (\mathcal{B}), rather than β as is the case for first- and second-generation LQs. This is because β is not equal to \mathcal{B} for third-generation LQs due to the sizable top-quark mass.

ATLAS and CMS have published searches for LQs coupling to the first, second and third generations [18–27]. Each generation of LQs is split into up-type and down-type LQs with different electric charges. For instance, for the third generation they are split into up-type LQs (LQ_3^u), which decay into $b\tau$ or $t\nu$, and down-type LQs (LQ_3^d), which decay into $t\tau$ or $b\nu$. Both types of LQs are currently excluded for masses below 1150 GeV for the BRW model, for all values of \mathcal{B} .

This paper updates the ATLAS search for an up-type LQ pair decaying into $b\tau$ [19], shown in Fig. 1, using the full Run 2 data sample and an updated analysis strategy, prioritising high LQ masses that are not yet excluded in the benchmark models considered. Analysis improvements include updated analysis-optimisation and background-estimation methods, as well as updates to several object identification algorithms. The analysis signature is two jets, at least one of which must be identified as containing a b -hadron, and two τ -leptons. For the τ -leptons, the cases considered are where both decay hadronically or where one τ -lepton decays into a light lepton (electron or muon, ℓ) and neutrinos and the other decays hadronically. The mass range considered for the LQ is from 300 to 2000 GeV . The extraction of the signals is performed through a simultaneous likelihood fit to multivariate

* e-mail: atlas.publications@cern.ch

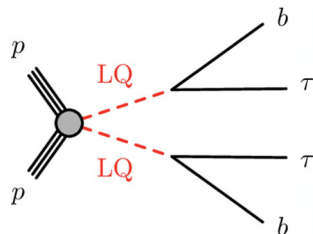


Fig. 1 Pair production of a leptoquark (LQ) and its subsequent decay into a b -quark and a τ -lepton

discriminants. For the results, both scalar and vector LQs are considered, with the limits on vector LQs interpreted in the context of two scenarios, the Yang–Mills scenario and the minimal-coupling scenario [28].

The paper is structured as follows. After a brief description of the ATLAS detector, the data sample, simulated backgrounds and simulated signals are described. This is followed by a description of the event reconstruction, the object selection, the event selections for the signal regions, and the multivariate discriminants that are used in the final fit. The next sections include a description of the data-driven background estimation methods, the systematic uncertainties, and finally the statistical methods and results.

2 ATLAS detector

The ATLAS detector [29] at the LHC is a multipurpose particle detector with a forward–backward symmetric cylindrical geometry and a near 4π coverage in solid angle.¹ The inner tracking detector consists of pixel and microstrip silicon detectors covering the pseudorapidity region $|\eta| < 2.5$, surrounded by a transition radiation tracker to enhance electron identification in the range of $|\eta| < 2.0$. An additional innermost pixel layer, the insertable B-layer [30,31], was added before Run 2 of the LHC. The inner detector (ID) is surrounded by a thin superconducting solenoid providing a 2 T axial magnetic field, and by a fine-granularity lead/liquid-argon (LAr) electromagnetic (EM) calorimeter covering $|\eta| < 3.2$. Hadronic calorimetry is provided by a steel/scintillator-tile calorimeter in the central pseudorapidity range ($|\eta| < 1.7$). The endcap and forward regions are instrumented with LAr calorimeters for both the EM and hadronic energy measurements up to $|\eta| = 4.9$. The muon spectrom-

eter (MS) surrounds the calorimeters and is based on three large superconducting air-core toroidal magnets with eight coils each. Three layers of high-precision tracking chambers provide coverage in the range of $|\eta| < 2.7$, while dedicated fast chambers allow triggering in the region $|\eta| < 2.4$. A two-level trigger system [32], consisting of a hardware-based first-level trigger followed by a software-based high-level trigger (HLT), is used to select events. An extensive software suite [33] is used in data simulation, in the reconstruction and analysis of real and simulated data, in detector operations, and in the trigger and data acquisition systems of the experiment.

3 Data and simulation samples

The data used in this search correspond to an integrated luminosity of 139 fb^{-1} of pp collision data collected by the ATLAS detector between 2015 and 2018 at a centre-of-mass energy $\sqrt{s} = 13 \text{ TeV}$. The uncertainty in the combined 2015–2018 integrated luminosity is 1.7% [34], obtained using the LUCID-2 detector [35] for the primary luminosity measurements. The presence of additional interactions in the same or neighbouring bunch crossing, referred to as pile-up, is characterised by the average number of such interactions, $\langle \mu \rangle$, which was 33.7 for the combined data sample. Only events recorded under stable beam conditions and for which all relevant detector subsystems were known to be in a good operating condition are used.

Dedicated Monte Carlo (MC) simulated samples are used to model SM processes and estimate the expected signal yields. All samples were passed through the full ATLAS detector simulation [36] based on GEANT4 [37], except for the signal samples that use a parameterised fast simulation of the calorimeter response [38] and GEANT4 for the other detector systems. The simulated events were reconstructed with the same algorithms as used for data, and contain a realistic modelling of pile-up interactions. The pile-up profiles match those of each data sample between 2015 and 2018, and are obtained by overlaying minimum-bias events simulated using the soft QCD processes of Pythia 8.186 [39] with the NNPDF2.3 leading-order (LO) [40] set of parton distribution functions (PDFs) and the A3 [41] set of tuned parameters (tune). The MC samples are corrected to account for the differences between simulation and data in terms of the pile-up, the energy and momentum scales, and the reconstruction and identification efficiencies of physics objects.

Simulated events with pair-produced up-type ($Q = +\frac{2}{3}$) scalar LQs were generated at next-to-leading order (NLO) in QCD with MADGRAPH5_AMC@NLO v2.6.0 [42], using the LQ model of Ref. [43], in which fixed-order NLO QCD calculations [44,45] are interfaced to PYTHIA 8.230 [46] for the parton shower (PS) and hadronisation. Parton luminosi-

¹ ATLAS uses a right-handed coordinate system with its origin at the nominal interaction point (IP) in the centre of the detector and the z -axis along the beam pipe. The x -axis points from the IP to the centre of the LHC ring, and the y -axis points upwards. Cylindrical coordinates (r, ϕ) are used in the transverse plane, ϕ being the azimuthal angle around the z -axis. The pseudorapidity is defined in terms of the polar angle θ as $\eta = -\ln \tan(\theta/2)$. Angular distance is measured in units of $\Delta R \equiv \sqrt{(\Delta\eta)^2 + (\Delta\phi)^2}$.

ties were provided by the five-flavour scheme NNPDF3.0 NLO [47] PDF set with $\alpha_s = 0.118$ and the underlying event (UE) was modelled with the A14 tune [48,49]. The coupling parameter λ was set to 0.3, resulting in a relative LQ width of approximately 0.2% and ensuring the LQs decay promptly. In all cases, $\beta = 0.5$ such that the couplings to charged leptons and neutrinos were equal and the decay products were interfaced to MADSPIN [50] to preserve spin correlations. Different values for \mathcal{B} were then obtained by reweighting the simulated events according to the generator information about their decay following the procedure in Ref. [19]. Signal cross-sections were obtained from the calculation of the pair production of scalar coloured particles, such as the hypothesised supersymmetric partner of the top quark, as these particles have the same production modes and their pair-production cross-section depends only on their mass. These processes were computed at approximate next-to-next-to-leading order (NNLO) in QCD with resummation of next-to-next-to-leading-logarithmic (NNLL) soft gluon terms [51–54]. The cross-sections do not include contributions from t -channel lepton exchange, which are neglected in Ref. [43] and may lead to corrections at the percent level [55]. The nominal cross-section and its uncertainty were derived using the PDF4LHC15_mc PDF set, following the recommendations of Ref. [56]. For LQ masses between 300 GeV and 2000 GeV, the cross-sections range from 10 pb to 0.01 fb.

Simulated events with pair-produced up-type vector LQs were generated at LO in QCD with MADGRAPH5_AMC@NLO v2.6.0, using the LQ model of Ref. [17] and the NNPDF3.0 NLO PDF set with $\alpha_s = 0.118$. Decays of the LQs were performed with MADSPIN, while PS and hadronisation were simulated using PYTHIA 8.244 with the A14 tune. The full model includes two additional vector states that are necessary to obtain a realistic extension of the SM, a colour singlet Z' and a colour octet G' . However, these are not present in the MADGRAPH model and hence do not contribute to the Feynman diagrams considered for pair production of vector leptoquarks. The samples were produced with a coupling strength $g_U = 3.0$, where g_U represents the overall coupling between the LQ and the fermion, motivated by a suppression of the production cross-section for the additional mediators in the ultraviolet completion of the model, which might otherwise be in tension with existing LHC limits. This choice of coupling results in a relative LQ width of around 10%. In all cases, $\beta = 0.5$ and the same reweighting as in the scalar LQ case is then used to probe different \mathcal{B} values. As mentioned, the model introduces two different coupling scenarios, the minimal-coupling scenario and the Yang–Mills scenario. In the latter case the LQ is a massive gauge boson and has additional couplings to the SM gauge bosons, resulting in enhanced cross-sections. \mathcal{B} is assumed to be unaffected by these couplings since the corresponding decays are either forbidden or heavily suppressed. Since no

higher-order cross-sections are available for this model, the LO MADGRAPH5_AMC@NLO cross-sections were used and vary between 94 pb (340 pb) and 0.05 fb (0.61 fb) for LQ masses between 300 GeV and 2000 GeV in the minimal-coupling (Yang–Mills) case. Above 500 GeV, kinematic differences between the two scenarios are negligible.

Scalar (vector) LQ samples were produced with LQ masses between 300 GeV to 2000 GeV, with a mass interval of 50 GeV in the range of 800–1600 GeV (1400–1600 GeV) and 100 GeV otherwise.

Background samples were simulated using different MC event generators depending on the process. All background processes are normalised to the most accurate available theoretical calculation of their respective cross-sections. The most relevant event generators, the accuracy of theoretical cross-sections, the UE parameter tunes, and the PDF sets used in simulating the SM background processes are summarised in Table 1. For all samples, except those generated using SHERPA, the EVTGEN v1.2.0 [87] program was used to simulate the properties of the b - and c -hadron decays.

4 Event reconstruction and object definitions

The LQ signature of interest in this search gives rise to a set of reconstructed objects that consist primarily of τ -leptons, which may decay into light leptons or hadronically, and jets from the hadronisation of quarks, specifically b -quarks. In addition, neutrinos produced in the decay of τ -leptons and the semileptonic decay of b -hadrons contribute to the missing transverse momentum $\mathbf{p}_T^{\text{miss}}$ of the event. To be considered for analysis, events are required to have at least one p_T interaction vertex, reconstructed from two or more charged-particle tracks with transverse momentum $p_T > 500 \text{ MeV}$; the one with the highest summed p_T^2 of associated tracks is selected as the primary vertex.

Electron candidates are reconstructed by matching ID tracks to energy clusters in the EM calorimeter. They must satisfy $p_T > 7 \text{ GeV}$ and lie in the range of $|\eta| < 2.47$, excluding the transition region between the barrel and endcap detectors ($1.37 < |\eta| < 1.52$). Electrons are further identified using a likelihood-based method, based on the track quality, the profile of the shower measured in the EM calorimeter and the consistency between the track and the energy cluster [88]. Two identification criteria are used to select electrons in this analysis: ‘veto electrons’² are required to satisfy the ‘loose’ identification working point, while ‘signal electrons’ are required to satisfy the more stringent ‘tight’ working point.

² ‘Veto’ leptons are used to reject events with additional leptons as discussed in Sect. 5.1

Table 1 The list of generators used for the simulation of the SM background processes. Information is given on the matrix element (ME) generator (including the perturbative QCD order), the PDF set, the parton shower (PS) and the underlying event (UE). The perturbative order (in QCD unless otherwise specified) of the cross-section used to normalise the different samples is also presented. (§) The $t\bar{t} - Wt$ interference

Process	ME generator	ME QCD order	ME PDF	PS and hadronisation	UE tune	Cross-section order
<i>Top-quark</i>						
$t\bar{t}$ (§)	POWHEG- BOX v2 [63]	NLO	NNPDF3.0NLO	PYTHIA 8.230	A14	NNLO+NNLL [64]
t -channel	POWHEG- BOX v2	NLO	NNPDF3.0NLO	PYTHIA 8.230	A14	NLO [65]
s -channel	POWHEG- BOX v2	NLO	NNPDF3.0NLO	PYTHIA 8.230	A14	NLO [66]
Wt (§)	POWHEG- BOX v2	NLO	NNPDF3.0NLO	PYTHIA 8.230	A14	NLO [67]
<i>Top-quark + W/Z</i>						
$t\bar{t}Z$	SHERPA 2.2.1 [68–70]	NLO	NNPDF3.0NNLO	SHERPA 2.2.1	Default	NLO ^(†)
$t\bar{t}W$	SHERPA 2.2.8	NLO	NNPDF3.0NNLO	SHERPA 2.2.8	Default	NLO ^(†)
<i>Vector boson + jets</i>						
$W/Z+jets$	SHERPA 2.2.1	NLO (≤ 2 jets) LO (3,4 jets)	NNPDF3.0NNLO	SHERPA 2.2.1	Default	NNLO [71]
<i>Diboson</i>						
WW, WZ, ZZ	SHERPA 2.2.1	NLO (≤ 1 jet) LO (2,3 jets)	NNPDF3.0NNLO	SHERPA 2.2.1	Default	NLO ^(†)
<i>Higgs boson</i>						
ggF	POWHEG- BOX v2	NNLO	NNPDF3.0NLO	PYTHIA 8.212	AZNLO [72]	N3LO(QCD)+NLO(EW) [73–77]
VBF	POWHEG- BOX v2	NLO	NNPDF3.0NLO	PYTHIA 8.212	AZNLO	NNLO(QCD)+NLO(EW) [73,78–80]
$qq \rightarrow WH$	POWHEG- BOX v2	NLO	NNPDF3.0NLO	PYTHIA 8.212	AZNLO	NNLO(QCD)+NLO(EW) [57–60,62,81]
$qq \rightarrow ZH$	POWHEG- BOX v2	NLO	NNPDF3.0NLO	PYTHIA 8.212	AZNLO	NNLO(QCD)+NLO(EW) ^(‡)
$gg \rightarrow ZH$	POWHEG- BOX v2	NLO	NNPDF3.0NLO	PYTHIA 8.212	AZNLO	NLO+NLL [82–86]
$t\bar{t}H$	POWHEG- BOX v2	NLO	NNPDF3.0NLO	PYTHIA 8.230	A14	NLO [73]

Muon candidates are reconstructed from tracks in the MS, matched with compatible tracks in the ID where coverage allows; in regions where the MS is only partially instrumented ($|\eta| < 0.1$) an energy deposit in the calorimeter compatible with a minimum-ionising particle is combined with a compatible ID track instead. They must satisfy $p_T > 7\text{ GeV}$ and lie in the range of $|\eta| < 2.7$. Muons are further identified based on the number of hits in the various ID subdetectors and MS stations, the compatibility between the measurements in the two detectors and the properties of the resulting track fit. Two identification criteria [89] are used to select muons: ‘veto muons’ (See footnote 2) must satisfy a ‘loose’ identification requirement, while the ‘signal muons’ are required to satisfy the ‘medium’ (‘high- p_T ’) working point if the p_T is less than (greater than) 800 GeV. The more stringent high- p_T requirements remove around 20% of muons but improve the p_T resolution by $\approx 30\%$ above 1.5 TeV, significantly suppressing potential backgrounds [90].

To suppress misidentified light leptons or those arising from hadron decays, all light-lepton candidates must satisfy an isolation criterion that limits the presence of tracks

was handled using the diagram removal scheme. (†) The cross-sections from SHERPA at NLO were used to normalise the WW , WZ , ZZ and $t\bar{t}W/Z$ events. (‡) The $qq \rightarrow ZH$ process was normalised to the NNLO (QCD) + NLO(EW) cross-section for the $pp \rightarrow ZH$ process [57–62], after subtracting the $gg \rightarrow ZH$ contribution

(calorimeter deposits) in a p_T -dependent (fixed) radius cone. The resulting efficiency is above 99% for both electrons and muons in the signal regions. Finally, signal leptons must satisfy stricter requirements on their p_T depending on the data-taking period, as detailed in Sect. 5.

Jets are reconstructed from topological energy clusters and charged-particle tracks, resulting from a particle-flow algorithm [91], using the anti- k_t algorithm with a radius parameter of $R = 0.4$ [92,93]. They are required to satisfy $p_T > 20\text{ GeV}$ and lie in the range of $|\eta| < 2.5$. To suppress jets from pile-up, jets with $p_T < 60\text{ GeV}$ and $|\eta| < 2.4$ are required to originate from the primary vertex using a multivariate ‘jet vertex tagger’ [94]. A multivariate algorithm based on a deep neural network, known as the ‘DL1r tagger’ [95–97], is used to identify jets containing b -hadrons (b -jets) based on the jet kinematics, the impact parameters of tracks associated with the jet and the reconstruction of displaced vertices. This analysis uses a working point with a 77% efficiency for true b -jets, as measured in simulated $t\bar{t}$

events, and corresponding rejection factors³ for light-flavour jets, charm jets and τ -leptons of 170, 5 and 21, respectively [98, 99].

Hadronically decaying τ -lepton candidates are seeded by jets, which are required to have one or three associated tracks (referred to hereafter as ‘one-prong’ or ‘three-prong’ candidates, respectively) with a total charge of ± 1 [100]. The visible decay products ($\tau_{\text{had-vis}}$) must satisfy $p_T > 20 \text{ GeV}$ and lie in the range of $|\eta| < 2.47$, excluding the transition region defined above. True $\tau_{\text{had-vis}}$ candidates are discriminated from quark- and gluon-initiated jets via a recurrent neural network (RNN) using calorimeter- and tracking-based variables as input and trained separately on one- and three-prong candidates [101]. The ‘loose’ working point used has an efficiency of approximately 85% and 75% for one- and three-prong $\tau_{\text{had-vis}}$ respectively. A further boosted decision tree (BDT) is used to reject one-prong $\tau_{\text{had-vis}}$ candidates originating from electrons with an efficiency of about 95% [102]. For the estimation of the background from jets misidentified as $\tau_{\text{had-vis}}$ (described in Sect. 6), anti- $\tau_{\text{had-vis}}$ candidates are defined in the same way as above but are required to fail to satisfy the nominal loose RNN working point requirements and instead satisfy a looser requirement that has an efficiency of 99% for selecting true $\tau_{\text{had-vis}}$ candidates.

The $\mathbf{p}_T^{\text{miss}}$ (with magnitude E_T^{miss}) is computed from the negative vectorial sum of the selected and calibrated objects described above, along with an extra track-based ‘soft term’ to account for the energy of particles originating from the primary vertex but not associated to any of the reconstructed objects [103, 104].

To resolve ambiguities whereby the same detector signature may be reconstructed as more than one physics object, a sequential overlap-removal procedure is applied. First, electron candidates are discarded if they share a track with a more energetic electron or a muon identified in the MS; if the muon is identified in the calorimeter it is removed instead. Any $\tau_{\text{had-vis}}$ candidate within $\Delta R = 0.2$ of an electron or a muon (which must be reconstructed in the MS if the $\tau_{\text{had-vis}}$ p_T is above 50 GeV) is then rejected. Jets are discarded if they lie within $\Delta R = 0.2$ of an electron or have fewer than three associated tracks and lie within the same distance of a muon. Electron or muon ($\tau_{\text{had-vis}}$) candidates within $\Delta R = 0.4$ ($\Delta R = 0.2$) of any remaining jet are then removed. Finally, ambiguities between anti- $\tau_{\text{had-vis}}$ candidates and jets within $\Delta R = 0.2$ are resolved in favour of the jet if it is b -tagged or the anti- $\tau_{\text{had-vis}}$ otherwise.

³ The rejection factor is defined as the reciprocal of the efficiency to mistag a jet not containing B -hadrons as a b -jet.

5 Event selection

The event selection targets a signature consisting of a pair of τ -leptons and a pair of b -quarks. It splits the events into two orthogonal signal categories based on the τ -lepton decay mode: the $\tau_{\text{lep}}\tau_{\text{had}}$ channel, which selects events with a light lepton, an oppositely charged $\tau_{\text{had-vis}}$ and one or two b -jets, and the $\tau_{\text{had}}\tau_{\text{had}}$ channel, which selects events with two opposite-charge $\tau_{\text{had-vis}}$ and one or two b -jets. Multivariate techniques are used to search for a LQ-pair signal in the two signal regions (SRs).

5.1 Signal regions

Candidate events were recorded using a combination of single-light-lepton [105, 106] and single- $\tau_{\text{had-vis}}$ triggers [107]. The single-lepton trigger used in the $\tau_{\text{lep}}\tau_{\text{had}}$ channel required a reconstructed light lepton at the HLT, with a minimum E_T threshold ranging from 24 to 26 GeV for electrons and a minimum p_T threshold ranging from 20 to 25 GeV for the muons, depending on the data-taking period. Offline leptons are required to be geometrically matched to the corresponding trigger object and have a p_T threshold 1–2 GeV above the HLT threshold so that the trigger was fully efficient. The single- $\tau_{\text{had-vis}}$ triggers used in the $\tau_{\text{had}}\tau_{\text{had}}$ channel required a reconstructed HLT $\tau_{\text{had-vis}}$ with a period-dependent minimum p_T threshold ranging between 80 GeV and 160 GeV. The corresponding p_T -threshold for the offline $\tau_{\text{had-vis}}$, which is again required to be geometrically matched to the trigger object, ranges between 100 GeV and 180 GeV, while the non-trigger-matched $\tau_{\text{had-vis}}$ is required to have $p_T > 20 \text{ GeV}$.

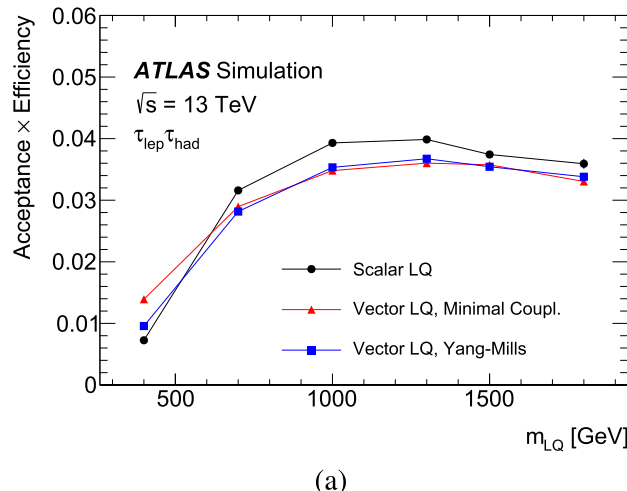
Following the trigger selection, the $\tau_{\text{lep}}\tau_{\text{had}}$ category requires exactly one ‘signal’ light lepton and an oppositely charged $\tau_{\text{had-vis}}$, while the $\tau_{\text{had}}\tau_{\text{had}}$ category requires exactly two opposite-charge $\tau_{\text{had-vis}}$ and no ‘veto’ light leptons. Both categories require at least two jets, one or two of which must be b -tagged, with $p_T > 45$ (20) GeV for the leading (sub-leading) jet.

The invariant mass of the two τ -lepton decay products is an important variable with which to reject the $Z + \text{jets}$ background. It is calculated using the missing mass calculator (MMC) [108], with the light lepton and the $\tau_{\text{had-vis}}$ (two $\tau_{\text{had-vis}}$) and the $\mathbf{p}_T^{\text{miss}}$ as input in the $\tau_{\text{lep}}\tau_{\text{had}}$ ($\tau_{\text{had}}\tau_{\text{had}}$) category, and it is required to satisfy $m_{\tau\tau}^{\text{MMC}} \notin 40\text{--}150 \text{ GeV}$. Two further selections are applied to target the characteristic LQ signature while reducing the large multi-jet background. The scalar sum of the transverse momenta (s_T), calculated taking into account the light lepton or $\tau_{\text{had-vis}}$, two leading jets and the E_T^{miss} , is a powerful discriminator. It is required to satisfy $s_T > 600 \text{ GeV}$, while the E_T^{miss} itself is required to exceed 100 GeV.

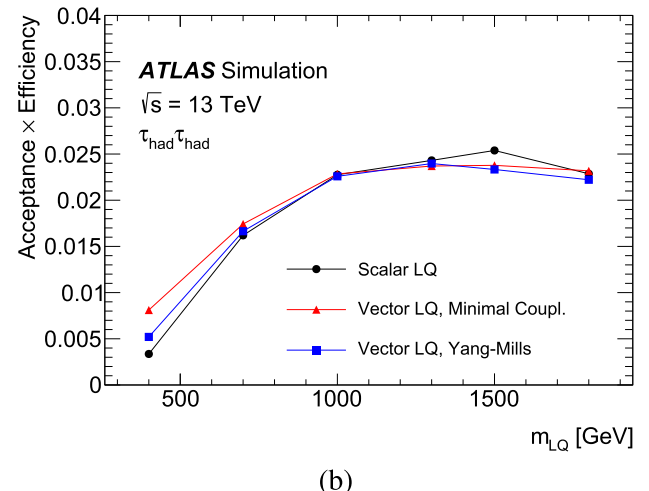
The full event selection is summarised in Table 2 and the resulting acceptance times efficiency is shown in Fig. 2 as

Table 2 Summary of the event selections for the $\tau_{\text{lep}}\tau_{\text{had}}$ and $\tau_{\text{had}}\tau_{\text{had}}$ categories. Where two objects are required, the thresholds on the sub-leading object are given in parenthesis. Where the selection depends on

	$\tau_{\text{lep}}\tau_{\text{had}}$ channel	$\tau_{\text{had}}\tau_{\text{had}}$ channel
e/μ selection	$= 1$ ‘signal’ e or μ $p_T^e > 25, 27 \text{ GeV}$ $p_T^\mu > 21, 27 \text{ GeV}$	No ‘veto’ e or μ
$\tau_{\text{had-vis}}$ selection	$= 1 \tau_{\text{had-vis}}$ $p_T^\tau > 100 \text{ GeV}$	$= 2 \tau_{\text{had-vis}}$ $p_T^\tau > 100, 140, 180 (20) \text{ GeV}$
Jet selection		≥ 2 jets $p_T^{\text{jet}} > 45 (20) \text{ GeV}$ 1 or 2 b -jets
Additional selection		Opposite charge $e, \mu, \tau_{\text{had}}$ and τ_{had} $m_{\tau\tau}^{\text{MMC}} \notin 40 - 150 \text{ GeV}$ $E_T^{\text{miss}} > 100 \text{ GeV}$ $s_T > 600 \text{ GeV}$



(a)



(b)

Fig. 2 The expected acceptance times efficiency (including object identification and reconstruction, triggering, and event selection) for the scalar and vector LQs, with both the minimal-coupling and the Yang–Mills scenarios, at $\beta = 0.5$ as a function of m_{LQ} in the **a** $\tau_{\text{lep}}\tau_{\text{had}}$

and **b** $\tau_{\text{had}}\tau_{\text{had}}$ channels. The values include the leptonic and hadronic branching ratios of the tau lepton. The error bars, which are in general smaller than the markers, indicate the statistical uncertainty

a function of m_{LQ} . Since the analysis prioritises high mass LQs that have not yet been excluded in the benchmark models under consideration, it is not optimal for low LQ masses.

5.2 Multivariate signal extraction

Following the event selection, the LQ signal is extracted using a multivariate discriminant. To obtain near-optimal sensitivity and continuity over the full range of LQ masses considered, a parameterised neural network (PNN) [109], parameterised in terms of the generated LQ mass, is chosen. The PNN consists of three hidden layers, each with 32 nodes,

implemented in Keras [110] with the Tensorflow [111] backend.

The PNN inputs consist of a combination of multiplicity, kinematic and angular quantities that discriminate between the signal and the dominant background. In the case of the $b\tau$ invariant mass, the most likely combination of the τ -lepton and a b -jet⁴ is chosen based on a mass-pairing strategy that minimises the mass difference between the two resulting LQ candidates. The variables, which are similar for both the

⁴ In the case of only one b -jet, the highest- p_T non- b -jet is taken as the second jet.

Table 3 Summary of variables used as inputs to the PNN in the $\tau_{\text{lep}}\tau_{\text{had}}$ and $\tau_{\text{had}}\tau_{\text{had}}$ categories. The variables are defined in the text

Variable	$\tau_{\text{lep}}\tau_{\text{had}}$ channel	$\tau_{\text{had}}\tau_{\text{had}}$ channel
$\tau_{\text{had-vis}} p_{\text{T}}^0$	✓	✓
s_{T}	✓	✓
$N_{b-\text{jets}}$	✓	✓
$m(\tau, \text{jet})_{0,1}$		✓
$m(\ell, \text{jet}), m(\tau_{\text{had}}, \text{jet})$	✓	
$\Delta R(\tau, \text{jet})$	✓	✓
$\Delta\phi(\ell, E_{\text{T}}^{\text{miss}})$	✓	
$E_{\text{T}}^{\text{miss}} \phi$ centrality	✓	✓

$\tau_{\text{lep}}\tau_{\text{had}}$ and $\tau_{\text{had}}\tau_{\text{had}}$ categories, are summarised in Table 3 and defined as follows:

- $\tau_{\text{had-vis}} p_{\text{T}}^0$ is the transverse momentum of the highest- p_{T} $\tau_{\text{had-vis}}$;
- s_{T} is the scalar sum of the transverse momenta defined above;
- $N_{b-\text{jets}}$ is the number of b -jets;
- $m(\tau, \text{jet})_{0,1}$ are the larger (0) and smaller (1) of the two LQ masses obtained via the mass-pairing strategy ($\tau_{\text{had}}\tau_{\text{had}}$ channel only);
- $m(\ell, \text{jet})$ and $m(\tau_{\text{had}}, \text{jet})$ are the mass of the light-lepton or $\tau_{\text{had-vis}}$, respectively, combined with its mass-paired b -jet ($\tau_{\text{lep}}\tau_{\text{had}}$ channel only);
- $\Delta R(\ell, \text{jet})$ ($\Delta R(\tau_{\text{had}}, \text{jet})$) is the ΔR between the light lepton (leading $\tau_{\text{had-vis}}$) and the mass-paired jet in the $\tau_{\text{lep}}\tau_{\text{had}}$ ($\tau_{\text{had}}\tau_{\text{had}}$) category;
- $\Delta\phi(\ell, E_{\text{T}}^{\text{miss}})$ is the azimuthal opening angle between the lepton and the $E_{\text{T}}^{\text{miss}}$ ($\tau_{\text{lep}}\tau_{\text{had}}$ category only);
- $E_{\text{T}}^{\text{miss}} \phi$ centrality quantifies the transverse direction of the $p_{\text{T}}^{\text{miss}}$ relative to the light lepton and $\tau_{\text{had-vis}}$ (two $\tau_{\text{had-vis}}$) in the $\tau_{\text{lep}}\tau_{\text{had}}$ ($\tau_{\text{had}}\tau_{\text{had}}$) category and is defined in Ref. [112].

A selection of representative input distributions, after the background corrections described in Sect. 6, are presented in Figures 3 and 4 for the $\tau_{\text{lep}}\tau_{\text{had}}$ SR and the $\tau_{\text{had}}\tau_{\text{had}}$ SR, respectively. While the relative importance of the variables varies with LQ mass, the s_{T} and mass variables are generally the most performant.

The PNNs are trained on all scalar LQ signal masses simultaneously against the main $t\bar{t}$ and single-top backgrounds, taking into account both the true and misidentified $\tau_{\text{had-vis}}$ components with the latter corrected as described in Sect. 6. The same PNN training is used for both vector LQ models since separate trainings are found to provide a negligible improvement in sensitivity. For the signals, the generated LQ mass is used as the parameterisation input in addition

to the input variables described above, while in the case of the backgrounds a mock LQ mass is randomly assigned from the range of signal LQ masses such that the resulting training is independent of the mass. In all cases, the input variables are standardised by subtracting the median value and dividing by the interquartile range. Comparing the output between the training dataset and an independent testing dataset showed no sign of overtraining. The resulting PNN score distributions, which peak at higher values for LQ signals than for the background processes, are used as the final analysis discriminants.

6 Background modelling

The dominant background in the $\tau_{\text{had}}\tau_{\text{had}}$ and $\tau_{\text{lep}}\tau_{\text{had}}$ channels is top production, including $t\bar{t}$ and single-top-quark production. A subdominant background is Z boson production in association with heavy-flavour quarks (bb , bc , cc), termed $Z + \text{HF}$ hereafter. Both top production and $Z + \text{HF}$ are estimated from simulation to which data-driven corrections are applied. In the $\tau_{\text{had}}\tau_{\text{had}}$ channel, multi-jet events form a non-negligible background that is estimated by using data-driven techniques. Small contributions to the background from all other processes are estimated by using simulated events. This section describes the background estimation methods used for top-quark-pair and single-top backgrounds, multi-jet backgrounds, and the $Z + \text{HF}$ background. The background is validated for $\tau_{\text{had}}\tau_{\text{had}}$ and $\tau_{\text{lep}}\tau_{\text{had}}$ events in a region with an inverted s_{T} selection, as well as a region with a low PNN score and the signal region selection. In addition, the $\tau_{\text{had}}\tau_{\text{had}}$ multi-jet estimate is validated in a region where the two $\tau_{\text{had-vis}}$ have the same electric charge. The potential signal contamination in all regions described in this section is negligible.

The process of estimating the backgrounds follows several steps. First, an overall shape correction is determined for the top background, as described in Sect. 6.1.1. Then, with this in place, a shape and normalisation correction is determined for the top backgrounds with jets misidentified as $\tau_{\text{had-vis}}$, as described in Sect. 6.1.2. After applying these corrections, a prediction for the shape and normalisation of multi-jet backgrounds is determined for the $\tau_{\text{had}}\tau_{\text{had}}$ channel in Sect. 6.2. Finally, with all relevant corrections in place, a normalisation factor is determined for the $Z + \text{HF}$ backgrounds, as described in Sect. 6.3. The resulting corrections are only weakly coupled due to the high purity of each control region, meaning that corrections for a specific background process do not significantly affect the overall background in control regions targeting other backgrounds. All of these corrections are applied in the final SR fit.

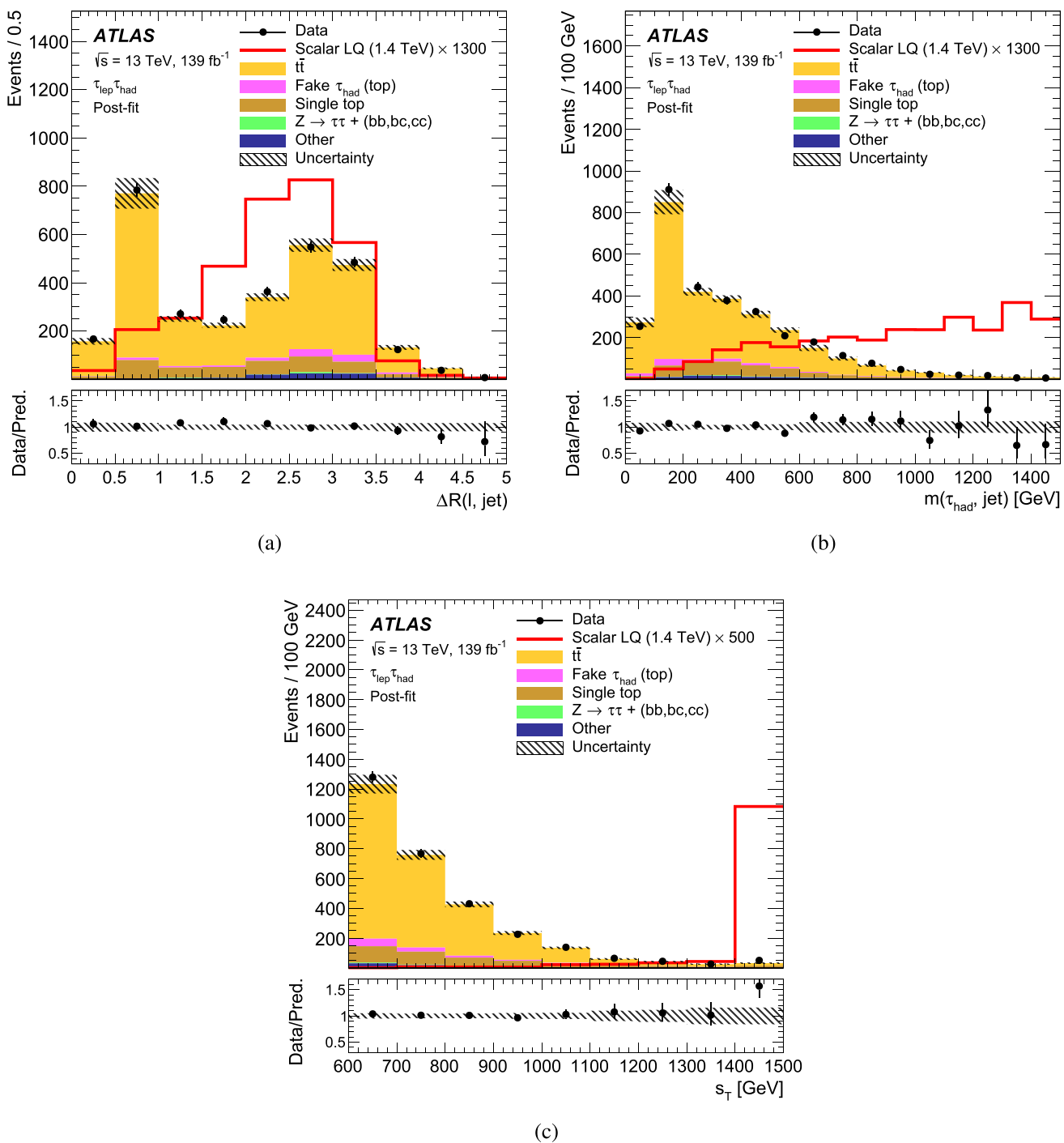


Fig. 3 Signal (solid lines), post-fit background (filled histograms) and data (dots with statistical error bars) distributions of representative PNN input variables in the $\tau_{\text{lep}} \tau_{\text{had}}$ SR: **a** $\Delta R(\ell, \text{jet})$, **b** $m(\tau_{\text{had}}, \text{jet})$ and **c** s_T . The normalisation and shape of the backgrounds are determined from the background-only likelihood fit to data and the ratios of the data to the sum of the predicted backgrounds are shown in the lower panels. ‘Other’

refers to the sum of minor backgrounds (vector boson + jets, diboson and Higgs boson). The hatched band indicates the combined statistical and systematic uncertainty in the total background prediction. The expected signal for a 1.4 TeV scalar LQ, scaled by the indicated factor for visibility, is overlaid. The last bin includes the overflow

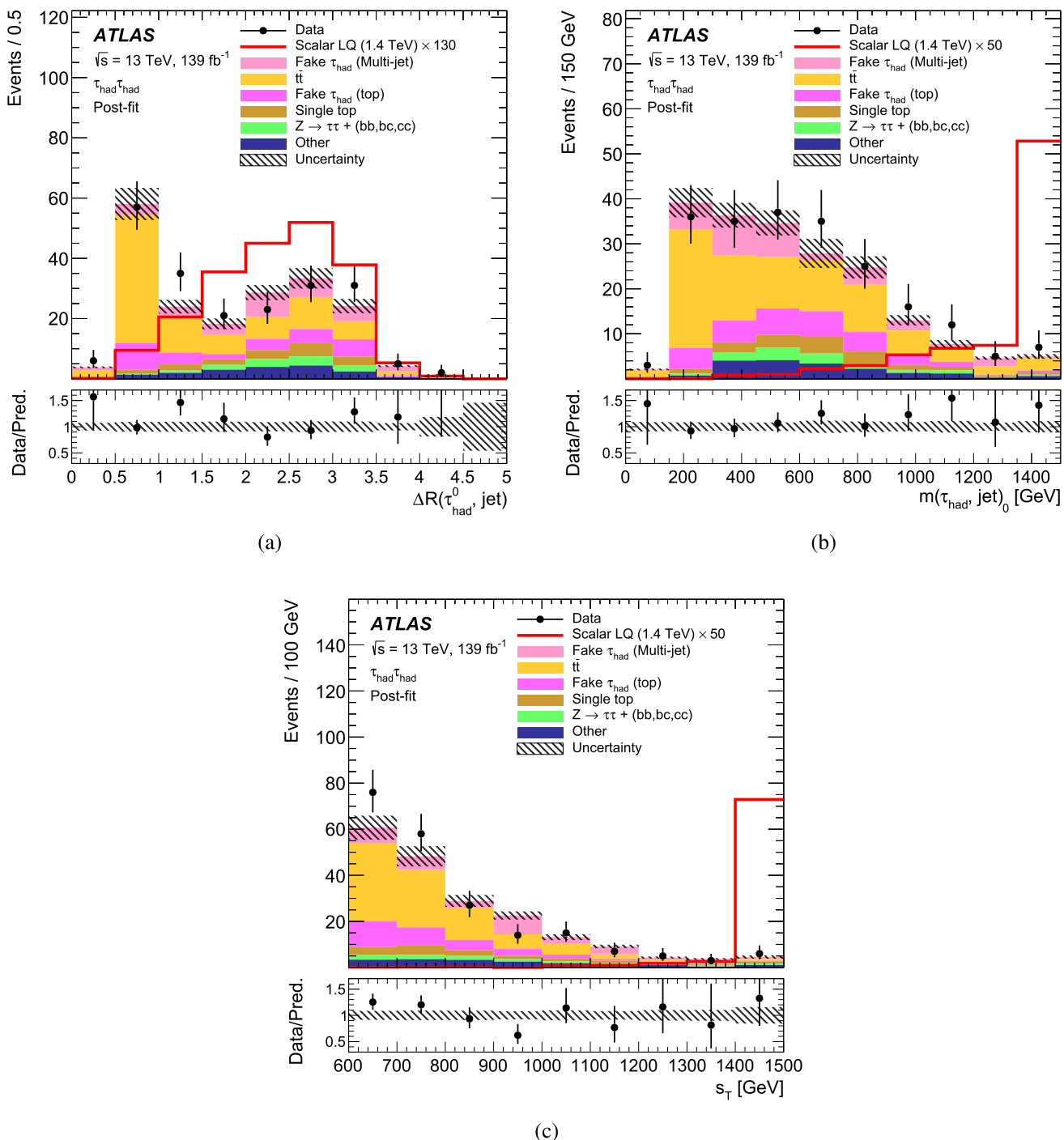


Fig. 4 Signal (solid lines), post-fit background (filled histograms) and data (dots with statistical error bars) distributions of representative PNN input variables in the $\tau_{\text{had}}\tau_{\text{had}}$ SR: **a** $\Delta R(\tau_{\text{had}}^0, \text{jet})$ where τ_{had}^0 is the leading τ -lepton, **b** the larger of the two τ -jet mass combinations $m(\tau_{\text{had}}, \text{jet})_0$ and **c** s_T . The normalisation and shape of the backgrounds are determined from the background-only likelihood fit to data and the ratios of the data to the sum of the predicted backgrounds are shown in

the lower panels. ‘Other’ refers to the sum of minor backgrounds (vector boson + jets, diboson and Higgs boson). The hatched band indicates the combined statistical and systematic uncertainty in the total background prediction. The expected signal for a 1.4 TeV scalar LQ, scaled by the indicated factor for visibility, is overlaid. The last bin includes the overflow

6.1 Top quark backgrounds

For top-quark-pair and single-top-quark production (top backgrounds), events are estimated separately based on whether the $\tau_{\text{had-vis}}$ candidate in the event is correctly identified (referred to as a true $\tau_{\text{had-vis}}$) or whether it is a quark- or gluon-initiated jet misidentified as a $\tau_{\text{had-vis}}$ (referred to as a fake $\tau_{\text{had-vis}}$). The small contributions from light leptons that are misidentified as $\tau_{\text{had-vis}}$ are considered together with the true $\tau_{\text{had-vis}}$ contribution. Events with a true $\tau_{\text{had-vis}}$ and a hadronic jet misidentified as a light lepton contribute negligibly to the $\tau_{\text{lep}}\tau_{\text{had}}$ channel and are not considered.

These backgrounds are estimated in a multi-step data-driven process that is applied to simulated events. First, all top backgrounds are scaled by an s_T -dependent reweighting factor (RF), and then simulated background events with misidentified $\tau_{\text{had-vis}}$ are further corrected by a scale factor (SF) that is binned in the $\tau_{\text{had-vis}} p_T$.

6.1.1 Overall reweighting of top backgrounds

The motivation for scaling the $t\bar{t}$ and single-top backgrounds arises from mismodelling of the data by simulation observed in control regions (CRs). It is seen that this effect becomes more pronounced for events with higher momentum top quarks, which is where this analysis is primarily focused. This mismodelling has also been observed in ATLAS measurements of the $t\bar{t}$ differential cross-section, where it is seen that the number of events is overestimated at high top-quark p_T [113–115].

For this reason, a CR is defined to determine a binned shape and normalisation correction of the simulated top quark events to data. Events in this CR are required to have two b -jets with p_T greater than 45 and 20 GeV, exactly two light leptons (ee , $\mu\mu$ or $e\mu$) with opposite charge, $E_T^{\text{miss}} > 100$ GeV, and a dilepton mass ($m_{\ell\ell}$) > 110 GeV. They are also required to have $m_{b\ell} > 250$ GeV, where $m_{b\ell} = \min(\max(m_{b_0\ell_0}, m_{b_1\ell_1}), \max(m_{b_0\ell_1}, m_{b_1\ell_0}))$, where the 0 and 1 indices refer to the leading and sub-leading b -tagged jets and leptons in order of transverse momentum. This region is orthogonal to the SRs and is over 99% pure in $t\bar{t}$ events.

The RFs are derived by subtracting all non-top backgrounds, as estimated using simulation, from data. A ratio of the remaining events to the prediction of $t\bar{t}$ and single-top events in simulation is then calculated. This factor is binned in s_T , with one bin up to 400 GeV, steps of 100 GeV from 400 to 1400 GeV, and then one bin for values greater than 1400 GeV. The values of the RFs decrease from 0.97 at low s_T to approximately 0.62 in the highest s_T bin. Even in the highest s_T bin, the signal contamination remains at the percent level. The largest relative contribution of single-top events is also at high s_T . This reweighting is applied in both

the $\tau_{\text{lep}}\tau_{\text{had}}$ and $\tau_{\text{had}}\tau_{\text{had}}$ SRs for $t\bar{t}$ and single-top events with true and misidentified τ -leptons, as well as in all CRs. The uncertainty in this RF is taken from the statistical uncertainty in the factor, bin-by-bin in s_T , and its impact on the shape and normalisation of the final PNN score distribution are considered. In addition, top background modelling uncertainties are propagated through the reweighting process, so that modified RFs are applied when evaluating such uncertainties in the final fit.

6.1.2 Top backgrounds with jets misidentified as $\tau_{\text{had-vis}}$

In addition to this overall RF, the estimation of top backgrounds with jets misidentified as $\tau_{\text{had-vis}}$ in the SRs is performed using simulated events with additional data-driven corrections. A fit is performed in a $\tau_{\text{lep}}\tau_{\text{had}}$ -based CR to simultaneously correct the overall normalisation of true $\tau_{\text{had-vis}}$ and misidentified $\tau_{\text{had-vis}}$ events while deriving an SF to be applied to misidentified $\tau_{\text{had-vis}}$ events in the $\tau_{\text{lep}}\tau_{\text{had}}$ and $\tau_{\text{had}}\tau_{\text{had}}$ SRs. The RF for top backgrounds is applied to this CR before the fit. The SFs obtained are then applied in the SRs, in order to correct the $\tau_{\text{had-vis}}$ misidentification rate in simulation to that observed in data.

The CR has the same selection as the SR for the $\tau_{\text{lep}}\tau_{\text{had}}$ channel, except that the $\tau_{\text{had-vis}} p_T > 100$ GeV requirement is removed and s_T is required to be in a range of 400–600 GeV. This region is 97% pure in $t\bar{t}$ events, with a mixture of both correctly identified and misidentified $\tau_{\text{had-vis}}$ that varies with $\tau_{\text{had-vis}} p_T$.

The distribution used for this estimation is the transverse mass of the light lepton and missing transverse momentum, defined as $m_T(\ell, E_T^{\text{miss}}) = \sqrt{(E_T^{\text{miss}} + p_{T,\ell})^2 - (E_{T,x}^{\text{miss}} + p_{x,\ell})^2 - (E_{T,y}^{\text{miss}} + p_{y,\ell})^2}$. The expected shapes for top backgrounds with true and misidentified $\tau_{\text{had-vis}}$ in this distribution differ significantly, making it possible to constrain the two background sources. The normalisation of the true and misidentified $\tau_{\text{had-vis}}$ background is allowed to vary freely, and SFs for the misidentified $\tau_{\text{had-vis}}$ background are determined in bins of $\tau_{\text{had-vis}} p_T$. All detector-related uncertainties and top background modelling uncertainties are included as nuisance parameters in the fit. An example fit in a single bin of p_T is shown in Fig. 5 for the $\tau_{\text{had-vis}}$ CRs. Depending on $\tau_{\text{had-vis}} p_T$, the SFs run from 0.90 in the lowest p_T bin down to 0.56 in the highest p_T bin.

For the estimation of top backgrounds with misidentified $\tau_{\text{had-vis}}$, an uncertainty is considered that arises from the limited number of events and an additional uncertainty is defined by comparing the nominal SFs to SFs derived with a more inclusive s_T selection ($s_T < 600$ GeV). This last uncertainty is intended to address a possible s_T -dependence in the mismodelling of top backgrounds. The difference between the

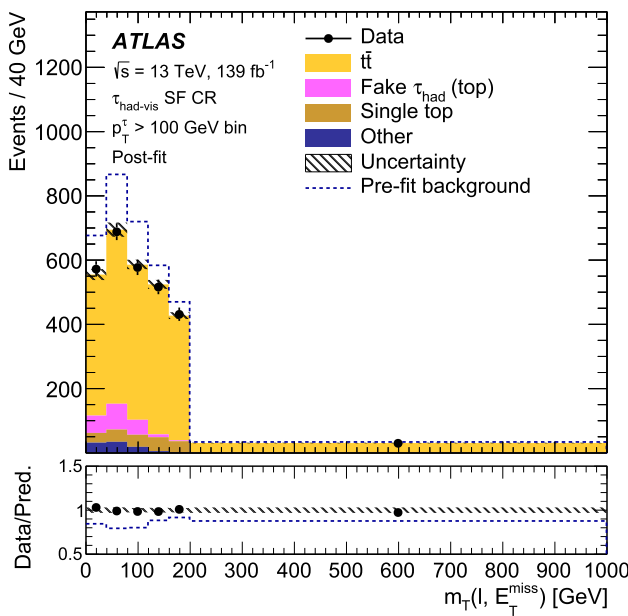


Fig. 5 Post-fit plots for true and misidentified $\tau_{\text{had-vis}}$ in the $\tau_{\text{had-vis}}$ CR, in an example p_T bin ($\tau_{\text{had-vis}} p_T > 100 \text{ GeV}$). ‘Other’ refers to the sum of minor backgrounds (vector boson + jets, diboson and Higgs boson). The lower panels show the ratios of the data to the sum of the predicted backgrounds. The hatched bands indicate the combined statistical and systematic uncertainty in the total background predictions. The dashed lines denote the total pre-fit backgrounds for comparison, while the last bins include the overflow

central values for SFs measured with these two s_T selections is taken as the s_T -dependence uncertainty.

6.2 Multi-jet backgrounds with jets misidentified as $\tau_{\text{had-vis}}$

For the $\tau_{\text{had}}\tau_{\text{had}}$ channel, multi-jet processes can contribute to the SR at non-negligible levels. For this reason, the $\tau_{\text{had}}\tau_{\text{had}}$ channel uses a data-driven fake-factor (FF) method to estimate this background. These FFs are measured in a CR with the same selection as the $\tau_{\text{had}}\tau_{\text{had}}$ SR, except that the two $\tau_{\text{had-vis}}$ candidates have the same charge and the E_T^{miss} requirement is loosened to 80 GeV. The FF is defined as the ratio of events where both $\tau_{\text{had-vis}}$ are loose to the number of events where one $\tau_{\text{had-vis}}$ is loose and the other is an anti- $\tau_{\text{had-vis}}$. These FFs are derived as a function of transverse momentum and the number of charged-particle tracks of the $\tau_{\text{had-vis}}$ candidate. The FFs are measured from data after subtracting all predicted non-multi-jet background contributions. The FFs range between approximately zero and 0.25.

The non-multi-jet background contributions that are subtracted, however, suffer from the same mismodelling issues described in the previous two sections. The top backgrounds are therefore corrected by the RFs and SFs derived as described in Sects. 6.1.1 and 6.1.2, respectively. Since the SFs are anticipated to be different for fake $\tau_{\text{had-vis}}$ passing the $\tau_{\text{had-vis}}$ and anti- $\tau_{\text{had-vis}}$ requirements, dedicated SFs are mea-

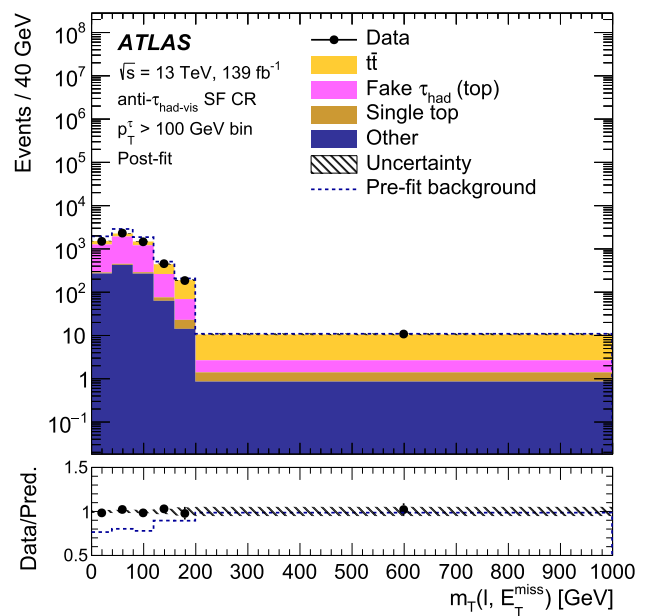


Fig. 6 Post-fit plot for true and misidentified $\tau_{\text{had-vis}}$ in the the anti- $\tau_{\text{had-vis}}$ CR, in an example p_T bin ($\tau_{\text{had-vis}} p_T > 100 \text{ GeV}$). ‘Other’ refers to the sum of minor backgrounds (vector boson + jets, diboson and Higgs boson). The lower panels show the ratios of the data to the sum of the predicted backgrounds. The hatched bands indicate the combined statistical and systematic uncertainty in the total background predictions. The dashed lines denote the total pre-fit backgrounds for comparison, while the last bins include the overflow

sured for this data-driven estimation. Specifically, the anti- $\tau_{\text{had-vis}}$ region uses SFs that are derived in a CR as described in Sect. 6.1.2, except that the $\tau_{\text{had-vis}}$ identification requirement is changed to that of an anti- $\tau_{\text{had-vis}}$. An example fit in a single bin of p_T is shown in Fig. 6 for the anti- $\tau_{\text{had-vis}}$ CR. Depending on $\tau_{\text{had-vis}} p_T$, these SFs vary between 0.77 and 0.95.

To construct the background estimate, FFs are applied to a region with the $\tau_{\text{had}}\tau_{\text{had}}$ SR selection, except that the $\tau_{\text{had-vis}}$ identification requirement is changed to that of an anti- $\tau_{\text{had-vis}}$. This provides both a shape and a normalisation for the multi-jet contribution in the PNN score distribution.

For the estimation of multi-jet backgrounds in $\tau_{\text{had}}\tau_{\text{had}}$, uncertainties are considered due to the statistical uncertainty of the FFs, decorrelated in p_T bins, and to the uncertainty in the subtraction of different backgrounds using simulation. Top events with a correctly identified $\tau_{\text{had-vis}}$, top events with a misidentified $\tau_{\text{had-vis}}$, and other small backgrounds are considered separately. The top events are varied by the overall uncertainty defined by the procedure to determine the modelling uncertainties, but evaluated in the anti- $\tau_{\text{had-vis}}$ region, resulting in an uncertainty of approximately 50%. The other backgrounds are varied by a conservative value of 30%; inflating the size of this uncertainty further was found

to have negligible impact on the result. In addition, a 20% overall uncertainty in the estimate is applied based on checks of the method in the validation regions described above. The total uncertainty in the multi-jet background is -64% and $+61\%$.

6.3 $Z + \text{HF}$ background

The normalisation of the $Z + \text{HF}$ background, which is a relatively small contribution in the SRs, is observed to be in disagreement with the NLO cross-section in SHERPA (e.g. Ref. [116]). It is therefore determined from data using a $Z + \text{HF}$ CR that targets events containing a Z boson decaying into a light-lepton pair and produced in association with two heavy-flavour jets. The composition of this control region is approximately 60% $Z + \text{HF}$ events and 40% $t\bar{t}$ events, with less than 1% arising from backgrounds with misidentified $\tau_{\text{had-vis}}$. Since the contribution from backgrounds with misidentified $\tau_{\text{had-vis}}$ is negligible, only the RF for the $t\bar{t}$ shape is included in this CR.

Data for the CR was recorded using a combination of the single-lepton triggers described above and additional dilepton triggers requiring pairs of same-flavour leptons. At the analysis level exactly two oppositely-charged same-flavour leptons, passing the ‘veto’ quality requirements and p_T thresholds based on the corresponding trigger thresholds, are required. The invariant mass of the resulting lepton pair $m_{\ell\ell}$ is required to lie between 75 GeV and 110 GeV. In addition, exactly two b -jets with $p_T > 20$ GeV are required and their invariant mass m_{bb} is required to be less than 40 GeV or greater than 150 GeV to avoid the Higgs boson mass peak. The RFs for top backgrounds derived in Sect. 6.1.1 are then applied.

A fit to the $m_{\ell\ell}$ distribution is performed to discriminate between the $Z + \text{HF}$ and top backgrounds, with the normalisation of both processes allowed to vary freely and all systematic uncertainties described in Sect. 7 included. The resulting $Z + \text{HF}$ normalisation factor is 1.36 ± 0.11 and is used to correct the $Z + \text{HF}$ background entering into the final fit (described in Sect. 8), which is allowed to vary within the associated uncertainty.

7 Systematic uncertainties

The systematic uncertainties considered include detector-related uncertainties, modelling and theoretical uncertainties, and uncertainties derived for the data-driven background estimates, the latter of which have already been described in Sect. 6. Uncertainties are evaluated by shifting the central value upward or downward by one standard deviation, and then propagating the differences to the PNN score distributions that are used in the final fit.

Detector-related uncertainties are defined as uncertainties relating to the detector response, object reconstruction and object identification. There are systematic uncertainties associated with each of the reconstructed objects considered, as well as the E_T^{miss} . For light leptons, $\tau_{\text{had-vis}}$, and jets, uncertainties are considered for energy scale and resolution, reconstruction and identification, while uncertainties in isolation are also considered for light leptons. For the $\tau_{\text{lep}}\tau_{\text{had}}$ and $\tau_{\text{had}}\tau_{\text{had}}$ channel, uncertainties associated with the lepton and $\tau_{\text{had-vis}}$ trigger efficiencies, respectively, are considered. For b -jets, additional uncertainties are considered for the efficiency of (mis)tagging b -jets, c -jets, and light-quark-initiated jets. Uncertainties related to energy scale and resolution, and the inclusion of soft terms, are considered for the E_T^{miss} . Finally, there is also an uncertainty associated with shape and normalisation components that arises from uncertainties in the simulation of pile-up collisions.

Theoretical and modelling uncertainties include uncertainties in the cross-section calculations, which have only a normalisation component, and uncertainties in the acceptance, for which normalisation and shape components are considered. For top backgrounds, relative acceptance uncertainties are also defined to take into account normalisation differences for $\tau_{\text{lep}}\tau_{\text{had}}$ and $\tau_{\text{had}}\tau_{\text{had}}$ SRs.

For $t\bar{t}$ processes, shape and normalisation uncertainties are considered that arise from changing the matrix element and parton shower simulation software, and from varying the initial and final state radiation, PDF, and α_s . The matrix element uncertainty is determined by comparing the POWHEG+PYTHIA 8 sample with an AMC@NLO+PYTHIA 8 sample. The parton shower uncertainty is determined by comparing the POWHEG+PYTHIA 8 sample with a POWHEG+HERWIG 7 [117, 118] sample. The other modelling uncertainties are evaluated using internal weights in the nominal $t\bar{t}$ sample.

For single-top processes, acceptance uncertainties with shape and normalisation components are considered. Uncertainties are considered from changing the matrix element, parton shower, and impacts of diagram interference. In addition, variations of initial- and final-state radiation and PDFs are considered. The matrix element uncertainty is determined by comparing the POWHEG+PYTHIA 8 sample with an AMC@NLO+PYTHIA 8 sample. The parton shower uncertainty is determined by comparing the POWHEG+PYTHIA 8 sample with a POWHEG+HERWIG 7 sample. The diagram interference uncertainty is evaluated by comparing the nominal single top samples, which use a diagram removal scheme, with alternative samples that utilise a diagram subtraction scheme [119]. The other modelling uncertainties are evaluated using internal weights in the nominal single-top samples.

All $t\bar{t}$ and single-top modelling uncertainties are also propagated through the top reweighting procedure, such that there

Table 4 Post-fit yields for background events, determined from a background-only fit, compared with the observed number of data events in the $\tau_{\text{lep}}\tau_{\text{had}}$ and $\tau_{\text{had}}\tau_{\text{had}}$ SRs. ‘Fake τ_{had} (top)’ refers to top backgrounds where a jet is misidentified as the $\tau_{\text{had-vis}}$ of the event. ‘Other’ refers to the sum of minor backgrounds (vector boson + jets, diboson and Higgs boson); it is primarily composed of $Z \rightarrow \tau\tau$ in association with light-flavour quarks and $W \rightarrow \ell\nu + \text{jets}$ events. The total background is not identical to the sum of the individual components since the latter are rounded for presentation, while the sum is calculated with the full precision before being subsequently rounded. Systematic uncertainties are included. Due to the large correlations, individual uncertainties can be significantly larger than the total uncertainty

	$\tau_{\text{lep}}\tau_{\text{had}}$ channel	$\tau_{\text{had}}\tau_{\text{had}}$ channel
$t\bar{t}$	2430 ± 110	94 ± 12
Single-top	365 ± 26	20 ± 5
Fake τ_{had} (top)	140 ± 100	36 ± 11
$Z \rightarrow \tau\tau + (\text{bb}, \text{bc}, \text{cc})$	13.1 ± 2.7	10.1 ± 1.3
Multi-jet	—	30 ± 16
Other	91 ± 35	18 ± 7
Total background	3040 ± 60	207 ± 14
Data	3031	211

is an uncertainty in the RF corresponding to each modelling uncertainty.

For all $Z + \text{jets}$ processes, uncertainties due to the choice of generator are evaluated by comparing the nominal SHERPA simulated samples with alternative samples simulated by MADGRAPH with LO-accurate matrix elements that contain up to four final-state partons, using PYTHIA for parton showering. In addition, uncertainties are considered by taking an envelope of variations in the renormalisation and factorisation scales and PDF values using internal weights in the simulated SHERPA sample. For this process specifically, uncertainties are also included based on varying the matrix element matching scale and the resummation scale for soft-gluon emission. Uncertainties are considered separately for the $Z + \text{HF}$ background and the remaining $Z + (bl, cl, ll)$ background, where l indicates a light-flavour jet, and only normalization is taken into account. All of these uncertainties are included in the $Z + \text{HF}$ fit described in Sect. 6.3, and their sum in quadrature, taking relative acceptance uncertainties into account, is considered as the uncertainty in the SRs for the final fit.

For other minor backgrounds, the following uncertainties are considered. A conservative uncertainty of 50% on the normalization of the diboson backgrounds is included. For $W + \text{jets}$ processes, which form a background to the analysis due to a jet being misidentified as a light lepton or a τ_{had} , a conservative 100% uncertainty is taken into account, decorrelated between the $\tau_{\text{lep}}\tau_{\text{had}}$ and $\tau_{\text{had}}\tau_{\text{had}}$ channels. Within the $\tau_{\text{lep}}\tau_{\text{had}}$ channel, the uncertainty is also decorrelated between the cases where it is the light lepton or the τ_{had} that is misiden-

tified. In both cases, the choice of the size of these uncertainties has a negligible impact on the results.

For signal samples, uncertainties arising from variations of scale, initial-state radiation, PDF, and α_s are considered, using alternative weights internal to the signal samples. Differences in shape are observed to be negligibly small in the PNN score distributions, so only variations in normalisation are included for the final fit.

The relative impact of the different sources of uncertainty on the analysis varies depending on the LQ model considered and the mass probed. Generally, the largest impact comes from the statistical uncertainties, which increase with m_{LQ} . In the scalar LQ case, for example, the statistical impact on the limit ranges from 60% at the lowest m_{LQ} evaluated to 80% above 1000 GeV. The main systematic uncertainties come from the $t\bar{t}$ and single-top-quark modelling uncertainties, including their interference, and normalisation. There is also a significant effect from the signal acceptance uncertainties, which increases with m_{LQ} , particularly for the vector LQ models.

8 Statistical interpretation and results

The data are compared with the expectation, including the background modelling corrections outlined in Sect. 6, by performing simultaneous binned maximum-likelihood fits to the PNN score distributions, separately for each LQ hypothesis, in the $\tau_{\text{lep}}\tau_{\text{had}}$ and $\tau_{\text{had}}\tau_{\text{had}}$ SRs. For each hypothesis, the binning of the PNN score distributions is chosen separately to maximise the expected sensitivity, while ensuring sufficient background events in the signal-enhanced PNN bins and preserving the stability of the fit. In addition to the relative signal-strength modifier, μ , the top normalisation is free to float in the fit and is constrained by the background-enhanced PNN bins.

The statistical and systematic uncertainties affecting the signal and background model, described in Sect. 7, are represented by deviations from the nominal model scaled by Gaussian- or Poisson-constrained nuisance parameters that are profiled in the fit. Common sources of systematic uncertainty are correlated across the SRs.

The resulting event yields in the $\tau_{\text{lep}}\tau_{\text{had}}$ and $\tau_{\text{had}}\tau_{\text{had}}$ SRs, based on a background-only fit to the data, are presented in Table 4. Corresponding post-fit PNN score distributions for representative LQ signals at masses of 500 GeV, 1.1 TeV and 1.4 TeV are shown in Fig. 7 (Fig. 8) for the $\tau_{\text{lep}}\tau_{\text{had}}$ ($\tau_{\text{had}}\tau_{\text{had}}$) SR. At high values of the PNN score, top backgrounds dominate in the $\tau_{\text{lep}}\tau_{\text{had}}$ channel, while the $\tau_{\text{had}}\tau_{\text{had}}$ background consists of a roughly even mixture of all background sources. Overall, good agreement with the SM background expectation is observed in all cases, although there is a slight deficit

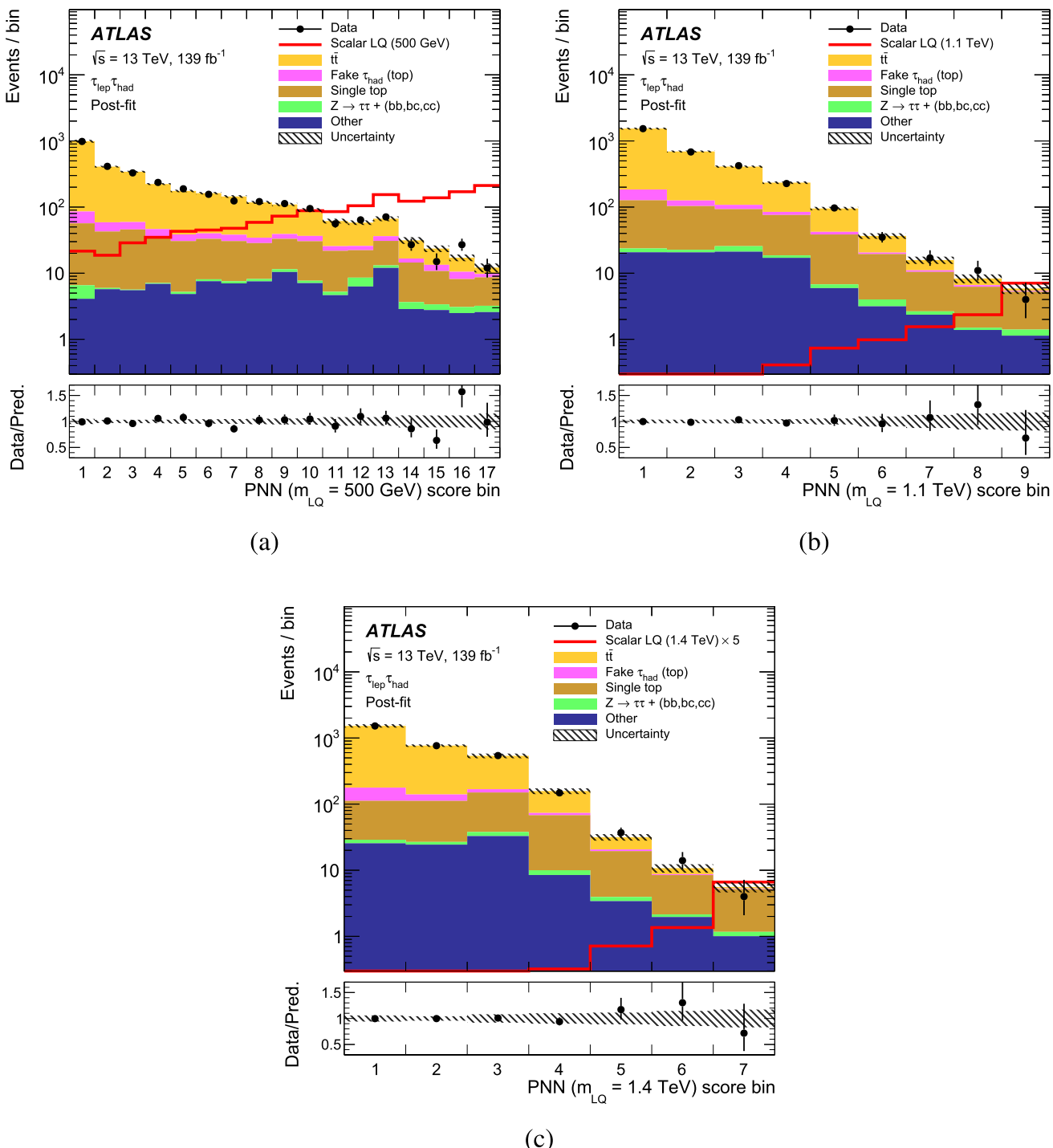


Fig. 7 The PNN score distributions in the $\tau_{\text{lep}}\tau_{\text{had}}$ SR for **a** $m_{\text{LQ}} = 500 \text{ GeV}$, **b** $m_{\text{LQ}} = 1.1 \text{ TeV}$, **c** $m_{\text{LQ}} = 1.4 \text{ TeV}$. The normalisation and shape of the backgrounds are determined from the background-only likelihood fit to data and the ratios of the data to the sum of the backgrounds are shown in the lower panels. ‘Other’ refers to the sum of minor backgrounds (vector boson + jets, diboson and Higgs

boson). The hatched bands indicate the combined statistical and systematic uncertainty in the total background predictions. The expected signals for scalar LQs with the corresponding masses, scaled by the indicated factors for visibility, are overlaid. Since the PNN score itself is not a physical quantity, it is represented solely by the bin number

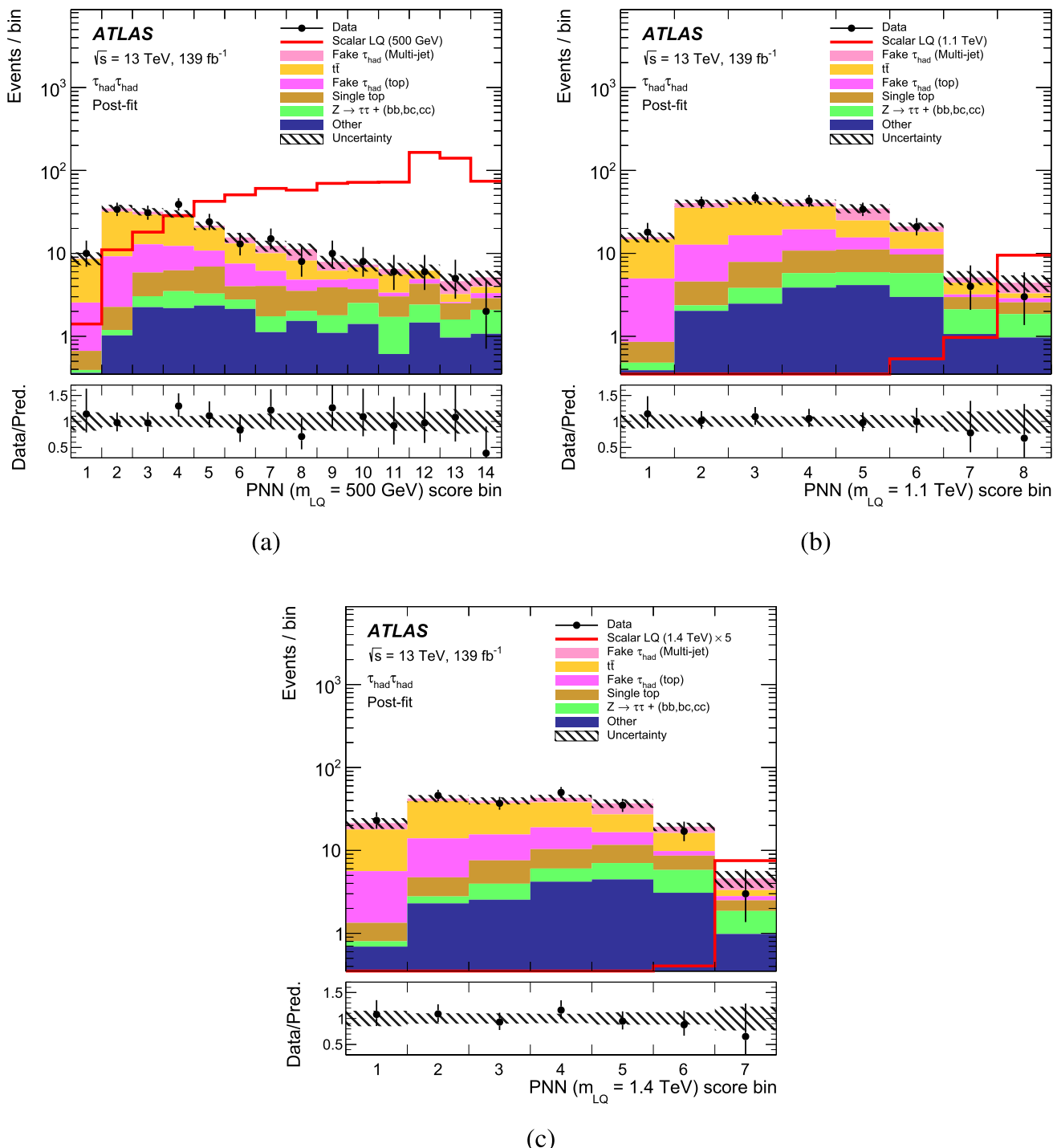


Fig. 8 The PNN score distributions in the $\tau_{\text{had}}\tau_{\text{had}}$ SR for **a** $m_{\text{LQ}} = 500 \text{ GeV}$, **b** $m_{\text{LQ}} = 1.1 \text{ TeV}$, **c** $m_{\text{LQ}} = 1.4 \text{ TeV}$. The normalisation and shape of the backgrounds are determined from the background-only likelihood fit to data and the ratios of the data to the sum of the backgrounds are shown in the lower panels. ‘Other’ refers to the sum of minor backgrounds (vector boson + jets, diboson and Higgs

boson). The hatched bands indicate the combined statistical and systematic uncertainty in the total background predictions. The expected signals for scalar LQs with the corresponding masses, scaled by the indicated factors for visibility, are overlaid. Since the PNN score itself is not a physical quantity, it is represented solely by the bin number

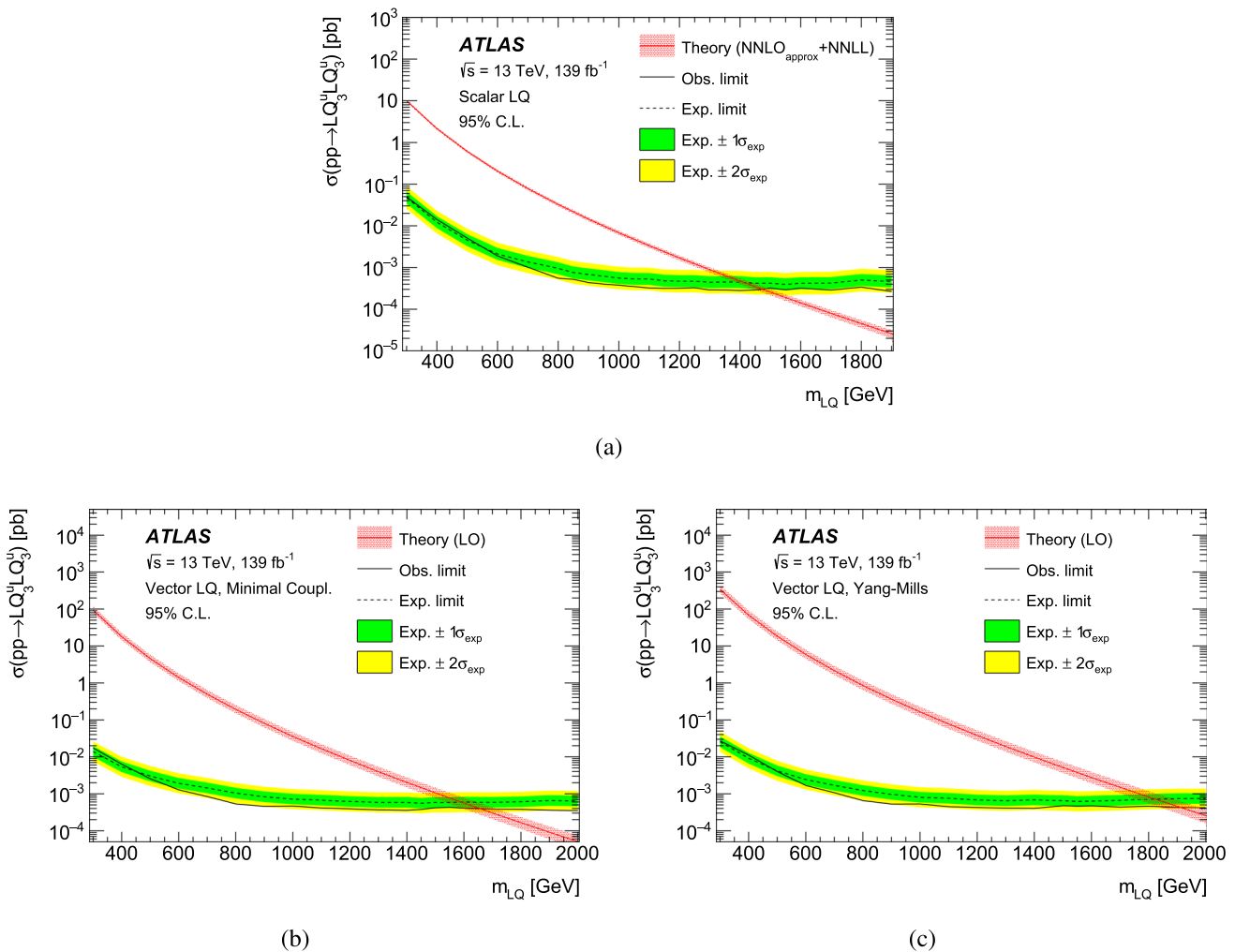


Fig. 9 The observed (solid line) and expected (dashed line) 95% CL upper limits on the LQ pair production cross-sections assuming $\mathcal{B} = 1$ as a function of m_{LQ} for **a** the scalar LQ case, **b** the vector LQ case in the minimal-coupling scenario, **c** vector LQs in the Yang–Mills scenario.

The surrounding shaded bands correspond to the ± 1 and ± 2 standard deviation ($\pm 1\sigma$, $\pm 2\sigma$) uncertainty in the expected limit. The theoretical prediction in each model, along with its uncertainty, is shown by the lines with the hatched bands

Table 5 Observed and expected lower limits on the LQ mass at 95% CL for the three different LQ models, assuming $\mathcal{B} = 1$

	Obs. limit [GeV]	Exp. limit [GeV]
Scalar LQ	1460	1410
Vector LQ (minimal-coupling)	1650	1590
Vector LQ (Yang–Mills)	1910	1820

of data relative to the background prediction in the highest PNN score bin for the $\tau_{\text{had}} \tau_{\text{had}}$ channel.

Since no significant excess is observed, upper limits on the scalar and vector LQ pair production cross-sections for each mass hypothesis are computed based on the modified frequentist CL_s method [120], using a profile likelihood test statistic [121] under the asymptotic approximation. The

resulting observed and expected limits, assuming $\mathcal{B} = 1$, as a function of m_{LQ} at 95% confidence level (CL) are shown in Fig. 9 for all LQ models. The expected contributions of the $\tau_{\text{lep}} \tau_{\text{had}}$ and $\tau_{\text{had}} \tau_{\text{had}}$ channels are approximately equal at high m_{LQ} , while the $\tau_{\text{had}} \tau_{\text{had}}$ is up to a factor of two more sensitive at low m_{LQ} . The improvement in the observed limit compared with the expectation is driven by the data deficit in the highest $\tau_{\text{had}} \tau_{\text{had}}$ PNN score bin mentioned above and is larger at high m_{LQ} since the signal becomes more localised at high PNN score as m_{LQ} increases. The theoretical prediction for the cross-section of scalar or vector LQ pair production is indicated by the solid line along with its uncertainties.

The corresponding expected and observed 95% CL lower limits on the LQ mass for the three different LQ models are summarised in Table 5, providing an improvement in mass reach for a scalar LQ of more than 450 GeV compared with

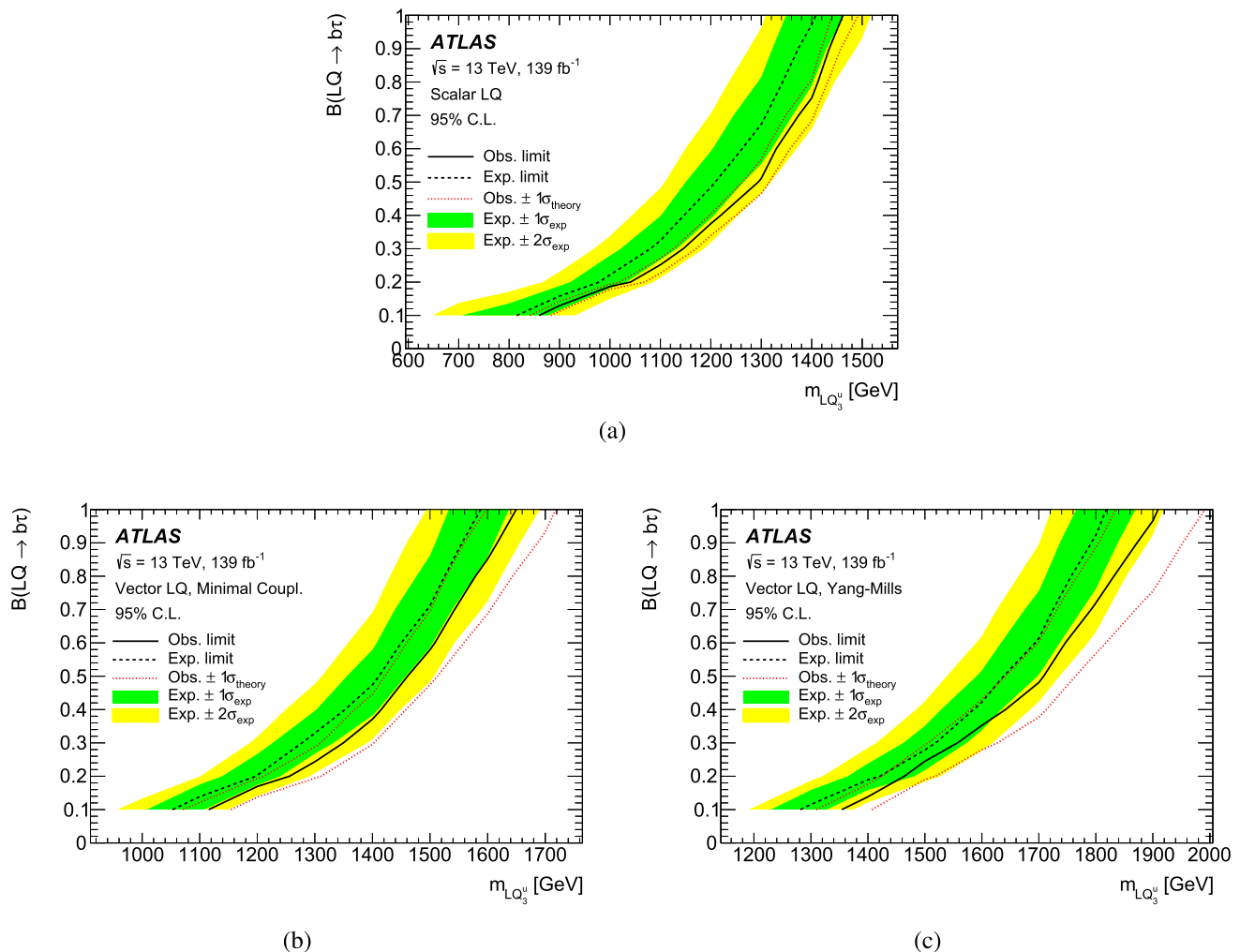


Fig. 10 The observed (solid line) and expected (dashed line) 95% CL upper limits on the branching ratio into charged leptons as a function of m_{LQ} for **a** the scalar LQ case, **b** the vector LQ case in the minimal-coupling scenario, **c** vector LQs in the Yang–Mills scenario. The observed exclusion region is above the solid line, with the theoretical uncertainty in the model indicated by the dotted lines around this. The expected limit is indicated by the dashed line and the surrounding shaded bands correspond to the ± 1 and ± 2 standard deviation ($\pm 1\sigma$, $\pm 2\sigma$) uncertainty in the expected limit. No limits are presented for $B < 0.1$ due to the lack of expected signal events in this final state

retical uncertainty in the model indicated by the dotted lines around this. The expected limit is indicated by the dashed line and the surrounding shaded bands correspond to the ± 1 and ± 2 standard deviation ($\pm 1\sigma$, $\pm 2\sigma$) uncertainty in the expected limit. No limits are presented for $B < 0.1$ due to the lack of expected signal events in this final state

the previous 36 fb^{-1} result in this channel [19]. They extend the full Run 2 ATLAS reach for third-generation up-type LQs by around 200 GeV in all three models compared with the search in the $LQLQ \rightarrow t\nu t\nu$ decay mode [27].

The results are also expressed as upper limits on the branching ratio to charged leptons as a function of m_{LQ} for each LQ model in Fig. 10. For all models investigated, constraints on the LQ mass are reduced by no more than 15% going from $B = 1$ to $B = 0.5$, while scalar LQ masses up to around 850 GeV are excluded for couplings into charged leptons as low as 0.1; the corresponding $B = 0.1$ exclusion for vector LQ is around 1100 GeV (1300 GeV) in the minimal-coupling (Yang–Mills) scenario.

9 Conclusion

A search for pair-produced scalar or vector leptoquarks decaying into a b -quark and a τ -lepton is presented. The analysis exploits the full data sample recorded with the ATLAS detector in Run 2 of the LHC, corresponding to 139 fb^{-1} of proton-proton collisions at $\sqrt{s} = 13 \text{ TeV}$. No significant deviations from the Standard Model expectation are observed and upper limits on the production cross-section are derived as a function of LQ mass and branching ratio into a charged lepton. Scalar LQs with masses below 1460 GeV are excluded assuming a 100% branching ratio, while for vector LQs the corresponding limit is 1650 GeV (1910 GeV) in the minimal-coupling (Yang–Mills) scenario. For branching ratios as low as 10%, scalar LQ masses below around

860 GeV are excluded; the corresponding mass limits for vector LQs are 1120 GeV (1360 GeV) in the minimal-coupling (Yang–Mills) scenario. These results significantly improve the sensitivity compared to previous ATLAS LQ searches, extending the mass reach for third-generation up-type LQs by more than 200 GeV in all models and surpassing the previous ATLAS search in this final state by more than 450 GeV for scalar LQs. In addition to the increased luminosity, this is due to upgraded hadronic τ -lepton and b -jet identification, improved multivariate techniques and better background estimation methods.

Acknowledgements We thank CERN for the very successful operation of the LHC, as well as the support staff from our institutions without whom ATLAS could not be operated efficiently. We acknowledge the support of ANPCyT, Argentina; YerPhI, Armenia; ARC, Australia; BMWFW and FWF, Austria; ANAS, Azerbaijan; CNPq and FAPESP, Brazil; NSERC, NRC and CFI, Canada; CERN; ANID, Chile; CAS, MOST and NSFC, China; Minciencias, Colombia; MEYS CR, Czech Republic; DNRF and DNSRC, Denmark; IN2P3-CNRS and CEA-DRF/IRFU, France; SRNSFG, Georgia; BMBF, HGF and MPG, Germany; GSRI, Greece; RGC and Hong Kong SAR, China; ISF and Benoziyo Center, Israel; INFN, Italy; MEXT and JSPS, Japan; CNRST, Morocco; NWO, Netherlands; RCN, Norway; MEIN, Poland; FCT, Portugal; MNE/IFA, Romania; MESTD, Serbia; MSSR, Slovakia; ARRS and MIZŠ, Slovenia; DSNI/NRF, South Africa; MICINN, Spain; SRC and Wallenberg Foundation, Sweden; SERI, SNSF and Cantons of Bern and Geneva, Switzerland; MOST, Taiwan; TENMAK, Türkiye; STFC, United Kingdom; DOE and NSF, United States of America. In addition, individual groups and members have received support from BCKDF, CANARIE, Compute Canada and CRC, Canada; PRIMUS 21/SCI/017 and UNCE SCI/013, Czech Republic; COST, ERC, ERDF, Horizon 2020 and Marie Skłodowska-Curie Actions, European Union; Investissements d’Avenir Labex, Investissements d’Avenir Idex and ANR, France; DFG and AvH Foundation, Germany; Herakleitos, Thales and Aristeia programmes co-financed by EU-ESF and the Greek NSRF, Greece; BSF-NSF and MINERVA, Israel; Norwegian Financial Mechanism 2014–2021, Norway; NCN and NAWA, Poland; La Caixa Banking Foundation, CERCA Programme Generalitat de Catalunya and PROMETEO and GenT Programmes Generalitat Valenciana, Spain; Göran Gustafssons Stiftelse, Sweden; The Royal Society and Leverhulme Trust, United Kingdom. The crucial computing support from all WLCG partners is acknowledged gratefully, in particular from CERN, the ATLAS Tier-1 facilities at TRIUMF (Canada), NDGF (Denmark, Norway, Sweden), CC-IN2P3 (France), KIT/GridKA (Germany), INFN-CNAF (Italy), NL-T1 (Netherlands), PIC (Spain), ASGC (Taiwan), RAL (UK) and BNL (USA), the Tier-2 facilities worldwide and large non-WLCG resource providers. Major contributors of computing resources are listed in Ref. [122].

Data Availability Statement This manuscript has no associated data or the data will not be deposited. [Authors’ comment: “All ATLAS scientific output is published in journals, and preliminary results are made available in Conference Notes. All are openly available, without restriction on use by external parties beyond copyright law and the standard conditions agreed by CERN. Data associated with journal publications are also made available: tables and data from plots (e.g. cross section values, likelihood profiles, selection efficiencies, cross section limits, ...) are stored in appropriate repositories such as HEPDATA (<http://hepdata.ceder.ac.uk/>). ATLAS also strives to make additional material related to the paper available that allows a reinterpretation of the data in the context of new theoretical models. For example, an extended encapsulation of the analysis is often provided for measurements in the

framework of RIVET (<http://rivet.hepforge.org/>).” This information is taken from the ATLAS Data Access Policy, which is a public document that can be downloaded from <http://opendata.cern.ch/record/413> [opendata.cern.ch].]

Open Access This article is licensed under a Creative Commons Attribution 4.0 International License, which permits use, sharing, adaptation, distribution and reproduction in any medium or format, as long as you give appropriate credit to the original author(s) and the source, provide a link to the Creative Commons licence, and indicate if changes were made. The images or other third party material in this article are included in the article’s Creative Commons licence, unless indicated otherwise in a credit line to the material. If material is not included in the article’s Creative Commons licence and your intended use is not permitted by statutory regulation or exceeds the permitted use, you will need to obtain permission directly from the copyright holder. To view a copy of this licence, visit <http://creativecommons.org/licenses/by/4.0/>.

Funded by SCOAP³. SCOAP³ supports the goals of the International Year of Basic Sciences for Sustainable Development.

References

1. J.C. Pati, A. Salam, Lepton number as the fourth “color”. *Phys. Rev. D* **10**, 275 (1974). <https://doi.org/10.1103/PhysRevD.10.275>
2. H. Georgi, S.L. Glashow, Unity of all elementary-particle forces. *Phys. Rev. Lett.* **32**, 438 (1974). <https://doi.org/10.1103/PhysRevLett.32.438>
3. S. Dimopoulos, L. Susskind, Mass without scalars. *Nucl. Phys. B* **155**, 237 (1979). [https://doi.org/10.1016/0550-3213\(79\)90364-X](https://doi.org/10.1016/0550-3213(79)90364-X)
4. S. Dimopoulos, Technicoloured signatures. *Nucl. Phys. B* **168**, 69 (1980). [https://doi.org/10.1016/0550-3213\(80\)90277-1](https://doi.org/10.1016/0550-3213(80)90277-1)
5. E. Eichten, K. Lane, Dynamical breaking of weak interaction symmetries. *Phys. Lett. B* **90**, 125 (1980). [https://doi.org/10.1016/0370-2693\(80\)90065-9](https://doi.org/10.1016/0370-2693(80)90065-9)
6. V.D. Angelopoulos et al., Search for new quarks suggested by the superstring. *Nucl. Phys. B* **292**, 59 (1987). [https://doi.org/10.1016/0550-3213\(87\)90637-7](https://doi.org/10.1016/0550-3213(87)90637-7)
7. W. Buchmüller, D. Wyler, Constraints on SU(5)-type leptoquarks. *Phys. Lett. B* **177**, 377 (1986). [https://doi.org/10.1016/0370-2693\(86\)90771-9](https://doi.org/10.1016/0370-2693(86)90771-9)
8. G. Hiller, M. Schmaltz, R_K and future $b \rightarrow s\ell\ell$ physics beyond the standard model opportunities. *Phys. Rev. D* **90**, 054014 (2014). <https://doi.org/10.1103/PhysRevD.90.054014>. arXiv:1408.1627 [hep-ph]
9. B. Gripaios, M. Nardecchia, S.A. Renner, Composite leptoquarks and anomalies in B-meson decays. *JHEP* **05**, 006 (2015). [https://doi.org/10.1007/JHEP05\(2015\)006](https://doi.org/10.1007/JHEP05(2015)006). arXiv:1412.1791 [hep-ph]
10. M. Freytsis, Z. Ligeti, J.T. Ruderman, Flavor models for $B - D^{(*)}\tau\bar{\nu}$. *Phys. Rev. D* **92**, 054018 (2015). <https://doi.org/10.1103/PhysRevD.92.054018>. arXiv:1506.08896 [hep-ph]
11. M. Bauer, M. Neubert, Minimal leptoquark explanation for the $R_{D^{(*)}}$, R_K , and $(g - 2)_\mu$ anomalies. *Phys. Rev. Lett.* **116**, 141802 (2016). <https://doi.org/10.1103/PhysRevLett.116.141802>. arXiv:1511.01900 [hep-ph]
12. L. Di Luzio, M. Nardecchia, What is the scale of new physics behind the B-flavour anomalies? *Eur. Phys. J. C* **77**, 536 (2017). <https://doi.org/10.1140/epjc/s10052-017-5118-9>. arXiv:1706.01868 [hep-ph]
13. D. Buttazzo, A. Greljo, G. Isidori, D. Marzocca, B-physics anomalies: a guide to combined explanations. *JHEP* **11**, 044 (2017). [https://doi.org/10.1007/JHEP11\(2017\)044](https://doi.org/10.1007/JHEP11(2017)044). arXiv:1706.07808 [hep-ph]

14. R. Aaij et al., Test of lepton universality using $B^+ \rightarrow K^+\ell^+\ell^-$ decays. *Phys. Rev. Lett.* **113**, 151601 (2014). <https://doi.org/10.1103/PhysRevLett.113.151601>. arXiv:1406.6482 [hep-ex]
15. W. Buchmüller, R. Rückl, D. Wyler, Leptoquarks in lepton-quark collisions. *Phys. Lett. B* **191**, 442 (1987). [https://doi.org/10.1016/0370-2693\(87\)90637-X](https://doi.org/10.1016/0370-2693(87)90637-X)
16. J. Blumlein, E. Boos, A. Kryukov, Leptoquark pair production in hadronic interactions. *Z. Phys. C* **76**, 137 (1997). <https://doi.org/10.1007/s002880050538>. arXiv:hep-ph/9610408
17. M.J. Baker, J. Fuentes-Martín, G. Isidori, M. König, High-pr signatures in vector-leptoquark models. *Eur. Phys. J. C* **79**, 334 (2019). <https://doi.org/10.1140/epjc/s10052-019-6853-x>. arXiv:1901.10480 [hep-ph]
18. ATLAS Collaboration, Search for pair production of scalar leptoquarks decaying into first- or second-generation leptons and top quarks in proton-proton collisions at $\sqrt{s} = 13$ TeV with the ATLAS detector. *Eur. Phys. J. C* **81**, 313 (2021). <https://doi.org/10.1140/epjc/s10052-021-09009-8>. arXiv:2010.02098 [hep-ex]
19. ATLAS Collaboration, Searches for third-generation scalar leptoquarks in $\sqrt{s} = 13$ TeV pp collisions with the ATLAS detector. *JHEP* **06**, 144 (2019). [https://doi.org/10.1007/JHEP06\(2019\)144](https://doi.org/10.1007/JHEP06(2019)144). arXiv:1902.08103 [hep-ex]
20. ATLAS Collaboration, Search for pair production of third-generation scalar leptoquarks decaying into a top quark and a τ -lepton in pp collisions at $\sqrt{s} = 13$ TeV with the ATLAS detector. *JHEP* **06**, 179 (2021). [https://doi.org/10.1007/JHEP06\(2021\)179](https://doi.org/10.1007/JHEP06(2021)179). arXiv:2101.11582 [hep-ex]
21. ATLAS Collaboration, Search for a scalar partner of the top quark in the all-hadronic $t\bar{t}$ plus missing transverse momentum final state at $\sqrt{s} = 13$ TeV with the ATLAS detector. *Eur. Phys. J. C* **80**, 737 (2020). <https://doi.org/10.1140/epjc/s10052-020-8102-8>. arXiv:2004.14060 [hep-ex]
22. ATLAS Collaboration, Search for new phenomena in final states with b-jets and missing transverse momentum in $\sqrt{s} = 13$ TeV pp collisions with the ATLAS detector. *JHEP* **05**, 093 (2021). [https://doi.org/10.1007/JHEP05\(2021\)093](https://doi.org/10.1007/JHEP05(2021)093). arXiv:2101.12527 [hep-ex]
23. C.M.S. Collaboration, Search for singly and pair-produced leptoquarks coupling to third-generation fermions in proton-proton collisions at $\sqrt{s} = 13$ TeV. *Phys. Lett. B* **819**, 136446 (2020). <https://doi.org/10.1016/j.physletb.2021.136446>. arXiv:2012.04178 [hep-ex]
24. C.M.S. Collaboration, Search for pair production of first-generation scalar leptoquarks at $\sqrt{s} = 13$ TeV. *Phys. Rev. D* **99**, 052002 (2019). <https://doi.org/10.1103/PhysRevD.99.052002>. arXiv:1811.01197 [hep-ex]
25. CMS Collaboration, Search for heavy neutrinos and third-generation leptoquarks in hadronic states of two τ leptons and two jets in proton-proton collisions at $\sqrt{s} = 13$ TeV. *JHEP* **03**, 170 (2019). [https://doi.org/10.1007/JHEP03\(2019\)170](https://doi.org/10.1007/JHEP03(2019)170). arXiv:1811.00806 [hep-ex]
26. C.M.S. Collaboration, Search for pair production of second-generation leptoquarks at $\sqrt{s} = 13$ TeV. *Phys. Rev. D* **99**, 032014 (2019). <https://doi.org/10.1103/PhysRevD.99.032014>. arXiv:1808.05082 [hep-ex]
27. ATLAS Collaboration, Search for new phenomena in pp collisions in final states with tau leptons, b-jets, and missing transverse momentum with the ATLAS detector. *Phys. Rev. D* **104**, 112005 (2021). <https://doi.org/10.1103/PhysRevD.104.112005>. arXiv:2108.07665 [hep-ex]
28. B. Diaz, M. Schmaltz, Y.-M. Zhong, The leptoquark hunter's guide: pair production. *JHEP* **10**, 097 (2017). [https://doi.org/10.1007/JHEP10\(2017\)097](https://doi.org/10.1007/JHEP10(2017)097). arXiv:1706.05033 [hep-ph]
29. ATLAS Collaboration, The ATLAS Experiment at the CERN Large Hadron Collider. *JINST* **3**, S08003 (2008). <https://doi.org/10.1088/1748-0221/3/08/S08003>
30. ATLAS Collaboration, ATLAS Insertable B-Layer: Technical Design Report, ATLAS-TDR-19; CERN-LHCC-2010-013 (2010). <https://cds.cern.ch/record/1291633>, Addendum: ATLAS-TDR-19-ADD-1; CERN-LHCC-2012-009 (2012). <https://cds.cern.ch/record/1451888>
31. B. Abbott et al., Production and integration of the ATLAS Insertable B-Layer. *JINST* **13**, T05008 (2018). <https://doi.org/10.1088/1748-0221/13/05/T05008>. arXiv:1803.00844 [physics.ins-det]
32. ATLAS Collaboration, Performance of the ATLAS trigger system. *Eur. Phys. J. C* **77**(2017), 317 (2015). <https://doi.org/10.1140/epjc/s10052-017-4852-3>. arXiv:1611.09661 [hep-ex]
33. ATLAS Collaboration, The ATLAS Collaboration Software and Firmware, ATL-SOFT-PUB-2021-001 (2021). <https://cds.cern.ch/record/2767187>
34. ATLAS Collaboration, Luminosity determination in pp collisions at $\sqrt{s} = 13$ TeV using the ATLAS detector at the LHC, ATLAS-CONF-2019-021 (2019). <https://cds.cern.ch/record/2677054>
35. G. Avoni et al., The new LUCID-2 detector for luminosity measurement and monitoring in ATLAS. *JINST* **13**, P07017 (2018). <https://doi.org/10.1088/1748-0221/13/07/P07017>
36. ATLAS Collaboration, The ATLAS simulation infrastructure. *Eur. Phys. J. C* **70**, 823 (2010). <https://doi.org/10.1140/epjc/s10052-010-1429-9>. arXiv:1005.4568 [physics.ins-det]
37. S. Agostinelli et al., GEANT4—a simulation toolkit. *Nucl. Instrum. Methods A* **506**, 250 (2003). [https://doi.org/10.1016/S0168-9002\(03\)01368-8](https://doi.org/10.1016/S0168-9002(03)01368-8)
38. ATLAS Collaboration, The simulation principle and performance of the ATLAS fast calorimeter simulation FastCaloSim, ATL-PHYS-PUB-2010-013 (2010). <https://cds.cern.ch/record/1300517>
39. T. Sjöstrand, S. Mrenna, P. Skands, A brief introduction to PYTHIA 8.1. *Comput. Phys. Commun.* **178**, 852 (2008). <https://doi.org/10.1016/j.cpc.2008.01.036>. arXiv:0710.3820 [hep-ph]
40. NNPDF Collaboration, R.D. Ball et al., Parton distributions with LHC data. *Nucl. Phys. B* **867**, 244 (2013). <https://doi.org/10.1016/j.nuclphysb.2012.10.003>. arXiv:1207.1303 [hep-ph]
41. ATLAS Collaboration, The Pythia 8 A3 tune description of ATLAS minimum bias and inelastic measurements incorporating the Donnachie–Landshoff diffractive model, ATL-PHYS-PUB-2016-017 (2016). <https://cds.cern.ch/record/2206965>
42. J. Alwall et al., The automated computation of tree-level and next-to-leading order differential cross sections, and their matching to parton shower simulations. *JHEP* **07**, 079 (2014). [https://doi.org/10.1007/JHEP07\(2014\)079](https://doi.org/10.1007/JHEP07(2014)079). arXiv:1405.0301 [hep-ph]
43. T. Mandal, S. Mitra, S. Seth, Pair Production of scalar leptoquarks at the LHC to NLO parton shower accuracy. *Phys. Rev. D* **93**, 035018 (2016). <https://doi.org/10.1103/PhysRevD.93.035018>. arXiv:1506.07369 [hep-ph]
44. M. Kramer, T. Plehn, M. Spira, P.M. Zerwas, Pair production of scalar leptoquarks at the CERN LHC. *Phys. Rev. D* **71**, 057503 (2005). <https://doi.org/10.1103/PhysRevD.71.057503>. arXiv:hep-ph/0411038
45. M. Kramer, T. Plehn, M. Spira, P.M. Zerwas, Pair production of scalar leptoquarks at the Fermilab Tevatron. *Phys. Rev. Lett.* **79**, 341 (1997). <https://doi.org/10.1103/PhysRevLett.79.341>. arXiv:hep-ph/9704322
46. T. Sjöstrand et al., An introduction to PYTHIA 8.2. *Comput. Phys. Commun.* **191** (2015) 159, <https://doi.org/10.1016/j.cpc.2015.01.024>. arXiv:1410.3012 [hep-ph]
47. The NNPDF Collaboration, R.D. Ball et al., Parton distributions for the LHC run II. *JHEP* **04**, 040 (2015). [https://doi.org/10.1007/JHEP04\(2015\)040](https://doi.org/10.1007/JHEP04(2015)040). arXiv:1410.8849 [hep-ph]
48. ATLAS Collaboration, ATLAS Pythia 8 tunes to 7 TeV data, ATL-PHYS-PUB-2014-021 (2014). <https://cds.cern.ch/record/1966419>

49. ATLAS Collaboration, Summary of ATLAS Pythia 8 tunes, ATL-PHYS-PUB-2012-003 (2012). <https://cds.cern.ch/record/1474107>
50. P. Artoisenet, R. Frederix, O. Mattelaer, R. Rietkerk, Automatic spin-entangled decays of heavy resonances in Monte Carlo simulations. *JHEP* **03**, 015 (2013). [https://doi.org/10.1007/JHEP03\(2013\)015](https://doi.org/10.1007/JHEP03(2013)015). arXiv:1212.3460 [hep-ph]
51. W. Beenakker, C. Borschensky, M. Krämer, A. Kulesza, E. Laenen, NNLL-fast: predictions for coloured supersymmetric particle production at the LHC with threshold and Coulomb resummation. *JHEP* **12**, 133 (2016). [https://doi.org/10.1007/JHEP12\(2016\)133](https://doi.org/10.1007/JHEP12(2016)133). arXiv:1607.07741 [hep-ph]
52. W. Beenakker, M. Kramer, T. Plehn, M. Spira, P.M. Zerwas, Stop production at hadron colliders. *Nucl. Phys. B* **515**, 3 (1998). [https://doi.org/10.1016/S0550-3213\(98\)00014-5](https://doi.org/10.1016/S0550-3213(98)00014-5). arXiv:hep-ph/9710451
53. W. Beenakker et al., Supersymmetric top and bottom squark production at hadron colliders. *JHEP* **08**, 098 (2010). [https://doi.org/10.1007/JHEP08\(2010\)098](https://doi.org/10.1007/JHEP08(2010)098). arXiv:1006.4771 [hep-ph]
54. W. Beenakker et al., NNLL resummation for stop pair-production at the LHC. *JHEP* **05**, 153 (2016). [https://doi.org/10.1007/JHEP05\(2016\)153](https://doi.org/10.1007/JHEP05(2016)153). arXiv:1601.02954 [hep-ph]
55. C. Borschensky, B. Fuks, A. Kulesza, D. Schwärtlander, Scalar leptoquark pair production at hadron colliders. *Phys. Rev. D* **101**, 115017 (2020). <https://doi.org/10.1103/PhysRevD.101.115017>. arXiv:2002.08971 [hep-ph]
56. J. Butterworth et al., PDF4LHC recommendations for LHC Run II. *J. Phys. G* **43**, 023001 (2016). <https://doi.org/10.1088/0954-3899/43/2/023001>. arXiv:1510.03865 [hep-ph]
57. M.L. Ciccolini, S. Dittmaier, M. Krämer, Electroweak radiative corrections to associated WH and ZH production at hadron colliders. *Phys. Rev. D* **68**, 073003 (2003). <https://doi.org/10.1103/PhysRevD.68.073003>. arXiv:hep-ph/0306234 [hep-ph]
58. O. Brein, A. Djouadi, R. Harlander, NNLO QCD corrections to the Higgs-strahlung processes at hadron colliders. *Phys. Lett. B* **579**, 149 (2004). <https://doi.org/10.1016/j.physletb.2003.10.112>. arXiv:hep-ph/0307206
59. G. Ferrera, M. Grazzini, F. Tramontano, Associated Higgs-W-boson production at hadron colliders: a fully exclusive QCD calculation at NNLO. *Phys. Rev. Lett.* **107**, 152003 (2011). <https://doi.org/10.1103/PhysRevLett.107.152003>. arXiv:1107.1164 [hep-ph]
60. O. Brein, R.V. Harlander, M. Wiesemann, T. Zirke, Top-quark mediated effects in hadronic Higgs-Strahlung. *Eur. Phys. J. C* **72**, 1868 (2012). <https://doi.org/10.1140/epjc/s10052-012-1868-6>. arXiv:1111.0761 [hep-ph]
61. G. Ferrera, M. Grazzini, F. Tramontano, Associated ZH production at hadron colliders: the fully differential NNLO QCD calculation. *Phys. Lett. B* **740**, 51 (2015). <https://doi.org/10.1016/j.physletb.2014.11.040>. arXiv:1407.4747 [hep-ph]
62. J.M. Campbell, R.K. Ellis, C. Williams, Associated production of a Higgs boson at NNLO. *JHEP* **06**, 179 (2016). [https://doi.org/10.1007/JHEP06\(2016\)179](https://doi.org/10.1007/JHEP06(2016)179). arXiv:1601.00658 [hep-ph]
63. S. Alioli, P. Nason, C. Oleari, E. Re, A general framework for implementing NLO calculations in shower Monte Carlo programs: the POWHEG BOX. *JHEP* **06**, 043 (2010). [https://doi.org/10.1007/JHEP06\(2010\)043](https://doi.org/10.1007/JHEP06(2010)043). arXiv:1002.2581 [hep-ph]
64. M. Czakon, A. Mitov, Top++: a program for the calculation of the top-pair cross-section at hadron colliders. *Comput. Phys. Commun.* **185**, 2930 (2014). <https://doi.org/10.1016/j.cpc.2014.06.021>. arXiv:1112.5675 [hep-ph]
65. N. Kidonakis, Next-to-next-to-leading logarithm resummation for s-channel single top quark production. *Phys. Rev. D* **81**, 054028 (2010). <https://doi.org/10.1103/PhysRevD.81.054028>. arXiv:1001.5034 [hep-ph]
66. N. Kidonakis, Next-to-next-to-leading-order collinear and soft gluon corrections for t-channel single top quark production. *Phys. Rev. D* **83**, 091503 (2011). <https://doi.org/10.1103/PhysRevD.83.091503>. arXiv:1103.2792 [hep-ph]
67. N. Kidonakis, Two-loop soft anomalous dimensions for single top quark associated production with aW^- or H^- . *Phys. Rev. D* **82**, 054018 (2010). <https://doi.org/10.1103/PhysRevD.82.054018>. arXiv:1005.4451 [hep-ph]
68. E. Bothmann et al., Event Generation with Sherpa 2.2. *SciPost Phys.* **7**, 034, (2019). <https://doi.org/10.21468/SciPostPhys.7.3.034>. arXiv:1905.09127 [hep-ph]
69. T. Gleisberg, S. Höche, Comix, a new matrix element generator. *JHEP* **12**, 039 (2008). <https://doi.org/10.1088/1126-6708/2008/12/039>. arXiv:0808.3674 [hep-ph]
70. F. Cascioli, P. Maierhöfer, S. Pozzorini, Scattering amplitudes with open loops. *Phys. Rev. Lett.* **108**, 111601 (2012). <https://doi.org/10.1103/PhysRevLett.108.111601>. arXiv:1111.5206 [hep-ph]
71. S. Catani, L. Cieri, G. Ferrera, D. de Florian, M. Grazzini, Vector boson production at hadron colliders: a fully exclusive QCD calculation at next-to-next-to-leading order. *Phys. Rev. Lett.* **103**, 082001 (2009). <https://doi.org/10.1103/PhysRevLett.103.082001>. arXiv:0903.2120 [hep-ph]
72. ATLAS Collaboration, Measurement of the Z/y^* boson transverse momentum distribution in pp collisions at $\sqrt{s} = 7$ TeV with the ATLAS detector. *JHEP* **09**, 145 (2014). [https://doi.org/10.1007/JHEP09\(2014\)145](https://doi.org/10.1007/JHEP09(2014)145). arXiv:1406.3660 [hep-ex]
73. D. de Florian et al., Handbook of LHC Higgs cross sections: 4. Deciphering the nature of the Higgs Sector (2016). <https://doi.org/10.23731/CYRM-2017-002>. arXiv:1610.07922 [hep-ph]
74. C. Anastasiou et al., High precision determination of the gluon fusion Higgs boson cross-section at the LHC. *JHEP* **05**, 058 (2016). [https://doi.org/10.1007/JHEP05\(2016\)058](https://doi.org/10.1007/JHEP05(2016)058). arXiv:1602.00695 [hep-ph]
75. C. Anastasiou, C. Duhr, F. Dulat, F. Herzog, B. Mistlberger, Higgs Boson gluon-fusion production in QCD at three loops. *Phys. Rev. Lett.* **114**, 212001 (2015). <https://doi.org/10.1103/PhysRevLett.114.212001>. arXiv:1503.06056 [hep-ph]
76. F. Dulat, A. Lazopoulos, B. Mistlberger, iHixs 2—inclusive Higgs cross sections. *Comput. Phys. Commun.* **233**, 243 (2018). <https://doi.org/10.1016/j.cpc.2018.06.025>. arXiv:1802.00827 [hep-ph]
77. S. Actis, G. Passarino, C. Sturm, S. Uccirati, NLO electroweak corrections to Higgs boson production at hadron colliders. *Phys. Lett. B* **670**, 12 (2008). <https://doi.org/10.1016/j.physletb.2008.10.018>. arXiv:0809.1301 [hep-ph]
78. M. Ciccolini, A. Denner, S. Dittmaier, Strong and electroweak corrections to the production of a Higgs boson + 2 Jets via weak interactions at the large hadron collider. *Phys. Rev. Lett.* **99**, 161803 (2007). <https://doi.org/10.1103/PhysRevLett.99.161803>. arXiv:0707.0381 [hep-ph]
79. M. Ciccolini, A. Denner, S. Dittmaier, Electroweak and QCD corrections to Higgs production via vector-boson fusion at the CERN LHC. *Phys. Rev. D* **77**, 013002 (2008). <https://doi.org/10.1103/PhysRevD.77.013002>. arXiv:0710.4749 [hep-ph]
80. P. Bolzoni, F. Maltoni, S.-O. Moch, M. Zaro, Higgs Boson production via vector-boson fusion at next-to-next-to-leading order in QCD. *Phys. Rev. Lett.* **105**, 011801 (2010). <https://doi.org/10.1103/PhysRevLett.105.011801>. arXiv:1003.4451 [hep-ph]
81. G. Ferrera, M. Grazzini, F. Tramontano, Higher-order QCD effects for associated WH production and decay at the LHC. *JHEP* **04**, 039 (2014). [https://doi.org/10.1007/JHEP04\(2014\)039](https://doi.org/10.1007/JHEP04(2014)039). arXiv:1312.1669 [hep-ph]
82. L. Altenkamp, S. Dittmaier, R.V. Harlander, H. Rzehak, T.J.E. Zirke, Gluon-induced Higgs-strahlung at next-to-leading order QCD. *JHEP* **02**, 078 (2013). [https://doi.org/10.1007/JHEP02\(2013\)078](https://doi.org/10.1007/JHEP02(2013)078). arXiv:1211.5015 [hep-ph]

83. B. Hespel, F. Maltoni, E. Vryonidou, Higgs and Z boson associated production via gluon fusion in the SM and the 2HDM. *JHEP* **06**, 065 (2015). [https://doi.org/10.1007/JHEP06\(2015\)065](https://doi.org/10.1007/JHEP06(2015)065). [arXiv:1503.01656](https://arxiv.org/abs/1503.01656) [hep-ph]
84. R.V. Harlander, A. Kulesza, V. Theeuwes, T. Zirke, Soft gluon resummation for gluon-induced Higgs Strahlung. *JHEP* **11**, 082 (2014). [https://doi.org/10.1007/JHEP11\(2014\)082](https://doi.org/10.1007/JHEP11(2014)082). [arXiv:1410.0217](https://arxiv.org/abs/1410.0217) [hep-ph]
85. R.V. Harlander, S. Liebler, T. Zirke, Higgs Strahlung at the Large Hadron Collider in the 2-Higgs-doublet model. *JHEP* **02**, 023 (2014). [https://doi.org/10.1007/JHEP02\(2014\)023](https://doi.org/10.1007/JHEP02(2014)023). [arXiv:1307.8122](https://arxiv.org/abs/1307.8122) [hep-ph]
86. O. Brein, R.V. Harlander, T.J.E. Zirke, vh@mnlo—Higgs Strahlung at hadron colliders. *Comput. Phys. Commun.* **184**, 998 (2013). <https://doi.org/10.1016/j.cpc.2012.11.002>. [arXiv:1210.5347](https://arxiv.org/abs/1210.5347) [hep-ph]
87. D.J. Lange, The EvtGen particle decay simulation package. *Nucl. Instrum. Methods A* **462**, 152 (2001). [https://doi.org/10.1016/S0168-9002\(01\)00089-4](https://doi.org/10.1016/S0168-9002(01)00089-4)
88. ATLAS Collaboration, Electron and photon performance measurements with the ATLAS detector using the 2015–2017 LHC proton-proton collision data. *JINST* **14**, P12006 (2019). <https://doi.org/10.1088/1748-0221/14/12/P12006>. [arXiv:1908.00005](https://arxiv.org/abs/1908.00005) [hep-ex]
89. ATLAS Collaboration, Muon reconstruction and identification efficiency in ATLAS using the full Run 2 pp collision data set at $\sqrt{s} = 13$ TeV. *Eur. Phys. J. C* **81**, 578 (2021). <https://doi.org/10.1140/epjc/s10052-021-09233-2>. [arXiv:2012.00578](https://arxiv.org/abs/2012.00578) [hep-ex]
90. ATLAS Collaboration, Muon reconstruction performance of the ATLAS detector in proton-proton collision data at $\sqrt{s} = 13$ TeV. *Eur. Phys. J. C* **76**, 292 (2016). <https://doi.org/10.1140/epjc/s10052-016-4120-y>. [arXiv:1603.05598](https://arxiv.org/abs/1603.05598) [hep-ex]
91. ATLAS Collaboration, Jet reconstruction and performance using particle flow with the ATLAS Detector. *Eur. Phys. J. C* **77**, 466 (2017). <https://doi.org/10.1140/epjc/s10052-017-5031-2>. [arXiv:1703.10485](https://arxiv.org/abs/1703.10485) [hep-ex]
92. M. Cacciari, G.P. Salam, G. Soyez, The $anti-k_t$ jet clustering algorithm. *JHEP* **04**, 063 (2008). <https://doi.org/10.1088/1126-6708/2008/04/063>. [arXiv:0802.1189](https://arxiv.org/abs/0802.1189) [hep-ph]
93. M. Cacciari, G.P. Salam, G. Soyez, FastJet user manual. *Eur. Phys. J. C* **72**, 1896 (2012). <https://doi.org/10.1140/epjc/s10052-012-1896-2>. [arXiv:1111.6097](https://arxiv.org/abs/1111.6097) [hep-ph]
94. ATLAS Collaboration, Performance of pile-up mitigation techniques for jets in pp collisions at $\sqrt{s} = 8$ TeV using the ATLAS detector. *Eur. Phys. J. C* **76**, 581 (2016). <https://doi.org/10.1140/epjc/s10052-016-4395-z>. [arXiv:1510.03823](https://arxiv.org/abs/1510.03823) [hep-ex]
95. ATLAS Collaboration, ATLAS b-jet identification performance and efficiency measurement with $t\bar{t}$ events in pp collisions $\sqrt{s} = 13$ TeV. *Eur. Phys. J. C* **79**, 970 (2019). <https://doi.org/10.1140/epjc/s10052-019-7450-8>. [arXiv:1907.05120](https://arxiv.org/abs/1907.05120) [hep-ex]
96. ATLAS Collaboration, Optimisation and performance studies of the ATLAS b-tagging algorithms for the 2017–18 LHC run, ATL-PHYS-PUB-2017-013 (2017). <https://cds.cern.ch/record/2273281>
97. ATLAS flavour-tagging algorithms for the LHC Run 2 pp collision dataset (2022). [arXiv:2211.16345](https://arxiv.org/abs/2211.16345) [physics.data-an]. <https://cds.cern.ch/record/2842028>
98. ATLAS Collaboration, Calibration of light-flavour b-jet mistagging rates using ATLAS proton-proton collision data at $\sqrt{s} = 13$ TeV, ATLAS-CONF-2018-006 (2018). <https://cds.cern.ch/record/2314418>
99. ATLAS Collaboration, Measurement of the c-jet mistagging efficiency in $t\bar{t}$ events using pp collision data at $\sqrt{s} = 13$ TeV collected with the ATLAS detector. *Eur. Phys. J. C* **82**, 95 (2022). <https://doi.org/10.1140/epjc/s10052-021-09843-w>. [arXiv:2109.10627](https://arxiv.org/abs/2109.10627) [hep-ex]
100. ATLAS Collaboration, Identification and energy calibration of hadronically decaying tau leptons with the ATLAS experiment in pp collisions at $\sqrt{s} = 8$ TeV. *Eur. Phys. J. C* **75**, 303 (2015). <https://doi.org/10.1140/epjc/s10052-015-3500-z>. [arXiv:1412.7086](https://arxiv.org/abs/1412.7086) [hep-ex]
101. ATLAS Collaboration, Identification of hadronic tau lepton decays using neural networks in the ATLAS experiment, ATL-PHYS-PUB-2019-033 (2019). <https://cds.cern.ch/record/2688062>
102. ATLAS Collaboration, Measurement of the tau lepton reconstruction and identification performance in the ATLAS experiment using pp collisions at $\sqrt{s} = 13$ TeV, ATLAS-CONF-2017-029 (2017). <https://cds.cern.ch/record/2261772>
103. ATLAS Collaboration, Performance of missing transverse momentum reconstruction with the ATLAS detector using proton-proton collisions at $\sqrt{s} = 13$ TeV. *Eur. Phys. J. C* **78**, 903 (2018). <https://doi.org/10.1140/epjc/s10052-018-6288-9>. [arXiv:1802.08168](https://arxiv.org/abs/1802.08168) [hep-ex]
104. ATLAS Collaboration, E_T^{miss} performance in the ATLAS detector using 2015–2016 LHC pp collisions, ATLAS-CONF-2018-023 (2018). <https://cds.cern.ch/record/2625233>
105. ATLAS Collaboration, Performance of electron and photon triggers in ATLAS during LHC Run 2. *Eur. Phys. J. C* **80**, 47 (2020). <https://doi.org/10.1140/epjc/s10052-019-7500-2>. [arXiv:1909.00761](https://arxiv.org/abs/1909.00761) [hep-ex]
106. ATLAS Collaboration, Performance of the ATLAS muon triggers in Run 2. *JINST* **15**, P09015 (2020). <https://doi.org/10.1088/1748-0221/15/09/p09015>. [arXiv:2004.13447](https://arxiv.org/abs/2004.13447) [hep-ex]
107. ATLAS Collaboration, The ATLAS Tau Trigger in Run 2, ATLAS-CONF-2017-061 (2017). <https://cds.cern.ch/record/2274201>
108. A. Elagin, P. Murat, A. Pranko, A. Safonov, A new mass reconstruction technique for resonances decaying to $\tau\tau$. *Nucl. Instrum. Methods A* **654**, 481 (2011). <https://doi.org/10.1016/j.nima.2011.07.009>. [arXiv:1012.4686](https://arxiv.org/abs/1012.4686) [hep-ex]
109. P. Baldi, K. Cranmer, T. Fauchet, P. Sadowski, D. Whiteson, Parameterized neural networks for high-energy physics. *Eur. Phys. J. C* **76**, 235 (2016). <https://doi.org/10.1140/epjc/s10052-016-4099-4>. [arXiv:1601.07913](https://arxiv.org/abs/1601.07913) [hep-ex]
110. F. Chollet et al., Keras (2015). <https://keras.io>
111. M Abadi et al., TensorFlow: Large-Scale Machine Learning on Heterogeneous Systems, Software available from tensorflow.org (2015). <https://www.tensorflow.org>
112. ATLAS Collaboration, A search for resonant and non-resonant Higgs boson pair production in the $b\bar{b}\tau^+\tau^-$ decay channel in pp collisions at $\sqrt{s} = 13$ TeV with the ATLAS detector. *Phys. Rev. Lett.* **121**, 191801 (2018). <https://doi.org/10.1103/PhysRevLett.121.191801>. [arXiv:1808.00336](https://arxiv.org/abs/1808.00336) [hep-ex]. [Erratum: *Phys. Rev. Lett.* **122**, 089901 (2019)]
113. ATLAS Collaboration, Measurement of the $t\bar{t}$ production cross-section and lepton differential distributions in $e\mu$ dilepton events from pp collisions at $\sqrt{s} = 13$ TeV with the ATLAS detector. *Eur. Phys. J. C* **80**, 528 (2020). <https://doi.org/10.1140/epjc/s10052-020-7907-9>. [arXiv:1910.08819](https://arxiv.org/abs/1910.08819) [hep-ex]
114. ATLAS Collaboration, Measurements of top-quark pair single- and double-differential cross-sections in the all-hadronic channel in pp collisions at $\sqrt{s} = 13$ TeV using the ATLAS detector. *JHEP* **01**, 033 (2021). [https://doi.org/10.1007/JHEP01\(2021\)033](https://doi.org/10.1007/JHEP01(2021)033). [arXiv:2006.09274](https://arxiv.org/abs/2006.09274) [hep-ex]
115. ATLAS Collaboration, Measurements of top-quark pair differential and double-differential cross-sections in the $\ell + jets$ channel with pp collisions at $\sqrt{s} = 13$ TeV using the ATLAS detector. *Eur. Phys. J. C* **79**, 1028 (2019). <https://doi.org/10.1140/epjc/s10052-019-7525-6>. [arXiv:1908.07305](https://arxiv.org/abs/1908.07305) [hep-ex]. [Erratum: *Eur. Phys. J. C* **80**, 1092 (2020)]

120. A.L. Read, Presentation of search results: the CL_s technique. *J. Phys. G* **28**, 2693 (2002). <https://doi.org/10.1088/0954-3899/28/10/313>
121. G. Cowan, K. Cranmer, E. Gross, O. Vitells, Asymptotic formulae for likelihood-based tests of new physics. *Eur. Phys. J. C* **71**, 1554 (2011). <https://doi.org/10.1140/epjc/s10052-011-1554-0>. arXiv:1007.1727 [physics.data-an]. [Erratum: *Eur. Phys. J. C* **73**, 2501 (2013)]
122. ATLAS Collaboration, ATLAS Computing Acknowledgements, ATL-SOFT-PUB-2021-003 (2021). <https://cds.cern.ch/record/2776662>

ATLAS Collaboration*

- G. Aad¹⁰², B. Abbott¹²⁰, K. Abeling⁵⁵, S. H. Abidi²⁹, A. Aboulhorma^{35c}, H. Abramowicz¹⁵¹, H. Abreu¹⁵⁰, Y. Abulaiti¹¹⁷, A. C. Abusleme Hoffman^{137a}, B. S. Acharya^{69a,69b,p}, C. Adam Bourdarios⁴, L. Adamczyk^{85a}, L. Adamek¹⁵⁵, S. V. Addepalli²⁶, J. Adelman¹¹⁵, A. Adiguzel^{21c}, S. Adorni⁵⁶, T. Adye¹³⁴, A. A. Affolder¹³⁶, Y. Afik³⁶, M. N. Agaras¹³, J. Agarwala^{73a,73b}, A. Aggarwal¹⁰⁰, C. Agheorghiesei^{27c}, J. A. Aguilar-Saavedra^{130f}, A. Ahmad³⁶, F. Ahmadov^{38,ab}, W. S. Ahmed¹⁰⁴, S. Ahuja⁹⁵, X. Ai⁴⁸, G. Aielli^{76a,76b}, M. Ait Tamlihat^{35e}, B. Aitbenchikh^{35a}, I. Aizenberg¹⁶⁹, M. Akbiyik¹⁰⁰, T. P. A. Åkesson⁹⁸, A. V. Akimov³⁷, K. Al Khoury⁴¹, G. L. Alberghi^{23b}, J. Albert¹⁶⁵, P. Albicocco⁵³, S. Alderweireldt⁵², M. Aleksa³⁶, I. N. Aleksandrov³⁸, C. Alexa^{27b}, T. Alexopoulos¹⁰, A. Alfonsi¹¹⁴, F. Alfonsi^{23b}, M. Alhroob¹²⁰, B. Ali¹³², S. Ali¹⁴⁸, M. Aliev³⁷, G. Alimonti^{71a}, W. Alkakhi⁵⁵, C. Allaire⁶⁶, B. M. M. Allbrooke¹⁴⁶, C. A. Allendes Flores^{137f}, P. P. Allport²⁰, A. Aloisio^{72a,72b}, F. Alonso⁹⁰, C. Alpigiani¹³⁸, M. Alvarez Estevez⁹⁹, A. Alvarez Fernandez¹⁰⁰, M. G. Alvaggi^{72a,72b}, M. Aly¹⁰¹, Y. Amaral Coutinho^{82b}, A. Ambler¹⁰⁴, C. Amelung³⁶, M. Amerl¹⁰¹, C. G. Ames¹⁰⁹, D. Amidei¹⁰⁶, S. P. Amor Dos Santos^{130a}, K. R. Amos¹⁶³, V. Ananiev¹²⁵, C. Anastopoulos¹³⁹, T. Andeen¹¹, J. K. Anders³⁶, S. Y. Andrean^{47a,47b}, A. Andreazza^{71a,71b}, S. Angelidakis⁹, A. Angerami^{41,ae}, A. V. Anisenkov³⁷, A. Annovi^{74a}, C. Antel⁵⁶, M. T. Anthony¹³⁹, E. Antipov¹⁴⁵, M. Antonelli⁵³, D. J. A. Antrim^{17a}, F. Anulli^{75a}, M. Aoki⁸³, T. Aoki¹⁵³, J. A. Aparisi Pozo¹⁶³, M. A. Aparo¹⁴⁶, L. Aperio Bella⁴⁸, C. Appelt¹⁸, N. Aranzabal³⁶, V. Araujo Ferraz^{82a}, C. Arcangeletti⁵³, A. T. H. Arce⁵¹, E. Arena⁹², J.-F. Arguin¹⁰⁸, S. Argyropoulos⁵⁴, J.-H. Arling⁴⁸, A. J. Armbruster³⁶, O. Arnaez⁴, H. Arnold¹¹⁴, Z. P. Arrubarrena Tame¹⁰⁹, G. Artoni^{75a,75b}, H. Asada¹¹¹, K. Asai¹¹⁸, S. Asai¹⁵³, N. A. Asbah⁶¹, J. Assahsah^{35d}, K. Assamagan²⁹, R. Astalos^{28a}, R. J. Atkin^{33a}, M. Atkinson¹⁶², N. B. Atlay¹⁸, H. Atmani^{62b}, P. A. Atmasiddha¹⁰⁶, K. Augsten¹³², S. Auricchio^{72a,72b}, A. D. Auriol²⁰, V. A. Astrup¹⁷¹, G. Avner¹⁵⁰, G. Avolio³⁶, K. Axiotis⁵⁶, G. Azuelos^{108,ai}, D. Babai^{28a}, H. Bachacou¹³⁵, K. Bachas^{152,s}, A. Bachiu³⁴, F. Backman^{47a,47b}, A. Badea⁶¹, P. Bagnaia^{75a,75b}, M. Bahmani¹⁸, A. J. Bailey¹⁶³, V. R. Bailey¹⁶², J. T. Baines¹³⁴, C. Bakalis¹⁰, O. K. Baker¹⁷², E. Bakos¹⁵, D. Bakshi Gupta⁸, R. Balasubramanian¹¹⁴, E. M. Baldin³⁷, P. Balek¹³³, E. Ballabene^{71a,71b}, F. Balli¹³⁵, L. M. Baltes^{63a}, W. K. Balunas³², J. Balz¹⁰⁰, E. Banas⁸⁶, M. Bandieramonte¹²⁹, A. Bandyopadhyay²⁴, S. Bansal²⁴, L. Barak¹⁵¹, E. L. Barberio¹⁰⁵, D. Barberis^{57a,57b}, M. Barbero¹⁰², G. Barbour⁹⁶, K. N. Barends^{33a}, T. Barillari¹¹⁰, M.-S. Barisits³⁶, T. Barklow¹⁴³, P. Baron¹²², D. A. Baron Moreno¹⁰¹, A. Baroncelli^{62a}, G. Barone²⁹, A. J. Barr¹²⁶, L. Barranco Navarro^{47a,47b}, F. Barreiro⁹⁹, J. Barreiro Guimarães da Costa^{14a}, U. Barron¹⁵¹, M. G. Barros Teixeira^{130a}, S. Barsov³⁷, F. Bartels^{63a}, R. Bartoldus¹⁴³, A. E. Barton⁹¹, P. Bartos^{28a}, A. Basan¹⁰⁰, M. Baselga⁴⁹, I. Bashta^{77a,77b}, A. Bassalat^{66,b}, M. J. Basso¹⁵⁵, C. R. Basson¹⁰¹, R. L. Bates⁵⁹, S. Batlamous^{35e}, J. R. Batley³², B. Batool¹⁴¹, M. Battaglia¹³⁶, D. Battulga¹⁸, M. Bauce^{75a,75b}, P. Bauer²⁴, J. B. Beacham⁵¹, T. Beau¹²⁷, P. H. Beauchemin¹⁵⁸, F. Becherer⁵⁴, P. Bechtle²⁴, H. P. Beck^{19,r}, K. Becker¹⁶⁷, A. J. Beddall^{21d}, V. A. Bednyakov³⁸, C. P. Bee¹⁴⁵, L. J. Beemster¹⁵, T. A. Beermann³⁶, M. Begalli^{82d}, M. Begel²⁹, A. Behera¹⁴⁵, J. K. Behr⁴⁸, C. Beirao Da Cruz E Silva³⁶, J. F. Beirer^{36,55}, F. Beisiegel²⁴, M. Belfkir¹⁵⁹, G. Bella¹⁵¹, L. Bellagamba^{23b}, A. Bellerive³⁴, P. Bellos²⁰, K. Beloborodov³⁷, N. L. Belyaev³⁷, D. Benchekroun^{35a}, F. Bendebba^{35a}, Y. Benhammou¹⁵¹, M. Benoit²⁹, J. R. Bensinger²⁶, S. Bentvelsen¹¹⁴, L. Beresford³⁶, M. Beretta⁵³, E. Bergeaas Kuutmann¹⁶¹, N. Berger⁴, B. Bergmann¹³², J. Beringer^{17a}, S. Berlendis⁷, G. Bernardi⁵, C. Bernius¹⁴³, F. U. Bernlochner²⁴, T. Berry⁹⁵, P. Berta¹³³, A. Berthold⁵⁰, I. A. Bertram⁹¹, S. Bethke¹¹⁰, A. Betti^{75a,75b}, A. J. Bevan⁹⁴, M. Bhamjee^{33c}, S. Bhatta¹⁴⁵, D. S. Bhattacharya¹⁶⁶, P. Bhattacharai²⁶, V. S. Bhopatkar¹²¹, R. Bi^{29,al}, R. M. Bianchi¹²⁹, O. Biebel¹⁰⁹, R. Bielski¹²³, M. Biglietti^{77a}, T. R. V. Billoud¹³², M. Bindi⁵⁵,

- A. Bingul^{21b}, C. Bini^{75a,75b}, A. Biondini⁹², C. J. Birch-sykes¹⁰¹, G. A. Bird^{20,134}, M. Birman¹⁶⁹, M. Biros¹³³, T. Bisanz³⁶, E. Bisceglie^{43a,43b}, D. Biswas¹⁷⁰, A. Bitadze¹⁰¹, K. Bjørke¹²⁵, I. Bloch⁴⁸, C. Blocker²⁶, A. Blue⁵⁹, U. Blumenschein⁹⁴, J. Blumenthal¹⁰⁰, G. J. Bobbink¹¹⁴, V. S. Bobrovnikov³⁷, M. Boehler⁵⁴, D. Bogavac³⁶, A. G. Bogdanchikov³⁷, C. Bohm^{47a}, V. Boisvert⁹⁵, P. Bokan⁴⁸, T. Bold^{85a}, M. Bomben⁵, M. Bona⁹⁴, M. Boonekamp¹³⁵, C. D. Booth⁹⁵, A. G. Borbély⁵⁹, H. M. Borecka-Bielska¹⁰⁸, L. S. Borgna⁹⁶, G. Borissov⁹¹, D. Bortoletto¹²⁶, D. Boscherini^{23b}, M. Bosman¹³, J. D. Bossio Sola³⁶, K. Bouaouda^{35a}, N. Bouchhar¹⁶³, J. Boudreau¹²⁹, E. V. Bouhouva-Thacker⁹¹, D. Boumediene⁴⁰, R. Bouquet⁵, A. Boveia¹¹⁹, J. Boyd³⁶, D. Boye²⁹, I. R. Boyko³⁸, J. Bracinik²⁰, N. Brahimi^{62d}, G. Brandt¹⁷¹, O. Brandt³², F. Braren⁴⁸, B. Brau¹⁰³, J. E. Brau¹²³, K. Brendlinger⁴⁸, R. Brener¹⁶⁹, L. Brenner¹¹⁴, R. Brenner¹⁶¹, S. Bressler¹⁶⁹, D. Britton⁵⁹, D. Britzger¹¹⁰, I. Brock²⁴, G. Brooijmans⁴¹, W. K. Brooks^{137f}, E. Brost²⁹, L. M. Brown¹⁶⁵, T. L. Bruckler¹²⁶, P. A. Bruckman de Renstrom⁸⁶, B. Brüers⁴⁸, D. Bruncko^{28b,*}, A. Bruni^{23b}, G. Bruni^{23b}, M. Bruschi^{23b}, N. Bruscino^{75a,75b}, T. Buanes¹⁶, Q. Buat¹³⁸, A. G. Buckley⁵⁹, I. A. Budagov^{38,*}, M. K. Bugge¹²⁵, O. Bulekov³⁷, B. A. Bullard¹⁴³, S. Burdin⁹², C. D. Burgard⁴⁹, A. M. Burger⁴⁰, B. Burghgrave⁸, J. T. P. Burr³², C. D. Burton¹¹, J. C. Burzynski¹⁴², E. L. Busch⁴¹, V. Büscher¹⁰⁰, P. J. Bussey⁵⁹, J. M. Butler²⁵, C. M. Buttar⁵⁹, J. M. Butterworth⁹⁶, W. Buttlinger¹³⁴, C. J. Buxo Vazquez¹⁰⁷, A. R. Buzykaev³⁷, G. Cabras^{23b}, S. Cabrera Urbán¹⁶³, D. Caforio⁵⁸, H. Cai¹²⁹, Y. Cai^{14a,14d}, V. M. M. Cairo³⁶, O. Cakir^{3a}, N. Calace³⁶, P. Calafiura^{17a}, G. Calderini¹²⁷, P. Calfayan⁶⁸, G. Callea⁵⁹, L. P. Caloba^{82b}, D. Calvet⁴⁰, S. Calvet⁴⁰, T. P. Calvet¹⁰², M. Calvetti^{74a,74b}, R. Camacho Toro¹²⁷, S. Camarda³⁶, D. Camarero Munoz²⁶, P. Camarri^{76a,76b}, M. T. Camerlingo^{72a,72b}, D. Cameron¹²⁵, C. Camincher¹⁶⁵, M. Campanelli⁹⁶, A. Camplani⁴², V. Canale^{72a,72b}, A. Canesse¹⁰⁴, M. Cano Bret⁸⁰, J. Cantero¹⁶³, Y. Cao¹⁶², F. Capocasa²⁶, M. Capua^{43a,43b}, A. Carbone^{71a,71b}, R. Cardarelli^{76a}, J. C. J. Cardenas⁸, F. Cardillo¹⁶³, T. Carli³⁶, G. Carlino^{72a}, J. I. Carlotto¹³, B. T. Carlson^{129,t}, E. M. Carlson^{156a,165}, L. Carminati^{71a,71b}, M. Carnesale^{75a,75b}, S. Caron¹¹³, E. Carquin^{137f}, S. Carrá^{71a,71b}, G. Carratta^{23a,23b}, F. Carrio Argos^{33g}, J. W. S. Carter¹⁵⁵, T. M. Carter⁵², M. P. Casado^{13,j}, A. F. Casha¹⁵⁵, M. Caspar⁴⁸, E. G. Castiglia¹⁷², F. L. Castillo^{63a}, L. Castillo Garcia¹³, V. Castillo Gimenez¹⁶³, N. F. Castro^{130a,130e}, A. Catinaccio³⁶, J. R. Catmore¹²⁵, V. Cavalieri²⁹, N. Cavalli^{23a,23b}, V. Cavasinni^{74a,74b}, E. Celebi^{21a}, F. Celli¹²⁶, M. S. Centonze^{70a,70b}, K. Cerny¹²², A. S. Cerqueira^{82a}, A. Cerri¹⁴⁶, L. Cerrito^{76a,76b}, F. Cerutti^{17a}, A. Cervelli^{23b}, G. Cesarin⁵³, S. A. Cetin^{21d}, Z. Chadi^{35a}, D. Chakraborty¹¹⁵, M. Chala^{130f}, J. Chan¹⁷⁰, W. Y. Chan¹⁵³, J. D. Chapman³², B. Chargeishvili^{149b}, D. G. Charlton²⁰, T. P. Charman⁹⁴, M. Chatterjee¹⁹, S. Chekanov⁶, S. V. Chekulaev^{156a}, G. A. Chelkov^{38,a}, A. Chen¹⁰⁶, B. Chen¹⁵¹, B. Chen¹⁶⁵, H. Chen^{14c}, H. Chen²⁹, J. Chen^{62c}, J. Chen¹⁴², S. Chen¹⁵³, S. J. Chen^{14c}, X. Chen^{62c}, X. Chen^{14b,ah}, Y. Chen^{62a}, C. L. Cheng¹⁷⁰, H. C. Cheng^{64a}, S. Cheong¹⁴³, A. Cheplakov³⁸, E. Cheremushkina⁴⁸, E. Cherepanova¹¹⁴, R. Cherkaoui El Moursli^{35e}, E. Cheu⁷, K. Cheung⁶⁵, L. Chevalier¹³⁵, V. Chiarella⁵³, G. Chiarella^{74a}, N. Chiedde¹⁰², G. Chiodini^{70a}, A. S. Chisholm²⁰, A. Chitan^{27b}, M. Chitishvili¹⁶³, M. V. Chizhov³⁸, K. Choi¹¹, A. R. Chomont^{75a,75b}, Y. Chou¹⁰³, E. Y. S. Chow¹¹⁴, T. Chowdhury^{33g}, L. D. Christopher^{33g}, K. L. Chu^{64a}, M. C. Chu^{64a}, X. Chu^{14a,14d}, J. Chudoba¹³¹, J. J. Chwastowski⁸⁶, D. Cieri¹¹⁰, K. M. Ciesla^{85a}, V. Cindro⁹³, A. Ciocio^{17a}, F. Cirotto^{72a,72b}, Z. H. Citron^{169,m}, M. Citterio^{71a}, D. A. Ciubotaru^{27b}, B. M. Ciungu¹⁵⁵, A. Clark⁵⁶, P. J. Clark⁵², J. M. Clavijo Columbie⁴⁸, S. E. Clawson¹⁰¹, C. Clement^{47a,47b}, J. Clercx⁴⁸, L. Clissa^{23a,23b}, Y. Coadou¹⁰², M. Cobal^{69a,69c}, A. Coccaro^{57b}, R. F. Coelho Barrue^{130a}, R. Coelho Lopes De Sa¹⁰³, S. Coelli^{71a}, H. Cohen¹⁵¹, A. E. C. Coimbra^{71a,71b}, B. Cole⁴¹, J. Collot⁶⁰, P. Conde Muiño^{130a,130g}, M. P. Connell^{33c}, S. H. Connell^{33c}, I. A. Connelly⁵⁹, E. I. Conroy¹²⁶, F. Conventi^{72a,aj}, H. G. Cooke²⁰, A. M. Cooper-Sarkar¹²⁶, F. Cormier¹⁶⁴, L. D. Corpe³⁶, M. Corradi^{75a,75b}, F. Corriveau^{104,z}, A. Cortes-Gonzalez¹⁸, M. J. Costa¹⁶³, F. Costanza⁴, D. Costanzo¹³⁹, B. M. Cote¹¹⁹, G. Cowan⁹⁵, J. W. Cowley³², K. Cranmer¹¹⁷, S. Crépé-Renaudin⁶⁰, F. Crescioli¹²⁷, M. Cristinziani¹⁴¹, M. Cristoforetti^{78a,78b,d}, V. Croft¹¹⁴, G. Crosetti^{43a,43b}, A. Cueto³⁶, T. Cuhadar Donszelmann¹⁶⁰, H. Cui^{14a,14d}, Z. Cui⁷, W. R. Cunningham⁵⁹, F. Curcio^{43a,43b}, P. Czodrowski³⁶, M. M. Czurylo^{63b}, M. J. Da Cunha Sargedas De Sousa^{62a}, J. V. Da Fonseca Pinto^{82b}, C. Da Via¹⁰¹, W. Dabrowski^{85a}, T. Dado⁴⁹, S. Dahbi^{33g}, T. Dai¹⁰⁶, C. Dallapiccola¹⁰³, M. Dam⁴², G. D'amen²⁹, V. D'Amico¹⁰⁹, J. Damp¹⁰⁰, J. R. Dandoy¹²⁸, M. F. Daneri³⁰, M. Danninger¹⁴², V. Dao³⁶, G. Darbo^{57b}, S. Darmora⁶, S. J. Das^{29,al}, S. D'Auria^{71a,71b}, C. David^{156b}, T. Davidek¹³³, B. Davis-Purcell³⁴, I. Dawson⁹⁴, K. De⁸, R. De Asmundis^{72a}, N. De Biase⁴⁸, S. De Castro^{23a,23b}, N. De Groot¹¹³, P. de Jong¹¹⁴, H. De la Torre¹⁰⁷, A. De Maria^{14c}, A. De Salvo^{75a}, U. De Sanctis^{76a,76b}, A. De Santo¹⁴⁶, J. B. De Vivie De Regie⁶⁰, D. V. Dedovich³⁸, J. Degens¹¹⁴, A. M. Deiana⁴⁴, F. Del Corso^{23a,23b}, J. Del Peso⁹⁹

- F. Del Rio^{63a}, F. Deliot¹³⁵, C. M. Delitzsch⁴⁹, M. Della Pietra^{72a,72b}, D. Della Volpe⁵⁶, A. Dell'Acqua³⁶, L. Dell'Asta^{71a,71b}, M. Delmastro⁴, P. A. Delsart⁶⁰, S. Demers¹⁷², M. Demichev³⁸, S. P. Denisov³⁷, L. D'Eramo¹¹⁵, D. Derendarz⁸⁶, F. Derue¹²⁷, P. Dervan⁹², K. Desch²⁴, K. Dette¹⁵⁵, C. Deutsch²⁴, F. A. Di Bello^{57a,57b}, A. Di Ciaccio^{76a,76b}, L. Di Ciaccio⁴, A. Di Domenico^{75a,75b}, C. Di Donato^{72a,72b}, A. Di Girolamo³⁶, G. Di Gregorio⁵, A. Di Luca^{78a,78b}, B. Di Micco^{77a,77b}, R. Di Nardo^{77a,77b}, C. Diaconu¹⁰², F. A. Dias¹¹⁴, T. Dias Do Vale¹⁴², M. A. Diaz^{137a,137b}, F. G. Diaz Capriles²⁴, M. Didenko¹⁶³, E. B. Diehl¹⁰⁶, L. Diehl⁵⁴, S. Díez Cornell⁴⁸, C. Diez Pardos¹⁴¹, C. Dimitriadi^{24,161}, A. Dimitrieva^{17a}, J. Dingfelder²⁴, I.-M. Dinu^{27b}, S. J. Dittmeier^{63b}, F. Dittus³⁶, F. Djama¹⁰², T. Djobava^{149b}, J. I. Djupsland¹⁶, C. Doglioni^{98,101}, J. Dolejsi¹³³, Z. Dolezal¹³³, M. Donadelli^{82c}, B. Dong¹⁰⁷, J. Donini⁴⁰, A. D'Onofrio^{77a,77b}, M. D'Onofrio⁹², J. Dopke¹³⁴, A. Doria^{72a}, M. T. Dova⁹⁰, A. T. Doyle⁵⁹, M. A. Draguet¹²⁶, E. Drechsler¹⁴², E. Dreyer¹⁶⁹, I. Drivas-koulouris¹⁰, A. S. Drobac¹⁵⁸, M. Drozdova⁵⁶, D. Du^{62a}, T. A. du Pree¹¹⁴, F. Dubinin³⁷, M. Dubovsky^{28a}, E. Duchovni¹⁶⁹, G. Duckeck¹⁰⁹, O. A. Ducu^{27b}, D. Duda¹¹⁰, A. Dudarev³⁶, E. R. Duden²⁶, M. D'uffizi¹⁰¹, L. Duflot⁶⁶, M. Dührssen³⁶, C. Dülsen¹⁷¹, A. E. Dumitriu^{27b}, M. Dunford^{63a}, S. Dungs⁴⁹, K. Dunne^{47a,47b}, A. Duperrin¹⁰², H. Duran Yildiz^{3a}, M. Düren⁵⁸, A. Durglishvili^{149b}, B. L. Dwyer¹¹⁵, G. I. Dyckes^{17a}, M. Dyndal^{85a}, S. Dysch¹⁰¹, B. S. Dziedzic⁸⁶, Z. O. Earnshaw¹⁴⁶, B. Eckerova^{28a}, S. Eggebrecht⁵⁵, M. G. Eggleston⁵¹, E. Egidio Purcino De Souza¹²⁷, L. F. Ehrke⁵⁶, G. Eigen¹⁶, K. Einsweiler^{17a}, T. Ekelof¹⁶¹, P. A. Ekman⁹⁸, Y. El Ghazali^{35b}, H. El Jarrari^{35e,148}, A. El Moussaouy^{35a}, V. Ellajosyula¹⁶¹, M. Ellert¹⁶¹, F. Ellinghaus¹⁷¹, A. A. Elliot⁹⁴, N. Ellis³⁶, J. Elmsheuser²⁹, M. Elsing³⁶, D. Emeliyanov¹³⁴, Y. Enari¹⁵³, I. Ene^{17a}, S. Epari¹³, J. Erdmann⁴⁹, P. A. Erland⁸⁶, M. Errenst¹⁷¹, M. Escalier⁶⁶, C. Escobar¹⁶³, E. Etzion¹⁵¹, G. Evans^{130a}, H. Evans⁶⁸, M. O. Evans¹⁴⁶, A. Ezhilov³⁷, S. Ezzarqoutouni^{35a}, F. Fabbri⁵⁹, L. Fabbri^{23a,23b}, G. Facini⁹⁶, V. Fadeyev¹³⁶, R. M. Fakhrutdinov³⁷, S. Falciano^{75a}, L. F. Falda Ulhoa Coelho³⁶, P. J. Falke²⁴, S. Falke³⁶, J. Faltova¹³³, Y. Fan^{14a}, Y. Fang^{14a,14d}, M. Fanti^{71a,71b}, M. Faraj^{69a,69b}, Z. Farazpay⁹⁷, A. Farbin⁸, A. Farilla^{77a}, T. Farooque¹⁰⁷, S. M. Farrington⁵², F. Fassi^{35e}, D. Fassouliotis⁹, M. Faucci Giannelli^{76a,76b}, W. J. Fawcett³², L. Fayard⁶⁶, P. Federic¹³³, P. Federicova¹³¹, O. L. Fedin^{37,a}, G. Fedotov³⁷, M. Feickert¹⁷⁰, L. Feligioni¹⁰², A. Fell¹³⁹, D. E. Fellers¹²³, C. Feng^{62b}, M. Feng^{14b}, Z. Feng¹¹⁴, M. J. Fenton¹⁶⁰, A. B. Fenyuk³⁷, L. Ferencz⁴⁸, R. A. M. Ferguson⁹¹, S. I. Fernandez Luengo^{137f}, J. Ferrando⁴⁸, A. Ferrari¹⁶¹, P. Ferrari^{113,114}, R. Ferrari^{73a}, D. Ferrere⁵⁶, C. Ferretti¹⁰⁶, F. Fiedler¹⁰⁰, A. Filipčič⁹³, E. K. Filmer¹, F. Filthaut¹¹³, M. C. N. Fiolhais^{130a,130c,c}, L. Fiorini¹⁶³, F. Fischer¹⁴¹, W. C. Fisher¹⁰⁷, T. Fitschen¹⁰¹, I. Fleck¹⁴¹, P. Fleischmann¹⁰⁶, T. Flick¹⁷¹, L. Flores¹²⁸, M. Flores^{33d,af}, L. R. Flores Castillo^{64a}, F. M. Follega^{78a,78b}, N. Fomin¹⁶, J. H. Foo¹⁵⁵, B. C. Forland⁶⁸, A. Formica¹³⁵, A. C. Forti¹⁰¹, E. Fortin¹⁰², A. W. Fortman⁶¹, M. G. Foti^{17a}, L. Fountas^{9,k}, D. Fournier⁶⁶, H. Fox⁹¹, P. Francavilla^{74a,74b}, S. Francescato⁶¹, S. Franchellucci⁵⁶, M. Franchini^{23a,23b}, S. Franchino^{63a}, D. Francis³⁶, L. Franco¹¹³, L. Franconi¹⁹, M. Franklin⁶¹, G. Frattari²⁶, A. C. Freegard⁹⁴, W. S. Freund^{82b}, Y. Y. Frid¹⁵¹, N. Fritzsche⁵⁰, A. Froch⁵⁴, D. Froidevaux³⁶, J. A. Frost¹²⁶, Y. Fu^{62a}, M. Fujimoto¹¹⁸, E. Fullana Torregrosa^{163,*}, J. Fuster¹⁶³, A. Gabrielli^{23a,23b}, A. Gabrielli¹⁵⁵, P. Gadow⁴⁸, G. Gagliardi^{57a,57b}, L. G. Gagnon^{17a}, G. E. Gallardo¹²⁶, E. J. Gallas¹²⁶, B. J. Gallop¹³⁴, R. Gamboa Goni⁹⁴, K. K. Gan¹¹⁹, S. Ganguly¹⁵³, J. Gao^{62a}, Y. Gao⁵², F. M. Garay Walls^{137a,137b}, B. Garcia^{29,al}, C. García¹⁶³, J. E. García Navarro¹⁶³, M. Garcia-Siveres^{17a}, R. W. Gardner³⁹, D. Garg⁸⁰, R. B. Garg^{143,q}, C. A. Garner¹⁵⁵, S. J. Gasiorowski¹³⁸, P. Gaspar^{82b}, G. Gaudio^{73a}, V. Gautam¹³, P. Gauzzi^{75a,75b}, I. L. Gavrilenko³⁷, A. Gavriluk³⁷, C. Gay¹⁶⁴, G. Gaycken⁴⁸, E. N. Gazis¹⁰, A. A. Geanta^{27,27e}, C. M. Gee¹³⁶, C. Gemme^{57b}, M. H. Genest⁶⁰, S. Gentile^{75a,75b}, S. George⁹⁵, W. F. George²⁰, T. Geralis⁴⁶, L. O. Gerlach⁵⁵, P. Gessinger-Befurt³⁶, M. E. Geyik¹⁷¹, M. Ghneimat¹⁴¹, K. Ghorbanian⁹⁴, A. Ghosal¹⁴¹, A. Ghosh¹⁶⁰, A. Ghosh⁷, B. Giacobbe^{23b}, S. Giagu^{75a,75b}, P. Giannetti^{74a}, A. Giannini^{62a}, S. M. Gibson⁹⁵, M. Gignac¹³⁶, D. T. Gil^{85b}, A. K. Gilbert^{85a}, B. J. Gilbert⁴¹, D. Gillberg³⁴, G. Gilles¹¹⁴, N. E. K. Gillwald⁴⁸, L. Ginabat¹²⁷, D. M. Gingrich^{2,ai}, M. P. Giordani^{69a,69c}, P. F. Giraud¹³⁵, G. Giugliarelli^{69a,69c}, D. Giugni^{71a}, F. Giuli³⁶, I. Gkalias^{9,k}, L. K. Gladilin³⁷, C. Glasman⁹⁹, G. R. Gledhill¹²³, M. Glisic¹²³, I. Gnesi^{43b,g}, Y. Go^{29,al}, M. Goblirsch-Kolb²⁶, B. Gocke⁴⁹, D. Godin¹⁰⁸, B. Gokturk^{21a}, S. Goldfarb¹⁰⁵, T. Golling⁵⁶, M. G. D. Gololo^{33g}, D. Golubkov³⁷, J. P. Gombas¹⁰⁷, A. Gomes^{130a,130b}, G. Gomes Da Silva¹⁴¹, A. J. Gomez Delegido¹⁶³, R. Gonçalo^{130a,130c}, G. Gonella¹²³, L. Gonella²⁰, A. Gongadze³⁸, F. Gonnella²⁰, J. L. Gonski⁴¹, R. Y. González Andana⁵², S. González de la Hoz¹⁶³, S. Gonzalez Fernandez¹³, R. Gonzalez Lopez⁹², C. Gonzalez Renteria^{17a}, R. Gonzalez Suarez¹⁶¹, S. Gonzalez-Sevilla⁵⁶, G. R. Gonzalvo Rodriguez¹⁶³, L. Goossens³⁶, P. A. Gorbounov³⁷, B. Gorini³⁶, E. Gorini^{70a,70b}, A. Gorišek⁹³, A. T. Goshaw⁵¹

- M. I. Gostkin³⁸, S. Goswami¹²¹, C. A. Gottardo³⁶, M. Gouighri^{35b}, V. Goumarre⁴⁸, A. G. Goussiou¹³⁸, N. Govender^{33c}, I. Grabowska-Bold^{85a}, K. Graham³⁴, E. Gramstad¹²⁵, S. Grancagnolo¹⁸, M. Grandi¹⁴⁶, V. Gratchev^{37,*}, P. M. Gravila^{27f}, F. G. Gravili^{70a,70b}, H. M. Gray^{17a}, M. Greco^{70a,70b}, C. Grefe²⁴, I. M. Gregor⁴⁸, P. Grenier¹⁴³, C. Grieco¹³, A. A. Grillo¹³⁶, K. Grimm^{31,n}, S. Grinstein^{13,v}, J.-F. Grivaz⁶⁶, E. Gross¹⁶⁹, J. Grosse-Knetter⁵⁵, C. Grud¹⁰⁶, J. C. Grundy¹²⁶, L. Guan¹⁰⁶, W. Guan²⁹, C. Gubbels¹⁶⁴, J. G. R. Guerrero Rojas¹⁶³, G. Guerrieri^{69a,69b}, F. Guescini¹¹⁰, R. Gugel¹⁰⁰, J. A. M. Guhit¹⁰⁶, A. Guida⁴⁸, T. Guillemin⁴, E. Guilloton^{134,167}, S. Guindon³⁶, F. Guo^{14a,14d}, J. Guo^{62c}, L. Guo⁶⁶, Y. Guo¹⁰⁶, R. Gupta⁴⁸, S. Gurbuz²⁴, S. S. Gurdasani⁵⁴, G. Gustavino³⁶, M. Guth⁵⁶, P. Gutierrez¹²⁰, L. F. Gutierrez Zagazeta¹²⁸, C. Gutschow⁹⁶, C. Gwenlan¹²⁶, C. B. Gwilliam⁹², E. S. Haaland¹²⁵, A. Haas¹¹⁷, M. Habedank⁴⁸, C. Haber^{17a}, H. K. Hadavand⁸, A. Hadef¹⁰⁰, S. Hadzic¹¹⁰, E. H. Haines⁹⁶, M. Haleem¹⁶⁶, J. Haley¹²¹, J. J. Hall¹³⁹, G. D. Hallewell¹⁰², L. Halser¹⁹, K. Hamano¹⁶⁵, H. Hamdaoui^{35e}, M. Hamer²⁴, G. N. Hamity⁵², E. J. Hampshire⁹⁵, J. Han^{62b}, K. Han^{62a}, L. Han^{14c}, L. Han^{62a}, S. Han^{17a}, Y. F. Han¹⁵⁵, K. Hanagaki⁸³, M. Hance¹³⁶, D. A. Hangal^{41,ae}, H. Hanif¹⁴², M. D. Hank¹²⁸, R. Hankache¹⁰¹, J. B. Hansen⁴², J. D. Hansen⁴², P. H. Hansen⁴², K. Hara¹⁵⁷, D. Harada⁵⁶, T. Harenberg¹⁷¹, S. Harkusha³⁷, Y. T. Harris¹²⁶, N. M. Harrison¹¹⁹, P. F. Harrison¹⁶⁷, N. M. Hartman¹⁴³, N. M. Hartmann¹⁰⁹, Y. Hasegawa¹⁴⁰, A. Hasib⁵², S. Haug¹⁹, R. Hauser¹⁰⁷, M. Havranek¹³², C. M. Hawkes²⁰, R. J. Hawkings³⁶, S. Hayashida¹¹¹, D. Hayden¹⁰⁷, C. Hayes¹⁰⁶, R. L. Hayes¹¹⁴, C. P. Hays¹²⁶, J. M. Hays⁹⁴, H. S. Hayward⁹², F. He^{62a}, Y. He¹⁵⁴, Y. He¹²⁷, N. B. Heatley⁹⁴, V. Hedberg⁹⁸, A. L. Heggelund¹²⁵, N. D. Hehir⁹⁴, C. Heidegger⁵⁴, K. K. Heidegger⁵⁴, W. D. Heidorn⁸¹, J. Heilmann³⁴, S. Heim⁴⁸, T. Heim^{17a}, J. G. Heinlein¹²⁸, J. J. Heinrich¹²³, L. Heinrich^{110,ag}, J. Hejbal¹³¹, L. Helary⁴⁸, A. Held¹⁷⁰, S. Hellesund¹²⁵, C. M. Helling¹⁶⁴, S. Hellman^{47a,47b}, C. Helsens³⁶, R. C. W. Henderson⁹¹, L. Henkelmann³², A. M. Henrique Correia³⁶, H. Herde⁹⁸, Y. Hernández Jiménez¹⁴⁵, L. M. Herrmann²⁴, T. Herrmann⁵⁰, G. Herten⁵⁴, R. Hertenberger¹⁰⁹, L. Hervas³⁶, N. P. Hessey^{156a}, H. Hib⁸⁴, S. J. Hillier²⁰, F. Hinterkeuser²⁴, M. Hirose¹²⁴, S. Hirose¹⁵⁷, D. Hirschbuehl¹⁷¹, T. G. Hitchings¹⁰¹, B. Hiti⁹³, J. Hobbs¹⁴⁵, R. Hobincu^{27e}, N. Hod¹⁶⁹, M. C. Hodgkinson¹³⁹, B. H. Hodgkinson³², A. Hoecker³⁶, J. Hofer⁴⁸, T. Holm²⁴, M. Holzbock¹¹⁰, L. B. A. H. Hommels³², B. P. Honan¹⁰¹, J. Hong^{62c}, T. M. Hong¹²⁹, J. C. Honig⁵⁴, B. H. Hooberman¹⁶², W. H. Hopkins⁶, Y. Horii¹¹¹, S. Hou¹⁴⁸, A. S. Howard⁹³, J. Howarth⁵⁹, J. Hoya⁶, M. Hrabovsky¹²², A. Hrynevich⁴⁸, T. Hrynevich⁴, P. J. Hsu⁶⁵, S.-C. Hsu¹³⁸, Q. Hu⁴¹, Y. F. Hu^{14a,14d,ak}, D. P. Huang⁹⁶, S. Huang^{64b}, X. Huang^{14c}, Y. Huang^{62a}, Y. Huang^{14a}, Z. Huang¹⁰¹, Z. Hubacek¹³², M. Huebner²⁴, F. Huegging²⁴, T. B. Huffman¹²⁶, M. Huhtinen³⁶, S. K. Huberts¹⁶, R. Hulskens¹⁰⁴, N. Huseynov^{12,a}, J. Huston¹⁰⁷, J. Huth⁶¹, R. Hyneman¹⁴³, G. Iacobucci⁵⁶, G. Iakovidis²⁹, I. Ibragimov¹⁴¹, L. Iconomidou-Fayard⁶⁶, P. Iengo^{72a,72b}, R. Iguchi¹⁵³, T. Iizawa⁵⁶, Y. Ikegami⁸³, A. Ilg¹⁹, N. Ilic¹⁵⁵, H. Imam^{35a}, T. Ingebretsen Carlson^{47a,47b}, G. Introzzi^{73a,73b}, M. Iodice^{77a}, V. Ippolito^{75a,75b}, M. Ishino¹⁵³, W. Islam¹⁷⁰, C. Issever^{18,48}, S. Istin^{21a,an}, H. Ito¹⁶⁸, J. M. Iturbe Ponce^{64a}, R. Iuppa^{78a,78b}, A. Ivina¹⁶⁹, J. M. Izen⁴⁵, V. Izzo^{72a}, P. Jacka^{131,132}, P. Jackson¹, R. M. Jacobs⁴⁸, B. P. Jaeger¹⁴², C. S. Jagfeld¹⁰⁹, P. Jain⁵⁴, G. Jäkel¹⁷¹, K. Jakobs⁵⁴, T. Jakoubek¹⁶⁹, J. Jamieson⁵⁹, K. W. Janas^{85a}, A. E. Jaspan⁹², M. Javurkova¹⁰³, F. Jeanneau¹³⁵, L. Jeanty¹²³, J. Jejelava^{149a,ac}, P. Jenni^{54,h}, C. E. Jessiman³⁴, S. Jézéquel⁴, C. Jia^{62b}, J. Jia¹⁴⁵, X. Jia⁶¹, X. Jia^{14a,14d}, Z. Jia^{14c}, Y. Jiang^{62a}, S. Jiggins⁴⁸, J. Jimenez Pena¹¹⁰, S. Jin^{14c}, A. Jinaru^{27b}, O. Jinnouchi¹⁵⁴, P. Johansson¹³⁹, K. A. Johns⁷, J. W. Johnson¹³⁶, D. M. Jones³², E. Jones¹⁶⁷, P. Jones³², R. W. L. Jones⁹¹, T. J. Jones⁹², R. Joshi¹¹⁹, J. Jovicevic¹⁵, X. Ju^{17a}, J. J. Junggeburth³⁶, T. Junkermann^{63a}, A. Juste Rozas^{13,v}, S. Kabana^{137e}, A. Kaczmar ska⁸⁶, M. Kado¹¹⁰, H. Kagan¹¹⁹, M. Kagan¹⁴³, A. Kahn⁴¹, A. Kahn¹²⁸, C. Kahra¹⁰⁰, T. Kajii¹⁶⁸, E. Kajomovitz¹⁵⁰, N. Kakati¹⁶⁹, C. W. Kalderon²⁹, A. Kamenshchikov¹⁵⁵, S. Kanayama¹⁵⁴, N. J. Kang¹³⁶, D. Kar^{33g}, K. Karava¹²⁶, M. J. Kareem^{156b}, E. Karentzos⁵⁴, I. Karkanias^{152,f}, S. N. Karpov³⁸, Z. M. Karpova³⁸, V. Kartvelishvili⁹¹, A. N. Karyukhin³⁷, E. Kasimi^{152,f}, J. Katzy⁴⁸, S. Kaur³⁴, K. Kawade¹⁴⁰, T. Kawamoto¹³⁵, G. Kawamura⁵⁵, E. F. Kay¹⁶⁵, F. I. Kaya¹⁵⁸, S. Kazakos¹³, V. F. Kazanin³⁷, Y. Ke¹⁴⁵, J. M. Keaveney^{33a}, R. Keeler¹⁶⁵, G. V. Kehris⁶¹, J. S. Keller³⁴, A. S. Kelly⁹⁶, D. Kelsey¹⁴⁶, J. J. Kempster¹⁴⁶, K. E. Kennedy⁴¹, P. D. Kennedy¹⁰⁰, O. Kepka¹³¹, B. P. Kerridge¹⁶⁷, S. Kersten¹⁷¹, B. P. Kerševan⁹³, S. Keshri⁶⁶, L. Keszeghova^{28a}, S. Ketabchi Haghhighat¹⁵⁵, M. Khandoga¹²⁷, A. Khanov¹²¹, A. G. Kharlamov³⁷, T. Kharlamova³⁷, E. E. Khoda¹³⁸, T. J. Khoo¹⁸, G. Khoriauli¹⁶⁶, J. Khubua^{149b}, Y. A. R. Khwaira⁶⁶, M. Kiehn³⁶, A. Kilgallon¹²³, D. W. Kim^{47a,47b}, E. Kim¹⁵⁴, Y. K. Kim³⁹, N. Kimura⁹⁶, A. Kirchhoff⁵⁵, C. Kirlfel²⁴, J. Kirk¹³⁴, A. E. Kiryumin¹¹⁰, T. Kishimoto¹⁵³, D. P. Kisliuk¹⁵⁵, C. Kitsaki¹⁰, O. Kivernyk²⁴, M. Klassen^{63a}, C. Klein³⁴, L. Klein¹⁶⁶, M. H. Klein¹⁰⁶, M. Klein⁹², S. B. Klein⁵⁶

- U. Klein⁹², P. Klimek³⁶, A. Klimentov²⁹, F. Klimentov¹¹⁰, T. Klioutchnikova³⁶, P. Kluit¹¹⁴, S. Kluth¹¹⁰, E. Knerner⁷⁹, T. M. Knight¹⁵⁵, A. Knue⁵⁴, R. Kobayashi⁸⁷, M. Kocian¹⁴³, P. Kodyš¹³³, D. M. Koeck¹⁴⁶, P. T. Koenig²⁴, T. Koffas³⁴, M. Kolb¹³⁵, I. Koletsou⁴, T. Komarek¹²², K. Koneke⁵⁴, A. X. Y. Kong¹, T. Kono¹¹⁸, N. Konstantinidis⁹⁶, B. Konya⁹⁸, R. Kopeliansky⁶⁸, S. Koperny^{85a}, K. Korcyl⁸⁶, K. Kordas^{152,f}, G. Koren¹⁵¹, A. Korn⁹⁶, S. Korn⁵⁵, I. Korolkov¹³, N. Korotkova³⁷, B. Kortman¹¹⁴, O. Kortner¹¹⁰, S. Kortner¹¹⁰, W. H. Kostecka¹¹⁵, V. V. Kostyukhin¹⁴¹, A. Kotsokechagia¹³⁵, A. Kotwal⁵¹, A. Koulouris³⁶, A. Kourkoumeli-Charalampidi^{73a,73b}, C. Kourkoumelis⁹, E. Kourlitis⁶, O. Kovanda¹⁴⁶, R. Kowalewski¹⁶⁵, W. Kozanecki¹³⁵, A. S. Kozhin³⁷, V. A. Kramarenko³⁷, G. Kramberger⁹³, P. Kramer¹⁰⁰, M. W. Krasny¹²⁷, A. Krasnzhorkay³⁶, J. A. Kremer¹⁰⁰, T. Kresse⁵⁰, J. Kretzschmar⁹², K. Kreul¹⁸, P. Krieger¹⁵⁵, S. Krishnamurthy¹⁰³, M. Krivos¹³³, K. Krizka²⁰, K. Kroeninger⁴⁹, H. Kroha¹¹⁰, J. Kroll¹³¹, J. Kroll¹²⁸, K. S. Krowppman¹⁰⁷, U. Kruchonak³⁸, H. Krüger²⁴, N. Krumnack⁸¹, M. C. Kruse⁵¹, J. A. Krzysiak⁸⁶, O. Kuchinskaia³⁷, S. Kuday^{3a}, S. Kuehn³⁶, R. Kuesters⁵⁴, T. Kuhl⁴⁸, V. Kukhtin³⁸, Y. Kulchitsky^{37,a}, S. Kuleshov^{137b,137d}, M. Kumar^{33g}, N. Kumari¹⁰², A. Kupco¹³¹, T. Kupfer⁴⁹, A. Kupich³⁷, O. Kuprash⁵⁴, H. Kurashige⁸⁴, L. L. Kurchaninov^{156a}, Y. A. Kurochkin³⁷, A. Kurova³⁷, M. Kuze¹⁵⁴, A. K. Kvam¹⁰³, J. Kvita¹²², T. Kwan¹⁰⁴, N. G. Kyriacou¹⁰⁶, L. A. O. Laatu¹⁰², C. Lacasta¹⁶³, F. Lacava^{75a,75b}, H. Lacker¹⁸, D. Lacour¹²⁷, N. N. Lad⁹⁶, E. Ladygin³⁸, B. Laforge¹²⁷, T. Lagouri^{137e}, S. Lai⁵⁵, I. K. Lakomiec^{85a}, N. Lalloue⁶⁰, J. E. Lambert¹²⁰, S. Lammers⁶⁸, W. Lampl⁷, C. Lampoudis^{152,f}, A. N. Lancaster¹¹⁵, E. Lançon²⁹, U. Landgraf⁵⁴, M. P. J. Landon⁹⁴, V. S. Lang⁵⁴, R. J. Langenberg¹⁰³, A. J. Lankford¹⁶⁰, F. Lanni³⁶, K. Lantzsch²⁴, A. Lanza^{73a}, A. Lapertosa^{57a,57b}, J. F. Laporte¹³⁵, T. Lari^{71a}, F. Lasagni Manghi^{23b}, M. Lassnig³⁶, V. Latonova¹³¹, A. Laudrain¹⁰⁰, A. Laurier¹⁵⁰, S. D. Lawlor⁹⁵, Z. Lawrence¹⁰¹, M. Lazzaroni^{71a,71b}, B. Le¹⁰¹, E. M. Le Boulicaut⁵¹, B. Leban⁹³, A. Lebedev⁸¹, M. LeBlanc³⁶, F. Ledroit-Guillon⁶⁰, A. C. A. Lee⁹⁶, G. R. Lee¹⁶, S. C. Lee¹⁴⁸, S. Lee^{47a,47b}, T. F. Lee⁹², L. L. Leeuw^{33c}, H. P. Lefebvre⁹⁵, M. Lefebvre¹⁶⁵, C. Leggett^{17a}, K. Lehmann¹⁴², G. Lehmann Miotti³⁶, M. Leigh⁵⁶, W. A. Leight¹⁰³, A. Leisos^{152,u}, M. A. L. Leite^{82c}, C. E. Leitgeb⁴⁸, R. Leitner¹³³, K. J. C. Leney⁴⁴, T. Lenz²⁴, S. Leone^{74a}, C. Leonidopoulos⁵², A. Leopold¹⁴⁴, C. Leroy¹⁰⁸, R. Les¹⁰⁷, C. G. Lester³², M. Levchenko³⁷, J. Levêque⁴, D. Levin¹⁰⁶, L. J. Levinson¹⁶⁹, M. P. Lewicki⁸⁶, D. J. Lewis⁴, A. Li⁵, B. Li^{62b}, C. Li^{62a}, C.-Q. Li^{62c}, H. Li^{62a}, H. Li^{62b}, H. Li^{14c}, H. Li^{62b}, J. Li^{62c}, K. Li¹³⁸, L. Li^{62c}, M. Li^{14a,14d}, Q. Y. Li^{62a}, S. Li^{14a,14d}, S. Li^{62c,62d,e}, T. Li^{62b}, X. Li¹⁰⁴, Z. Li^{62b}, Z. Li¹²⁶, Z. Li¹⁰⁴, Z. Li⁹², Z. Li^{14a,14d}, Z. Liang^{14a}, M. Liberatore⁴⁸, B. Liberti^{76a}, K. Lie^{64c}, J. Lieber Marin^{82b}, H. Lien⁶⁸, K. Lin¹⁰⁷, R. A. Linck⁶⁸, R. E. Lindley⁷, J. H. Lindon², A. Linss⁴⁸, E. Lipieles¹²⁸, A. Lipniacka¹⁶, A. Lister¹⁶⁴, J. D. Little⁴, B. Liu^{14a}, B. X. Liu¹⁴², D. Liu^{62c,62d}, J. B. Liu^{62a}, J. K. K. Liu³², K. Liu^{62c,62d}, M. Liu^{62a}, M. Y. Liu^{62a}, P. Liu^{14a}, Q. Liu^{62c,62d,138}, X. Liu^{62a}, Y. Liu^{14c,14d}, Y. L. Liu¹⁰⁶, Y. W. Liu^{62a}, J. Llorente Merino¹⁴², S. L. Lloyd⁹⁴, E. M. Lobodzinska⁴⁸, P. Loch⁷, S. Loffredo^{76a,76b}, T. Lohse¹⁸, K. Lohwasser¹³⁹, E. Loiacono⁴⁸, M. Lokajicek^{131,*}, J. D. Long¹⁶², I. Longarini¹⁶⁰, L. Longo^{70a,70b}, R. Longo¹⁶², I. Lopez Paz⁶⁷, A. Lopez Solis⁴⁸, J. Lorenz¹⁰⁹, N. Lorenzo Martinez⁴, A. M. Lory¹⁰⁹, X. Lou^{47a,47b}, X. Lou^{14a,14d}, A. Lounis⁶⁶, J. Love⁶, P. A. Love⁹¹, G. Lu^{14a,14d}, M. Lu⁸⁰, S. Lu¹²⁸, Y. J. Lu⁶⁵, H. J. Lubatti¹³⁸, C. Luci^{75a,75b}, F. L. Lucio Alves^{14c}, A. Lucotte⁶⁰, F. Luehring⁶⁸, I. Luise¹⁴⁵, O. Lukianchuk⁶⁶, O. Lundberg¹⁴⁴, B. Lund-Jensen¹⁴⁴, N. A. Luongo¹²³, M. S. Lutz¹⁵¹, D. Lynn²⁹, H. Lyons⁹², R. Lysak¹³¹, E. Lytken⁹⁸, V. Lyubushkin³⁸, T. Lyubushkina³⁸, M. M. Lyukova¹⁴⁵, H. Ma²⁹, L. L. Ma^{62b}, Y. Ma⁹⁶, D. M. Mac Donell¹⁶⁵, G. Maccarrone⁵³, J. C. MacDonald¹³⁹, R. Madar⁴⁰, W. F. Mader⁵⁰, J. Maeda⁸⁴, T. Maeno²⁹, M. Maerker⁵⁰, H. Maguire¹³⁹, A. Maio^{130a,130b,130d}, K. Maj^{85a}, O. Majersky⁴⁸, S. Majewski¹²³, N. Makovec⁶⁶, V. Maksimovic¹⁵, B. Malaescu¹²⁷, Pa. Malecki⁸⁶, V. P. Maleev³⁷, F. Malek⁶⁰, D. Malito^{43a,43b}, U. Mallik⁸⁰, C. Malone³², S. Maltezos¹⁰, S. Malyukov³⁸, J. Mamuzic¹³, G. Mancini⁵³, G. Manco^{73a,73b}, J. P. Mandalia⁹⁴, I. Mandic⁹³, L. Manhaes de Andrade Filho^{82a}, I. M. Maniatis¹⁶⁹, J. Manjarres Ramos^{102,ad}, D. C. Mankad¹⁶⁹, A. Mann¹⁰⁹, B. Mansoulie¹³⁵, S. Manzoni³⁶, A. Marantis^{152,u}, G. Marchiori⁵, M. Marcisovsky¹³¹, C. Marcon^{71a,71b}, M. Marinescu²⁰, M. Marjanovic¹²⁰, E. J. Marshall⁹¹, Z. Marshall^{17a}, S. Marti-Garcia¹⁶³, T. A. Martin¹⁶⁷, V. J. Martin⁵², B. Martin dit Latour¹⁶, L. Martinelli^{75a,75b}, M. Martinez^{13,v}, P. Martinez Agullo¹⁶³, V. I. Martinez Outschoorn¹⁰³, P. Martinez Suarez¹³, S. Martin-Haugh¹³⁴, V. S. Martoiu^{27b}, A. C. Martyniuk⁹⁶, A. Marzin³⁶, S. R. Maschek¹¹⁰, D. Mascione^{78a,78b}, L. Masetti¹⁰⁰, T. Mashimo¹⁵³, J. Masik¹⁰¹, A. L. Maslennikov³⁷, L. Massa^{23b}, P. Massarotti^{72a,72b}, P. Mastrandrea^{74a,74b}, A. Mastroberardino^{43a,43b}, T. Masubuchi¹⁵³, T. Mathisen¹⁶¹, N. Matsuzawa¹⁵³, J. Maurer^{27b}, B. Maček⁹³, D. A. Maximov³⁷, R. Mazini¹⁴⁸, I. Maznas^{152,f}, M. Mazza¹⁰⁷, S. M. Mazza¹³⁶, C. Mc Ginn²⁹, J. P. Mc Gowan¹⁰⁴,

- S. P. Mc Kee¹⁰⁶, E. F. McDonald¹⁰⁵, A. E. McDougall¹¹⁴, J. A. Mcfayden¹⁴⁶, G. Mchedlidze^{149b}, R. P. Mckenzie^{33g}, T. C. McLachlan⁴⁸, D. J. McLaughlin⁹⁶, K. D. McLean¹⁶⁵, S. J. McMahon¹³⁴, P. C. McNamara¹⁰⁵, C. M. Mcpartland⁹², R. A. McPherson^{165,z}, T. Megy⁴⁰, S. Mehlhase¹⁰⁹, A. Mehta⁹², D. Melimi¹⁵⁰, B. R. Mellado Garcia^{33g}, A. H. Melo⁵⁵, F. Meloni⁴⁸, A. M. Mendes Jacques Da Costa¹⁰¹, H. Y. Meng¹⁵⁵, L. Meng⁹¹, S. Menke¹¹⁰, M. Mentink³⁶, E. Meoni^{43a,43b}, C. Merlassino¹²⁶, L. Merola^{72a,72b}, C. Meroni^{71a,71b}, G. Merz¹⁰⁶, O. Meshkov³⁷, J. Metcalfe⁶, A. S. Mete⁶, C. Meyer⁶⁸, J.-P. Meyer¹³⁵, R. P. Middleton¹³⁴, L. Mijovic⁵², G. Mikenberg¹⁶⁹, M. Mikestikova¹³¹, M. Mikuž⁹³, H. Mildner¹³⁹, A. Milic³⁶, C. D. Milke⁴⁴, D. W. Miller³⁹, L. S. Miller³⁴, A. Milov¹⁶⁹, D. A. Milstead^{47a,47b}, T. Min^{14c}, A. A. Minaenko³⁷, I. A. Minashvili^{149b}, L. Mince⁵⁹, A. I. Mincer¹¹⁷, B. Mindur^{85a}, M. Mineev³⁸, Y. Mino⁸⁷, L. M. Mir¹³, M. Miralles Lopez¹⁶³, M. Mironova¹²⁶, M. C. Missio¹¹³, T. Mitani¹⁶⁸, A. Mitra¹⁶⁷, V. A. Mitsou¹⁶³, O. Miu¹⁵⁵, P. S. Miyagawa⁹⁴, Y. Miyazaki⁸⁹, A. Mizukami⁸³, T. Mkrtchyan^{63a}, M. Mlinarevic⁹⁶, T. Mlinarevic⁹⁶, M. Mlynarikova³⁶, S. Mobius⁵⁵, K. Mochizuki¹⁰⁸, P. Moder⁴⁸, P. Mogg¹⁰⁹, A. F. Mohammed^{14a,14d}, S. Mohapatra⁴¹, G. Mokgatitswane^{33g}, B. Mondal¹⁴¹, S. Mondal¹³², K. Mönig⁴⁸, E. Monnier¹⁰², L. Monsonis Romero¹⁶³, J. Montejo Berlingen⁸³, M. Montella¹¹⁹, F. Monticelli⁹⁰, N. Morange⁶⁶, A. L. Moreira De Carvalho^{130a}, M. Moreno Llacer¹⁶³, C. Moreno Martinez⁵⁶, P. Morettini^{57b}, S. Morgenstern¹⁶⁷, M. Morii⁶¹, M. Morinaga¹⁵³, A. K. Morley³⁶, F. Morodei^{75a,75b}, L. Morvaj³⁶, P. Moschovakos³⁶, B. Moser³⁶, M. Mosidze^{149b}, T. Moskalets⁵⁴, P. Moskvitina¹¹³, J. Moss^{31,o}, E. J. W. Moyse¹⁰³, O. Mtintsilana^{33g}, S. Muanza¹⁰², J. Mueller¹²⁹, D. Muenstermann⁹¹, R. Müller¹⁹, G. A. Mullier¹⁶¹, J. J. Mullin¹²⁸, D. P. Mungo¹⁵⁵, J. L. Munoz Martinez¹³, D. Munoz Perez¹⁶³, F. J. Munoz Sanchez¹⁰¹, M. Murin¹⁰¹, W. J. Murray^{134,167}, A. Murrone^{71a,71b}, J. M. Muse¹²⁰, M. Muškinja^{17a}, C. Mwewa²⁹, A. G. Myagkov^{37,a}, A. J. Myers⁸, A. A. Myers¹²⁹, G. Myers⁶⁸, M. Myska¹³², B. P. Nachman^{17a}, O. Nackenhorst⁴⁹, A. Nag⁵⁰, K. Nagai¹²⁶, K. Nagano⁸³, J. L. Nagle^{29,al}, E. Nagy¹⁰², A. M. Nairz³⁶, Y. Nakahama⁸³, K. Nakamura⁸³, H. Nanjo¹²⁴, R. Narayan⁴⁴, E. A. Narayanan¹¹², I. Naryshkin³⁷, M. Naseri³⁴, C. Nass²⁴, G. Navarro^{22a}, J. Navarro-Gonzalez¹⁶³, R. Nayak¹⁵¹, A. Nayaz¹⁸, P. Y. Nechaeva³⁷, F. Nechansky⁴⁸, L. Nedic¹²⁶, T. J. Neep²⁰, A. Negri^{73a,73b}, M. Negrini^{23b}, C. Nellist¹¹⁴, C. Nelson¹⁰⁴, K. Nelson¹⁰⁶, S. Nemecek¹³¹, M. Nessi^{36,i}, M. S. Neubauer¹⁶², F. Neuhaus¹⁰⁰, J. Neundorf⁴⁸, R. Newhouse¹⁶⁴, P. R. Newman²⁰, C. W. Ng¹²⁹, Y. W. Y. Ng⁴⁸, B. Ngair^{35e}, H. D. N. Nguyen¹⁰⁸, R. B. Nickerson¹²⁶, R. Nicolaïdou¹³⁵, J. Nielsen¹³⁶, M. Niemeyer⁵⁵, N. Nikiforou³⁶, V. Nikolaenko^{37,a}, I. Nikolic-Audit¹²⁷, K. Nikolopoulos²⁰, P. Nilsson²⁹, I. Ninca⁴⁸, H. R. Nindhito⁵⁶, G. Ninio¹⁵¹, A. Nisati^{75a}, N. Nishu², R. Nisius¹¹⁰, J.-E. Nitschke⁵⁰, E. K. Nkadieng^{33g}, S. J. Noacco Rosende⁹⁰, T. Nobe¹⁵³, D. L. Noel³², Y. Noguchi⁸⁷, T. Nommensen¹⁴⁷, M. A. Nomura²⁹, M. B. Norfolk¹³⁹, R. R. B. Norisam⁹⁶, B. J. Norman³⁴, J. Novak⁹³, T. Novak⁴⁸, L. Novotny¹³², R. Novotny¹¹², L. Nozka¹²², K. Ntekas¹⁶⁰, N. M. J. Nunes De Moura Junior^{82b}, E. Nurse⁹⁶, J. Ocariz¹²⁷, A. Ochi⁸⁴, I. Ochoa^{130a}, S. Oerdekk¹⁶¹, J. T. Offermann³⁹, A. Ogrodnik^{85a}, A. Oh¹⁰¹, C. C. Ohm¹⁴⁴, H. Oide⁸³, R. Oishi¹⁵³, M. L. Ojeda⁴⁸, Y. Okazaki⁸⁷, M. W. O'Keefe⁹², Y. Okumura¹⁵³, L. F. Oleiro Seabra^{130a}, S. A. Olivares Pino^{137d}, D. Oliveira Damazio²⁹, D. Oliveira Goncalves^{82a}, J. L. Oliver¹⁶⁰, M. J. R. Olsson¹⁶⁰, A. Olszewski⁸⁶, J. Olszowska^{86,*}, Ö. Ö. Öncel⁵⁴, D. C. O'Neil¹⁴², A. P. O'Neill¹⁹, A. Onofre^{130a,130e}, P. U. E. Onyisi¹¹, M. J. Oreglia³⁹, G. E. Orellana⁹⁰, D. Orestano^{77a,77b}, N. Orlando¹³, R. S. Orr¹⁵⁵, V. O'Shea⁵⁹, R. Ospanov^{62a}, G. Otero y Garzon³⁰, H. Otono⁸⁹, P. S. Ott^{63a}, G. J. Ottino^{17a}, M. Ouchrif^{35d}, J. Ouellette²⁹, F. Ould-Saada¹²⁵, M. Owen⁵⁹, R. E. Owen¹³⁴, K. Y. Oyulmaz^{21a}, V. E. Ozcan^{21a}, N. Ozturk⁸, S. Ozturk^{21d}, H. A. Pacey³², A. Pacheco Pages¹³, C. Padilla Aranda¹³, G. Padovano^{75a,75b}, S. Pagan Griso^{17a}, G. Palacino⁶⁸, A. Palazzo^{70a,70b}, S. Palestini³⁶, J. Pan¹⁷², T. Pan^{64a}, D. K. Panchal¹¹, C. E. Pandini¹¹⁴, J. G. Panduro Vazquez⁹⁵, H. Pang^{14b}, P. Pani⁴⁸, G. Panizzo^{69a,69c}, L. Paolozzi⁵⁶, C. Papadatos¹⁰⁸, S. Parajuli⁴⁴, A. Paramonov⁶, C. Paraskevopoulos¹⁰, D. Paredes Hernandez^{64b}, T. H. Park¹⁵⁵, M. A. Parker³², F. Parodi^{57a,57b}, E. W. Parrish¹¹⁵, V. A. Parrish⁵², J. A. Parsons⁴¹, U. Parzefall⁵⁴, B. Pascual Dias¹⁰⁸, L. Pascual Dominguez¹⁵¹, F. Pasquali¹¹⁴, E. Pasqualucci^{75a}, S. Passaggio^{57b}, F. Pastore⁹⁵, P. Pasuwan^{47a,47b}, P. Patel⁸⁶, U. M. Patel⁵¹, J. R. Pater¹⁰¹, T. Pauly³⁶, J. Pearkes¹⁴³, M. Pedersen¹²⁵, R. Pedro^{130a}, S. V. Peleganchuk³⁷, O. Penc³⁶, E. A. Pender⁵², H. Peng^{62a}, K. E. Penski¹⁰⁹, M. Penzin³⁷, B. S. Peralva^{82d}, A. P. Pereira Peixoto⁶⁰, L. Pereira Sanchez^{47a,47b}, D. V. Perepelitsa^{29,al}, E. Perez Codina^{156a}, M. Perganti¹⁰, L. Perini^{71a,71b,*}, H. Pernegger³⁶, A. Perrevoort¹¹³, O. Perrin⁴⁰, K. Peters⁴⁸, R. F. Y. Peters¹⁰¹, B. A. Petersen³⁶, T. C. Petersen⁴², E. Petit¹⁰², V. Petousis¹³², C. Petridou^{152,f}, A. Petrukhin¹⁴¹, M. Pettee^{17a}, N. E. Pettersson³⁶, A. Petukhov³⁷, K. Petukhova¹³³, A. Peyaud¹³⁵, R. Pezoa^{137f}, L. Pezzotti³⁶, G. Pezzullo¹⁷², T. M. Pham¹⁷⁰, T. Pham¹⁰⁵, P. W. Phillips¹³⁴, M. W. Phipps¹⁶²

- G. Piacquadio¹⁴⁵, E. Pianori^{17a}, F. Piazza^{71a,71b}, R. Piegaia³⁰, D. Pietreanu^{27b}, A. D. Pilkington¹⁰¹, M. Pinamonti^{69a,69c}, J. L. Pinfold², B. C. Pinheiro Pereira^{130a}, C. Pitman Donaldson⁹⁶, D. A. Pizzi³⁴, L. Pizzimenti^{76a,76b}, A. Pizzini¹¹⁴, M.-A. Pleier²⁹, V. Plesanovs⁵⁴, V. Pleskot¹³³, E. Plotnikova³⁸, G. Poddar⁴, R. Poettgen⁹⁸, L. Poggioli¹²⁷, D. Pohl²⁴, I. Pokharel⁵⁵, S. Polacek¹³³, G. Polesello^{73a}, A. Poley^{142,156a}, R. Polifka¹³², A. Polini^{23b}, C. S. Pollard¹⁶⁷, Z. B. Pollock¹¹⁹, V. Polychronakos²⁹, E. Pompa Pacchi^{75a,75b}, D. Ponomarenko¹¹³, L. Pontecorvo³⁶, S. Popa^{27a}, G. A. Popenciu^{27d}, D. M. Portillo Quintero^{156a}, S. Pospisil¹³², P. Postolache^{27c}, K. Potamianos¹²⁶, P. A. Potepa^{85a}, I. N. Potrap³⁸, C. J. Potter³², H. Potti¹, T. Poulsen⁴⁸, J. Poveda¹⁶³, M. E. Pozo Astigarraga³⁶, A. Prades Ibanez¹⁶³, M. M. Prapa⁴⁶, J. Pretel⁵⁴, D. Price¹⁰¹, M. Primavera^{70a}, M. A. Principe Martin⁹⁹, R. Privara¹²², M. L. Proffitt¹³⁸, N. Proklova¹²⁸, K. Prokofiev^{64c}, G. Proto^{76a,76b}, S. Protopopescu²⁹, J. Proudfoot⁶, M. Przybycien^{85a}, W. W. Przygoda^{85b}, J. E. Puddefoot¹³⁹, D. Pudzha³⁷, D. Pyatiizbyantseva³⁷, J. Qian¹⁰⁶, D. Qichen¹⁰¹, Y. Qin¹⁰¹, T. Qiu⁵², A. Quadt⁵⁵, M. Queitsch-Maitland¹⁰¹, G. Quetant⁵⁶, G. Rabanal Bolanos⁶¹, D. Rafanoharana⁵⁴, F. Ragusa^{71a,71b}, J. L. Rainbolt³⁹, J. A. Raine⁵⁶, S. Rajagopalan²⁹, E. Ramakott³⁷, K. Ran^{14d,48}, N. P. Rapheeha^{33g}, V. Raskina¹²⁷, D. F. Rassloff^{63a}, S. Rave¹⁰⁰, B. Ravina⁵⁵, I. Ravinovich¹⁶⁹, M. Raymond³⁶, A. L. Read¹²⁵, N. P. Readioff¹³⁹, D. M. Rebuzzi^{73a,73b}, G. Redlinger²⁹, K. Reeves⁴⁵, J. A. Reidelsturz¹⁷¹, D. Reikher¹⁵¹, A. Rej¹⁴¹, C. Rembser³⁶, A. Renardi⁴⁸, M. Renda^{27b}, M. B. Rendel¹¹⁰, F. Renner⁴⁸, A. G. Rennie⁵⁹, S. Resconi^{71a}, M. Ressegotti^{57a,57b}, E. D. Ressegueie^{17a}, S. Rettic³⁶, J. G. Reyes Rivera¹⁰⁷, B. Reynolds¹¹⁹, E. Reynolds^{17a}, M. Rezaei Estabragh¹⁷¹, O. L. Rezanova³⁷, P. Reznicek¹³³, N. Ribaric⁹¹, E. Ricci^{78a,78b}, R. Richter¹¹⁰, S. Richter^{47a,47b}, E. Richter-Was^{85b}, M. Ridel¹²⁷, S. Ridouani^{35d}, P. Rieck¹¹⁷, P. Riedler³⁶, M. Rijssenbeek¹⁴⁵, A. Rimoldi^{73a,73b}, M. Rimoldi⁴⁸, L. Rinaldi^{23a,23b}, T. T. Rinn²⁹, M. P. Rinnagel¹⁰⁹, G. Ripellino¹⁶¹, I. Riu¹³, P. Rivadeneira⁴⁸, J. C. Rivera Vergara¹⁶⁵, F. Rizatdinova¹²¹, E. Rizvi⁹⁴, C. Rizzi⁵⁶, B. A. Roberts¹⁶⁷, B. R. Roberts^{17a}, S. H. Robertson^{104,z}, M. Robin⁴⁸, D. Robinson³², C. M. Robles Gajardo^{137f}, M. Robles Manzano¹⁰⁰, A. Robson⁵⁹, A. Rocchi^{76a,76b}, C. Roda^{74a,74b}, S. Rodriguez Bosca^{63a}, Y. Rodriguez Garcia^{22a}, A. Rodriguez Rodriguez⁵⁴, A. M. Rodríguez Vera^{156b}, S. Roe³⁶, J. T. Roemer¹⁶⁰, A. R. Roepe-Gier¹³⁶, J. Roggel¹⁷¹, O. Røhne¹²⁵, R. A. Rojas¹⁰³, B. Roland⁵⁴, C. P. A. Roland⁶⁸, J. Roloff²⁹, A. Romanouk³⁷, E. Romano^{73a,73b}, M. Romano^{23b}, A. C. Romero Hernandez¹⁶², N. Rompotis⁹², L. Roos¹²⁷, S. Rosati^{75a}, B. J. Rosser³⁹, E. Rossi⁴, E. Rossi^{72a,72b}, L. P. Rossi^{57b}, L. Rossini⁴⁸, R. Rosten¹¹⁹, M. Rotaru^{27b}, B. Rottler⁵⁴, C. Rougier^{102,ad}, D. Rousseau⁶⁶, D. Rousseau³², G. Rovelli^{73a,73b}, A. Roy¹⁶², S. Roy-Garand¹⁵⁵, A. Rozanov¹⁰², Y. Rozen¹⁵⁰, X. Ruan^{33g}, A. Rubio Jimenez¹⁶³, A. J. Ruby⁹², V. H. Ruelas Rivera¹⁸, T. A. Ruggeri¹, F. Rühr⁵⁴, A. Ruiz-Martinez¹⁶³, A. Rummler³⁶, Z. Rurikova⁵⁴, N. A. Rusakovich³⁸, H. L. Russell¹⁶⁵, J. P. Rutherford⁷, K. Rybacki⁹¹, M. Rybar¹³³, E. B. Rye¹²⁵, A. Ryzhov³⁷, J. A. Sabater Iglesias⁵⁶, P. Sabatini¹⁶³, L. Sabetta^{75a,75b}, H. F.-W. Sadrozinski¹³⁶, F. Safai Tehrani^{75a}, B. Safarzadeh Samani¹⁴⁶, M. Safdari¹⁴³, S. Saha¹⁰⁴, M. Sahinsoy¹¹⁰, M. Saimpert¹³⁵, M. Saito¹⁵³, T. Saito¹⁵³, D. Salamani³⁶, A. Salnikov¹⁴³, J. Salt¹⁶³, A. Salvador Salas¹³, D. Salvatore^{43a,43b}, F. Salvatore¹⁴⁶, A. Salzburger³⁶, D. Sammel⁵⁴, D. Sampsonidis^{152,f}, D. Sampsonidou^{62c,62d}, J. Sánchez¹⁶³, A. Sanchez Pineda⁴, V. Sanchez Sebastian¹⁶³, H. Sandaker¹²⁵, C. O. Sander⁴⁸, J. A. Sandesara¹⁰³, M. Sandhoff¹⁷¹, C. Sandoval^{22b}, D. P. C. Sankey¹³⁴, T. Sano⁸⁷, A. Sansoni⁵³, L. Santi^{75a,75b}, C. Santoni⁴⁰, H. Santos^{130a,130b}, S. N. Santpur^{17a}, A. Santra¹⁶⁹, K. A. Saoucha¹³⁹, J. G. Saraiva^{130a,130d}, J. Sardain⁷, O. Sasaki⁸³, K. Sato¹⁵⁷, C. Sauer^{63b}, F. Sauerburger⁵⁴, E. Sauvan⁴, P. Savard^{155,ai}, R. Sawada¹⁵³, C. Sawyer¹³⁴, L. Sawyer⁹⁷, I. Sayago Galvan¹⁶³, C. Sbarra^{23b}, A. Sbrizzi^{23a,23b}, T. Scanlon⁹⁶, J. Schaarschmidt¹³⁸, P. Schacht¹¹⁰, D. Schaefer³⁹, U. Schäfer¹⁰⁰, A. C. Schaffer^{44,66}, D. Schaire¹⁰⁹, R. D. Schamberger¹⁴⁵, E. Schanet¹⁰⁹, C. Scharf¹⁸, M. M. Schefer¹⁹, V. A. Schegelsky³⁷, D. Scheirich¹³³, F. Schenck¹⁸, M. Schernau¹⁶⁰, C. Scheulen⁵⁵, C. Schiavi^{57a,57b}, Z. M. Schillaci²⁶, E. J. Schioppa^{70a,70b}, M. Schioppa^{43a,43b}, B. Schlag¹⁰⁰, K. E. Schleicher⁵⁴, S. Schlenker³⁶, J. Schmeing¹⁷¹, M. A. Schmidt¹⁷¹, K. Schmieden¹⁰⁰, C. Schmitt¹⁰⁰, S. Schmitt⁴⁸, L. Schoeffel¹³⁵, A. Schoening^{63b}, P. G. Scholer⁵⁴, E. Schopf¹²⁶, M. Schott¹⁰⁰, J. Schovancova³⁶, S. Schramm⁵⁶, F. Schroeder¹⁷¹, H.-C. Schultz-Coulon^{63a}, M. Schumacher⁵⁴, B. A. Schumm¹³⁶, Ph. Schune¹³⁵, H. R. Schwartz¹³⁶, A. Schwartzzman¹⁴³, T. A. Schwarz¹⁰⁶, Ph. Schwemling¹³⁵, R. Schwienhorst¹⁰⁷, A. Sciandra¹³⁶, G. Sciolla²⁶, F. Scuri^{74a}, F. Scutti¹⁰⁵, C. D. Sebastiani⁹², K. Sedlacek⁴⁹, P. Seema¹⁸, S. C. Seidel¹¹², A. Seiden¹³⁶, B. D. Seidlitz⁴¹, C. Seitz⁴⁸, J. M. Seixas^{82b}, G. Sekhniaidze^{72a}, S. J. Sekula⁴⁴, L. Selem⁴, N. Semprini-Cesari^{23a,23b}, S. Sen⁵¹, D. Sengupta⁵⁶, V. Senthilkumar¹⁶³, L. Serin⁶⁶, L. Serkin^{69a,69b}, M. Sessa^{77a,77b}, H. Severini¹²⁰, F. Sforza^{57a,57b}, A. Sfyrla⁵⁶, E. Shabalina⁵⁵, R. Shaheen¹⁴⁴

- J. D. Shahinian¹²⁸, D. Shaked Renous¹⁶⁹, L. Y. Shan^{14a}, M. Shapiro^{17a}, A. Sharma³⁶, A. S. Sharma¹⁶⁴, P. Sharma⁸⁰, S. Sharma⁴⁸, P. B. Shatalov³⁷, K. Shaw¹⁴⁶, S. M. Shaw¹⁰¹, Q. Shen^{5,62c}, P. Sherwood⁹⁶, L. Shi⁹⁶, C. O. Shimmin¹⁷², Y. Shimogama¹⁶⁸, J. D. Shinner⁹⁵, I. P. J. Shipsey¹²⁶, S. Shirabe⁶⁰, M. Shiyakova^{38,x}, J. Shlomi¹⁶⁹, M. J. Shochet³⁹, J. Shojaei¹⁰⁵, D. R. Shope¹²⁵, S. Shrestha^{119,am}, E. M. Shrif^{33g}, M. J. Shroff¹⁶⁵, P. Sicho¹³¹, A. M. Sickles¹⁶², E. Sideras Haddad^{33g}, A. Sidoti^{23b}, F. Siegert⁵⁰, Dj. Sijacki¹⁵, R. Sikora^{85a}, F. Sili⁹⁰, J. M. Silva²⁰, M. V. Silva Oliveira³⁶, S. B. Silverstein^{47a}, S. Simion⁶⁶, R. Simoniello³⁶, E. L. Simpson⁵⁹, H. Simpson¹⁴⁶, L. R. Simpson¹⁰⁶, N. D. Simpson⁹⁸, S. Simsek^{21d}, S. Sindhu⁵⁵, P. Sinervo¹⁵⁵, S. Singh¹⁴², S. Singh¹⁵⁵, S. Sinha⁴⁸, S. Sinha^{33g}, M. Sioli^{23a,23b}, I. Siral³⁶, S. Yu. Sivoklokov^{37,*}, J. Sjölin^{47a,47b}, A. Skaf⁵⁵, E. Skorda⁹⁸, P. Skubic¹²⁰, M. Slawinska⁸⁶, V. Smakhtin¹⁶⁹, B. H. Smart¹³⁴, J. Smiesko³⁶, S. Yu. Smirnov³⁷, Y. Smirnov³⁷, L. N. Smirnova^{37,a}, O. Smirnova⁹⁸, A. C. Smith⁴¹, E. A. Smith³⁹, H. A. Smith¹²⁶, J. L. Smith⁹², R. Smith¹⁴³, M. Smizanska⁹¹, K. Smolek¹³², A. Smykiewicz⁸⁶, A. A. Snesarev³⁷, H. L. Snoek¹¹⁴, S. Snyder²⁹, R. Sobie^{165,z}, A. Soffer¹⁵¹, C. A. Solans Sanchez³⁶, E. Yu. Soldatov³⁷, U. Soldevila¹⁶³, A. A. Solodkov³⁷, S. Solomon⁵⁴, A. Soloshenko³⁸, K. Solovieva⁵⁴, O. V. Solovyev⁴⁰, V. Solovyev³⁷, P. Sommer³⁶, A. Sonay¹³, W. Y. Song^{156b}, J. M. Sonneveld¹¹⁴, A. Sopczak¹³², A. L. Sopio⁹⁶, F. Sopkova^{28b}, V. Sothilingam^{63a}, S. Sottocornola⁶⁸, R. Soualah^{116b}, Z. Soumaimi^{35e}, D. South⁴⁸, S. Spagnolo^{70a,70b}, M. Spalla¹¹⁰, D. Sperlich⁵⁴, G. Spigo³⁶, M. Spina¹⁴⁶, S. Spinali⁹¹, D. P. Spiteri⁵⁹, M. Spousta¹³³, E. J. Staats³⁴, A. Stabile^{71a,71b}, R. Stamen^{63a}, M. Stamenkovic¹¹⁴, A. Stampekkis²⁰, M. Standke²⁴, E. Stancka⁸⁶, M. V. Stange⁵⁰, B. Stanislaus^{17a}, M. M. Stanitzki⁴⁸, M. Stankaityte¹²⁶, B. Stapf⁴⁸, E. A. Starchenko³⁷, G. H. Stark¹³⁶, J. Stark^{102,ad}, D. M. Starko^{156b}, P. Staroba¹³¹, P. Starovoitov^{63a}, S. Stärz¹⁰⁴, R. Staszewski⁸⁶, G. Stavropoulos⁴⁶, J. Steentoft¹⁶¹, P. Steinberg²⁹, B. Stelzer^{142,156a}, H. J. Stelzer¹²⁹, O. Stelzer-Chilton^{156a}, H. Stenzel⁵⁸, T. J. Stevenson¹⁴⁶, G. A. Stewart³⁶, J. R. Stewart¹²¹, M. C. Stockton³⁶, G. Stoicea^{27b}, M. Stolarski^{130a}, S. Stoniek¹¹⁰, A. Straessner⁵⁰, J. Strandberg¹⁴⁴, S. Strandberg^{47a,47b}, M. Strauss¹²⁰, T. Strebler¹⁰², P. Strizenec^{28b}, R. Ströhmer¹⁶⁶, D. M. Strom¹²³, L. R. Strom⁴⁸, R. Stroynowski⁴⁴, A. Strubig^{47a,47b}, S. A. Stucci²⁹, B. Stugu¹⁶, J. Stupak¹²⁰, N. A. Styles⁴⁸, D. Su¹⁴³, S. Su^{62a}, W. Su^{62c,62d,138}, X. Su^{62a,66}, K. Sugizaki¹⁵³, V. V. Sulin³⁷, M. J. Sullivan⁹², D. M. S. Sultan^{78a,78b}, L. Sultanaliyeva³⁷, S. Sultansoy^{3b}, T. Sumida⁸⁷, S. Sun¹⁰⁶, S. Sun¹⁷⁰, O. Sunneborn Gudnadottir¹⁶¹, M. R. Sutton¹⁴⁶, M. Svatos¹³¹, M. Swiatlowski^{156a}, T. Swirski¹⁶⁶, I. Sykora^{28a}, M. Sykora¹³³, T. Sykora¹³³, D. Ta¹⁰⁰, K. Tackmann^{48,w}, A. Taffard¹⁶⁰, R. Tafirout^{156a}, J. S. Tafoya Vargas⁶⁶, R. H. M. Taibah¹²⁷, R. Takashima⁸⁸, E. P. Takeva⁵², Y. Takubo⁸³, M. Talby¹⁰², A. A. Talyshев³⁷, K. C. Tam^{64b}, N. M. Tamir¹⁵¹, A. Tanaka¹⁵³, J. Tanaka¹⁵³, R. Tanaka⁶⁶, M. Tanasini^{57a,57b}, J. Tang^{62c}, Z. Tao¹⁶⁴, S. Tapia Araya^{137f}, S. Tapprogge¹⁰⁰, A. Tarek Abouelfadl Mohamed¹⁰⁷, S. Tarem¹⁵⁰, K. Tariq^{62b}, G. Tarna^{27b,102}, G. F. Tartarelli^{71a}, P. Tas¹³³, M. Tasevsky¹³¹, E. Tassi^{43a,43b}, A. C. Tate¹⁶², G. Tateno¹⁵³, Y. Tayalati^{35e,y}, G. N. Taylor¹⁰⁵, W. Taylor^{156b}, H. Teagle⁹², A. S. Tee¹⁷⁰, R. Teixeira De Lima¹⁴³, P. Teixeira-Dias⁹⁵, J. J. Teoh¹⁵⁵, K. Terashi¹⁵³, J. Terron⁹⁹, S. Terzo¹³, M. Testa⁵³, R. J. Teuscher^{155,z}, A. Thaler⁷⁹, O. Theiner⁵⁶, N. Themistokleous⁵², T. Theveneaux-Pelzer¹⁰², O. Thielmann¹⁷¹, D. W. Thomas⁹⁵, J. P. Thomas²⁰, E. A. Thompson^{17a}, P. D. Thompson²⁰, E. Thomson¹²⁸, E. J. Thorpe⁹⁴, Y. Tian⁵⁵, V. Tikhomirov^{37,a}, Yu.A. Tikhonov³⁷, S. Timoshenko³⁷, E. X. L. Ting¹, P. Tipton¹⁷², S. H. Tlou^{33g}, A. Tnourji⁴⁰, K. Todome^{23a,23b}, S. Todorova-Nova¹³³, S. Todt⁵⁰, M. Togawa⁸³, J. Tojo⁸⁹, S. Tokár^{28a}, K. Tokushuku⁸³, O. Toldaiev⁶⁸, R. Tombs³², M. Tomoto^{83,111}, L. Tompkins^{143,q}, K. W. Topolnicki^{85b}, P. Tornambe¹⁰³, E. Torrence¹²³, H. Torres⁵⁰, E. Torró Pastor¹⁶³, M. Toscani³⁰, C. Tosciri³⁹, M. Tost¹¹, D. R. Tovey¹³⁹, A. Traeet¹⁶, I. S. Trandafir^{27b}, T. Trefzger¹⁶⁶, A. Tricoli²⁹, I. M. Trigger^{156a}, S. Trincaz-Duvold¹²⁷, D. A. Trischuk²⁶, B. Trocmé⁶⁰, C. Troncon^{71a}, L. Truong^{33c}, M. Trzebinski⁸⁶, A. Trzupek⁸⁶, F. Tsai¹⁴⁵, M. Tsai¹⁰⁶, A. Tsiamis^{152,f}, P. V. Tsiareshka³⁷, S. Tsigaridas^{156a}, A. Tsirigotis^{152,u}, V. Tsiskaridze¹⁴⁵, E. G. Tskhadadze^{149a}, M. Tsopoulou^{152,f}, Y. Tsujikawa⁸⁷, I. I. Tsukerman³⁷, V. Tsulaia^{17a}, S. Tsuno⁸³, O. Tsur¹⁵⁰, D. Tsybychev¹⁴⁵, Y. Tu^{64b}, A. Tudorache^{27b}, V. Tudorache^{27b}, A. N. Tuna³⁶, S. Turchikhin³⁸, I. Turk Cakir^{3a}, R. Turra^{71a}, T. Turtuvshin^{38,aa}, P. M. Tuts⁴¹, S. Tzamarias^{152,f}, P. Tzanis¹⁰, E. Tzovara¹⁰⁰, K. Uchida¹⁵³, F. Ukegawa¹⁵⁷, P. A. Ulloa Poblete^{137c}, E. N. Umaka²⁹, G. Unal³⁶, M. Unal¹¹, A. Undrus²⁹, G. Unel¹⁶⁰, J. Urban^{28b}, P. Urquijo¹⁰⁵, G. Usai⁸, R. Ushioda¹⁵⁴, M. Usman¹⁰⁸, Z. Uysal^{21b}, L. Vacavant¹⁰², V. Vacek¹³², B. Vachon¹⁰⁴, K. O. H. Vadla¹²⁵, T. Vafeiadis³⁶, A. Vaitkus⁹⁶, C. Valderanis¹⁰⁹, E. Valdes Santurio^{47a,47b}, M. Valente^{156a}, S. Valentinetto^{23a,23b}, A. Valero¹⁶³, A. Vallier^{102,ad}, J. A. Valls Ferrer¹⁶³, D. R. Van Arneman¹¹⁴, T. R. Van Daalen¹³⁸, P. Van Gemmeren⁶, M. Van Rijnbach^{36,125}, S. Van Stroud⁹⁶, I. Van Vulpen¹¹⁴, M. Vanadia^{76a,76b}

- W. Vandelli³⁶, M. Vandenbroucke¹³⁵, E. R. Vandewall¹²¹, D. Vannicola¹⁵¹, L. Vannoli^{57a,57b}, R. Vari^{75a}, E. W. Varnes⁷, C. Varni^{17a}, T. Varol¹⁴⁸, D. Varouchas⁶⁶, L. Varriale¹⁶³, K. E. Varvell¹⁴⁷, M. E. Vasile^{27b}, L. Vaslin⁴⁰, G. A. Vasquez¹⁶⁵, F. Vazeille⁴⁰, T. Vazquez Schroeder³⁶, J. Veatch³¹, V. Vecchio¹⁰¹, M. J. Veen¹⁰³, I. Veliscek¹²⁶, L. M. Veloce¹⁵⁵, F. Veloso^{130a,130c}, S. Veneziano^{75a}, A. Ventura^{70a,70b}, A. Verbytskyi¹¹⁰, M. Verducci^{74a,74b}, C. Vergis²⁴, M. Verissimo De Araujo^{82b}, W. Verkerke¹¹⁴, J. C. Vermeulen¹¹⁴, C. Vernieri¹⁴³, P. J. Verschuur⁹⁵, M. Vessella¹⁰³, M. C. Vetterli^{142,ai}, A. Vgenopoulos^{152,f}, N. Viaux Maira^{137f}, T. Vickey¹³⁹, O. E. Vickey Boeriu¹³⁹, G. H. A. Viehhauser¹²⁶, L. Vigani^{63b}, M. Villa^{23a,23b}, M. Villaplana Perez¹⁶³, E. M. Villhauer⁵², E. Vilucchi⁵³, M. G. Vinchter³⁴, G. S. Virdee²⁰, A. Vishwakarma⁵², C. Vittori³⁶, I. Vivarelli¹⁴⁶, V. Vladimirov¹⁶⁷, E. Voevodina¹¹⁰, F. Vogel¹⁰⁹, P. Vokac¹³², J. Von Ahnen⁴⁸, E. Von Toerne²⁴, B. Vormwald³⁶, V. Vorobel¹³³, K. Vorobev³⁷, M. Vos¹⁶³, K. Voss¹⁴¹, J. H. Vossebeld⁹², M. Vozak¹¹⁴, L. Vozdecky⁹⁴, N. Vranjes¹⁵, M. Vranjes Milosavljevic¹⁵, M. Vreeswijk¹¹⁴, R. Vuillermet³⁶, O. Vujinovic¹⁰⁰, I. Vukotic³⁹, S. Wada¹⁵⁷, C. Wagner¹⁰³, J. M. Wagner^{17a}, W. Wagner¹⁷¹, S. Wahdan¹⁷¹, H. Wahlberg⁹⁰, R. Wakasa¹⁵⁷, M. Wakida¹¹¹, J. Walder¹³⁴, R. Walker¹⁰⁹, W. Walkowiak¹⁴¹, A. M. Wang⁶¹, A. Z. Wang¹⁷⁰, C. Wang¹⁰⁰, C. Wang^{62c}, H. Wang^{17a}, J. Wang^{64a}, R.-J. Wang¹⁰⁰, R. Wang⁶¹, R. Wang⁶, S. M. Wang¹⁴⁸, S. Wang^{62b}, T. Wang^{62a}, W. T. Wang⁸⁰, X. Wang^{14c}, X. Wang¹⁶², X. Wang^{62c}, Y. Wang^{62d}, Y. Wang^{14c}, Z. Wang¹⁰⁶, Z. Wang^{51,62c,62d}, Z. Wang¹⁰⁶, A. Warburton¹⁰⁴, R. J. Ward²⁰, N. Warrack⁵⁹, A. T. Watson²⁰, H. Watson⁵⁹, M. F. Watson²⁰, G. Watts¹³⁸, B. M. Waugh⁹⁶, C. Weber²⁹, H. A. Weber¹⁸, M. S. Weber¹⁹, S. M. Weber^{63a}, C. Wei^{62a}, Y. Wei¹²⁶, A. R. Weidberg¹²⁶, E. J. Weik¹¹⁷, J. Weingarten⁴⁹, M. Weirich¹⁰⁰, C. Weiser⁵⁴, C. J. Wells⁴⁸, T. Wenaus²⁹, B. Wendland⁴⁹, T. Wengler³⁶, N. S. Wenke¹¹⁰, N. Wermes²⁴, M. Wessels^{63a}, K. Whalen¹²³, A. M. Wharton⁹¹, A. S. White⁶¹, A. White⁸, M. J. White¹, D. Whiteson¹⁶⁰, L. Wickremasinghe¹²⁴, W. Wiedenmann¹⁷⁰, C. Wiel⁵⁰, M. Wielers¹³⁴, C. Wiglesworth⁴², L. A. M. Wiik-Fuchs⁵⁴, D. J. Wilbern¹²⁰, H. G. Wilkens³⁶, D. M. Williams⁴¹, H. H. Williams¹²⁸, S. Williams³², S. Willocq¹⁰³, B. J. Wilson¹⁰¹, P. J. Windischhofer³⁹, F. Winklmeier¹²³, B. T. Winter⁵⁴, J. K. Winter¹⁰¹, M. Wittgen¹⁴³, M. Wobisch⁹⁷, R. Wölker¹²⁶, J. Wollrath¹⁶⁰, M. W. Wolter⁸⁶, H. Wolters^{130a,130c}, V. W. S. Wong¹⁶⁴, A. F. Wongel⁴⁸, S. D. Worm⁴⁸, B. K. Wosiek⁸⁶, K. W. Woźniak⁸⁶, K. Wraight⁵⁹, J. Wu^{14a,14d}, M. Wu^{64a}, M. Wu¹¹³, S. L. Wu¹⁷⁰, X. Wu⁵⁶, Y. Wu^{62a}, Z. Wu^{62a,135}, J. Wuerzinger¹¹⁰, T. R. Wyatt¹⁰¹, B. M. Wynne⁵², S. Xella⁴², L. Xia^{14c}, M. Xia^{14b}, J. Xiang^{64c}, X. Xiao¹⁰⁶, M. Xie^{62a}, X. Xie^{62a}, S. Xin^{14a,14d}, J. Xiong^{17a}, I. Xiotidis¹⁴⁶, D. Xu^{14a}, H. Xu^{62a}, L. Xu^{62a}, R. Xu¹²⁸, T. Xu¹⁰⁶, Y. Xu^{14b}, Z. Xu^{62b}, Z. Xu^{14a}, B. Yabsley¹⁴⁷, S. Yacoob^{33a}, N. Yamaguchi⁸⁹, Y. Yamaguchi¹⁵⁴, H. Yamauchi¹⁵⁷, T. Yamazaki^{17a}, Y. Yamazaki⁸⁴, J. Yan^{62c}, S. Yan¹²⁶, Z. Yan²⁵, H. J. Yang^{62c,62d}, H. T. Yang^{62a}, S. Yang^{62a}, T. Yang^{64c}, X. Yang^{62a}, X. Yang^{14a}, Y. Yang⁴⁴, Y. Yang^{62a}, Z. Yang^{62a,106}, W.-M. Yao^{17a}, Y. C. Yap⁴⁸, H. Ye^{14c}, H. Ye⁵⁵, J. Ye⁴⁴, S. Ye²⁹, X. Ye^{62a}, Y. Yeh⁹⁶, I. Yeletskikh³⁸, B. K. Yeo^{17a}, M. R. Yexley⁹¹, P. Yin⁴¹, K. Yorita¹⁶⁸, S. Younas^{27b}, C. J. S. Young⁵⁴, C. Young¹⁴³, Y. Yu^{62a}, M. Yuan¹⁰⁶, R. Yuan^{62b,l}, L. Yue⁹⁶, M. Zaazoua^{35e}, B. Zabinski⁸⁶, E. Zaid⁵², T. Zakareishvili^{149b}, N. Zakharchuk³⁴, S. Zambito⁵⁶, J. A. Zamora Saa^{137b,137d}, J. Zang¹⁵³, D. Zanzi⁵⁴, O. Zaplatilek¹³², C. Zeitnitz¹⁷¹, H. Zeng^{14a}, J. C. Zeng¹⁶², D. T. Zenger Jr²⁶, O. Zenin³⁷, T. Ženiš^{28a}, S. Zenz⁹⁴, S. Zerradi^{35a}, D. Zerwas⁶⁶, M. Zhai^{14a,14d}, B. Zhang^{14c}, D. F. Zhang¹³⁹, J. Zhang^{62b}, J. Zhang⁶, K. Zhang^{14a,14d}, L. Zhang^{14c}, P. Zhang^{14a,14d}, R. Zhang¹⁷⁰, S. Zhang¹⁰⁶, T. Zhang¹⁵³, X. Zhang^{62c}, X. Zhang^{62b}, Y. Zhang^{5,62c}, Z. Zhang^{17a}, Z. Zhang⁶⁶, H. Zhao¹³⁸, P. Zhao⁵¹, T. Zhao^{62b}, Y. Zhao¹³⁶, Z. Zhao^{62a}, A. Zhemchugov³⁸, X. Zheng^{62a}, Z. Zheng¹⁴³, D. Zhong¹⁶², B. Zhou¹⁰⁶, C. Zhou¹⁷⁰, H. Zhou⁷, N. Zhou^{62c}, Y. Zhou⁷, C. G. Zhu^{62b}, H. L. Zhu^{62a}, J. Zhu¹⁰⁶, Y. Zhu^{62c}, Y. Zhu^{62a}, X. Zhuang^{14a}, K. Zhukov³⁷, V. Zhulanov³⁷, N. I. Zimine³⁸, J. Zinsser^{63b}, M. Ziolkowski¹⁴¹, L. Živković¹⁵, A. Zoccoli^{23a,23b}, K. Zoch⁵⁶, T. G. Zorbas¹³⁹, O. Zormpa⁴⁶, W. Zou⁴¹, L. Zwalinski³⁶

¹ Department of Physics, University of Adelaide, Adelaide, Australia

² Department of Physics, University of Alberta, Edmonton, AB, Canada

³ ^(a)Department of Physics, Ankara University, Ankara, Türkiye; ^(b)Division of Physics, TOBB University of Economics and Technology, Ankara, Türkiye

⁴ LAPP, Université Savoie Mont Blanc, CNRS/IN2P3, Annecy, France

⁵ APC, Université Paris Cité, CNRS/IN2P3, Paris, France

⁶ High Energy Physics Division, Argonne National Laboratory, Argonne, IL, USA

⁷ Department of Physics, University of Arizona, Tucson, AZ, USA

- ⁸ Department of Physics, University of Texas at Arlington, Arlington, TX, USA
⁹ Physics Department, National and Kapodistrian University of Athens, Athens, Greece
¹⁰ Physics Department, National Technical University of Athens, Zografou, Greece
¹¹ Department of Physics, University of Texas at Austin, Austin, TX, USA
¹² Institute of Physics, Azerbaijan Academy of Sciences, Baku, Azerbaijan
¹³ Institut de Física d'Altes Energies (IFAE), Barcelona Institute of Science and Technology, Barcelona, Spain
¹⁴ ^(a)Institute of High Energy Physics, Chinese Academy of Sciences, Beijing, China; ^(b)Physics Department, Tsinghua University, Beijing, China; ^(c)Department of Physics, Nanjing University, Nanjing, China; ^(d)University of Chinese Academy of Science (UCAS), Beijing, China
¹⁵ Institute of Physics, University of Belgrade, Belgrade, Serbia
¹⁶ Department for Physics and Technology, University of Bergen, Bergen, Norway
¹⁷ ^(a)Physics Division, Lawrence Berkeley National Laboratory, Berkeley, CA, USA; ^(b)University of California, Berkeley, CA, USA
¹⁸ Institut für Physik, Humboldt Universität zu Berlin, Berlin, Germany
¹⁹ Albert Einstein Center for Fundamental Physics and Laboratory for High Energy Physics, University of Bern, Bern, Switzerland
²⁰ School of Physics and Astronomy, University of Birmingham, Birmingham, UK
²¹ ^(a)Department of Physics, Bogazici University, Istanbul, Türkiye; ^(b)Department of Physics Engineering, Gaziantep University, Gaziantep, Türkiye; ^(c)Department of Physics, Istanbul University, Istanbul, Türkiye; ^(d)Istinye University, Sarıyer, Istanbul, Türkiye
²² ^(a)Facultad de Ciencias y Centro de Investigaciones, Universidad Antonio Nariño, Bogotá, Colombia; ^(b)Departamento de Física, Universidad Nacional de Colombia, Bogotá, Colombia
²³ ^(a)Dipartimento di Fisica e Astronomia A. Righi, Università di Bologna, Bologna, Italy; ^(b)INFN Sezione di Bologna, Bologna, Italy
²⁴ Physikalischs Institut, Universität Bonn, Bonn, Germany
²⁵ Department of Physics, Boston University, Boston, MA, USA
²⁶ Department of Physics, Brandeis University, Waltham, MA, USA
²⁷ ^(a)Transilvania University of Brasov, Brasov, Romania; ^(b)Horia Hulubei National Institute of Physics and Nuclear Engineering, Bucharest, Romania; ^(c)Department of Physics, Alexandru Ioan Cuza University of Iasi, Iasi, Romania ; ^(d)National Institute for Research and Development of Isotopic and Molecular Technologies, Physics Department, Cluj-Napoca, Romania; ^(e)University Politehnica Bucharest, Bucharest, Romania; ^(f)West University in Timisoara, Timisoara, Romania; ^(g)Faculty of Physics, University of Bucharest, Bucharest, Romania
²⁸ ^(a)Faculty of Mathematics, Physics and Informatics, Comenius University, Bratislava, Slovak Republic; ^(b)Department of Subnuclear Physics, Institute of Experimental Physics of the Slovak Academy of Sciences, Kosice, Slovak Republic
²⁹ Physics Department, Brookhaven National Laboratory, Upton, NY, USA
³⁰ Departamento de Física, Facultad de Ciencias Exactas y Naturales, y CONICET, Instituto de Física de Buenos Aires (IFIBA), Universidad de Buenos Aires, Buenos Aires, Argentina
³¹ California State University, Fresno, CA, USA
³² Cavendish Laboratory, University of Cambridge, Cambridge, UK
³³ ^(a)Department of Physics, University of Cape Town, Cape Town, South Africa; ^(b)iThemba Labs, Western Cape, South Africa; ^(c)Department of Mechanical Engineering Science, University of Johannesburg, Johannesburg, South Africa ; ^(d)National Institute of Physics, University of the Philippines Diliman (Philippines), Philippines; ^(e)University of South Africa, Department of Physics, Pretoria, South Africa; ^(f)University of Zululand, KwaDlangezwa, South Africa ; ^(g)School of Physics, University of the Witwatersrand, Johannesburg, South Africa
³⁴ Department of Physics, Carleton University, Ottawa, ON, Canada
³⁵ ^(a)Faculté des Sciences Ain Chock, Réseau Universitaire de Physique des Hautes Energies-Université Hassan II, Casablanca, Morocco; ^(b)Faculté des Sciences, Université Ibn-Tofail, Kénitra, Morocco ; ^(c)Faculté des Sciences Semlalia, LPHEA-Marrakech, Université Cadi Ayyad, Marrakech, Morocco; ^(d)LPMR, Faculté des Sciences, Université Mohamed Premier, Oujda, Morocco; ^(e)Faculté des sciences, Université Mohammed V, Rabat, Morocco; ^(f)Institute of Applied Physics, Mohammed VI Polytechnic University, Ben Guérir, Morocco
³⁶ CERN, Geneva, Switzerland
³⁷ Affiliated with an Institute Covered by a Cooperation Agreement with CERN, Geneva, Switzerland
³⁸ Affiliated with an International Laboratory Covered by a Cooperation Agreement with CERN, Geneva, Switzerland

- ³⁹ Enrico Fermi Institute, University of Chicago, Chicago, IL, USA
⁴⁰ LPC, CNRS/IN2P3, Université Clermont Auvergne, Clermont-Ferrand, France
⁴¹ Nevis Laboratory, Columbia University, Irvington, NY, USA
⁴² Niels Bohr Institute, University of Copenhagen, Copenhagen, Denmark
⁴³ ^(a)Dipartimento di Fisica, Università della Calabria, Rende, Italy; ^(b)Laboratori Nazionali di Frascati, INFN Gruppo Collegato di Cosenza, Cosenza, Italy
⁴⁴ Physics Department, Southern Methodist University, Dallas, TX, USA
⁴⁵ Physics Department, University of Texas at Dallas, Richardson, TX, USA
⁴⁶ National Centre for Scientific Research “Demokritos”, Agia Paraskevi, Greece
⁴⁷ ^(a)Department of Physics, Stockholm University, Stockholm, Sweden; ^(b)Oskar Klein Centre, Stockholm, Sweden
⁴⁸ Deutsches Elektronen-Synchrotron DESY, Hamburg and Zeuthen, Germany
⁴⁹ Fakultät Physik , Technische Universität Dortmund, Dortmund, Germany
⁵⁰ Institut für Kern- und Teilchenphysik, Technische Universität Dresden, Dresden, Germany
⁵¹ Department of Physics, Duke University, Durham, NC, USA
⁵² SUPA-School of Physics and Astronomy, University of Edinburgh, Edinburgh, UK
⁵³ INFN e Laboratori Nazionali di Frascati, Frascati, Italy
⁵⁴ Physikalisches Institut, Albert-Ludwigs-Universität Freiburg, Freiburg, Germany
⁵⁵ II. Physikalisches Institut, Georg-August-Universität Göttingen, Göttingen, Germany
⁵⁶ Département de Physique Nucléaire et Corpusculaire, Université de Genève, Geneva, Switzerland
⁵⁷ ^(a)Dipartimento di Fisica, Università di Genova, Genoa, Italy; ^(b)INFN Sezione di Genova, Genoa, Italy
⁵⁸ II. Physikalisches Institut, Justus-Liebig-Universität Giessen, Giessen, Germany
⁵⁹ SUPA-School of Physics and Astronomy, University of Glasgow, Glasgow, UK
⁶⁰ LPSC, CNRS/IN2P3, Grenoble INP, Université Grenoble Alpes, Grenoble, France
⁶¹ Laboratory for Particle Physics and Cosmology, Harvard University, Cambridge, MA, USA
⁶² ^(a)Department of Modern Physics and State Key Laboratory of Particle Detection and Electronics, University of Science and Technology of China, Hefei, China; ^(b)Institute of Frontier and Interdisciplinary Science and Key Laboratory of Particle Physics and Particle Irradiation (MOE), Shandong University, Qingdao, China; ^(c)School of Physics and Astronomy, Shanghai Jiao Tong University, Key Laboratory for Particle Astrophysics and Cosmology (MOE), SKLPPC, Shanghai, China; ^(d)Tsung-Dao Lee Institute, Shanghai, China
⁶³ ^(a)Kirchhoff-Institut für Physik, Ruprecht-Karls-Universität Heidelberg, Heidelberg, Germany; ^(b)Physikalisches Institut, Ruprecht-Karls-Universität Heidelberg, Heidelberg, Germany
⁶⁴ ^(a)Department of Physics, Chinese University of Hong Kong, Shatin, N.T., Hong Kong, China; ^(b)Department of Physics, University of Hong Kong, Hong Kong, China; ^(c)Department of Physics and Institute for Advanced Study, Hong Kong University of Science and Technology, Clear Water Bay, Kowloon, Hong Kong, China
⁶⁵ Department of Physics, National Tsing Hua University, Hsinchu, Taiwan
⁶⁶ IJCLab, CNRS/IN2P3, Université Paris-Saclay, 91405 Orsay, France
⁶⁷ Centro Nacional de Microelectrónica (IMB-CNM-CSIC), Barcelona, Spain
⁶⁸ Department of Physics, Indiana University, Bloomington, IN, USA
⁶⁹ ^(a)INFN Gruppo Collegato di Udine, Sezione di Trieste, Udine, Italy; ^(b)ICTP, Trieste, Italy; ^(c)Dipartimento Politecnico di Ingegneria e Architettura, Università di Udine, Udine, Italy
⁷⁰ ^(a)INFN Sezione di Lecce, Lecce, Italy; ^(b)Dipartimento di Matematica e Fisica, Università del Salento, Lecce, Italy
⁷¹ ^(a)INFN Sezione di Milano, Milan, Italy; ^(b)Dipartimento di Fisica, Università di Milano, Milan, Italy
⁷² ^(a)INFN Sezione di Napoli, Naples, Italy; ^(b)Dipartimento di Fisica, Università di Napoli, Naples, Italy
⁷³ ^(a)INFN Sezione di Pavia, Pavia, Italy; ^(b)Dipartimento di Fisica, Università di Pavia, Pavia, Italy
⁷⁴ ^(a)INFN Sezione di Pisa, Pisa, Italy; ^(b)Dipartimento di Fisica E. Fermi, Università di Pisa, Pisa, Italy
⁷⁵ ^(a)INFN Sezione di Roma, Rome, Italy; ^(b)Dipartimento di Fisica, Sapienza Università di Roma, Rome, Italy
⁷⁶ ^(a)INFN Sezione di Roma Tor Vergata, Rome, Italy; ^(b)Dipartimento di Fisica, Università di Roma Tor Vergata, Rome, Italy
⁷⁷ ^(a)INFN Sezione di Roma Tre, Rome, Italy; ^(b)Dipartimento di Matematica e Fisica, Università Roma Tre, Rome, Italy
⁷⁸ ^(a)INFN-TIFPA, Povo, Italy; ^(b)Università degli Studi di Trento, Trento, Italy
⁷⁹ Universität Innsbruck, Department of Astro and Particle Physics, Innsbruck, Austria
⁸⁰ University of Iowa, Iowa City, IA, USA
⁸¹ Department of Physics and Astronomy, Iowa State University, Ames, IA, USA

- 82 ^(a)Departamento de Engenharia Elétrica, Universidade Federal de Juiz de Fora (UFJF), Juiz de Fora, Brazil
; ^(b)Universidade Federal do Rio De Janeiro COPPE/EE/IF, Rio de Janeiro, Brazil; ^(c)Instituto de Física, Universidade de São Paulo, São Paulo, Brazil; ^(d)Rio de Janeiro State University, Rio de Janeiro, Brazil
- 83 KEK, High Energy Accelerator Research Organization, Tsukuba, Japan
- 84 Graduate School of Science, Kobe University, Kobe, Japan
- 85 ^(a)AGH University of Krakow, Faculty of Physics and Applied Computer Science, Kraków, Poland; ^(b)Marian Smoluchowski Institute of Physics, Jagiellonian University, Kraków, Poland
- 86 Institute of Nuclear Physics Polish Academy of Sciences, Kraków, Poland
- 87 Faculty of Science, Kyoto University, Kyoto, Japan
- 88 Kyoto University of Education, Kyoto, Japan
- 89 Research Center for Advanced Particle Physics and Department of Physics, Kyushu University, Fukuoka , Japan
- 90 Instituto de Física La Plata, Universidad Nacional de La Plata and CONICET, La Plata, Argentina
- 91 Physics Department, Lancaster University, Lancaster, UK
- 92 Oliver Lodge Laboratory, University of Liverpool, Liverpool, UK
- 93 Department of Experimental Particle Physics, Jožef Stefan Institute and Department of Physics, University of Ljubljana, Ljubljana, Slovenia
- 94 School of Physics and Astronomy, Queen Mary University of London, London, UK
- 95 Department of Physics, Royal Holloway University of London, Egham, UK
- 96 Department of Physics and Astronomy, University College London, London, UK
- 97 Louisiana Tech University, Ruston, LA, USA
- 98 Fysiska institutionen, Lunds universitet, Lund, Sweden
- 99 Departamento de Física Teorica C-15 and CIAFF, Universidad Autónoma de Madrid, Madrid, Spain
- 100 Institut für Physik, Universität Mainz, Mainz, Germany
- 101 School of Physics and Astronomy, University of Manchester, Manchester, UK
- 102 CPPM, CNRS/IN2P3, Aix-Marseille Université, Marseille, France
- 103 Department of Physics, University of Massachusetts, Amherst, MA, USA
- 104 Department of Physics, McGill University, Montreal, QC, Canada
- 105 School of Physics, University of Melbourne, Victoria, Australia
- 106 Department of Physics, University of Michigan, Ann Arbor, MI, USA
- 107 Department of Physics and Astronomy, Michigan State University, East Lansing, MI, USA
- 108 Group of Particle Physics, University of Montreal, Montreal, QC, Canada
- 109 Fakultät für Physik, Ludwig-Maximilians-Universität München, Munich, Germany
- 110 Max-Planck-Institut für Physik (Werner-Heisenberg-Institut), Munich, Germany
- 111 Graduate School of Science and Kobayashi-Maskawa Institute, Nagoya University, Nagoya, Japan
- 112 Department of Physics and Astronomy, University of New Mexico, Albuquerque, NM, USA
- 113 Institute for Mathematics, Astrophysics and Particle Physics, Radboud University/Nikhef, Nijmegen, The Netherlands
- 114 Nikhef National Institute for Subatomic Physics and University of Amsterdam, Amsterdam, The Netherlands
- 115 Department of Physics, Northern Illinois University, DeKalb, IL, USA
- 116 ^(a)New York University Abu Dhabi, Abu Dhabi, United Arab Emirates; ^(b)University of Sharjah, Sharjah, United Arab Emirates
- 117 Department of Physics, New York University, New York, NY, USA
- 118 Ochanomizu University, Otsuka, Bunkyo-ku, Tokyo, Japan
- 119 Ohio State University, Columbus, OH, USA
- 120 Homer L. Dodge Department of Physics and Astronomy, University of Oklahoma, Norman, OK, USA
- 121 Department of Physics, Oklahoma State University, Stillwater, OK, USA
- 122 Joint Laboratory of Optics, Palacký University, Olomouc, Czech Republic
- 123 Institute for Fundamental Science, University of Oregon, Eugene, OR, USA
- 124 Graduate School of Science, Osaka University, Osaka, Japan
- 125 Department of Physics, University of Oslo, Oslo, Norway
- 126 Department of Physics, Oxford University, Oxford, UK
- 127 LPNHE, CNRS/IN2P3, Sorbonne Université, Université Paris Cité, Paris, France
- 128 Department of Physics, University of Pennsylvania, Philadelphia, PA, USA
- 129 Department of Physics and Astronomy, University of Pittsburgh, Pittsburgh, PA, USA

- ¹³⁰ ^(a)Laboratório de Instrumentação e Física Experimental de Partículas-LIP, Lisbon, Portugal; ^(b)Departamento de Física, Faculdade de Ciências, Universidade de Lisboa, Lisbon, Portugal; ^(c)Departamento de Física, Universidade de Coimbra, Coimbra, Portugal; ^(d)Centro de Física Nuclear da Universidade de Lisboa, Lisbon, Portugal; ^(e)Departamento de Física, Universidade do Minho, Braga, Portugal; ^(f)Departamento de Física Teórica y del Cosmos, Universidad de Granada, Granada (Spain), Portugal; ^(g)Departamento de Física, Instituto Superior Técnico, Universidade de Lisboa, Lisbon, Portugal
- ¹³¹ Institute of Physics of the Czech Academy of Sciences, Prague, Czech Republic
- ¹³² Czech Technical University in Prague, Prague, Czech Republic
- ¹³³ Charles University, Faculty of Mathematics and Physics, Prague, Czech Republic
- ¹³⁴ Particle Physics Department, Rutherford Appleton Laboratory, Didcot, UK
- ¹³⁵ IRFU, CEA, Université Paris-Saclay, Gif-sur-Yvette, France
- ¹³⁶ Santa Cruz Institute for Particle Physics, University of California Santa Cruz, Santa Cruz, CA, USA
- ¹³⁷ ^(a)Departamento de Física, Pontificia Universidad Católica de Chile, Santiago, Chile; ^(b)Millennium Institute for Subatomic Physics at High Energy Frontier (SAPHIR), Santiago, Chile; ^(c)Instituto de Investigación Multidisciplinario en Ciencia y Tecnología, y Departamento de Física, Universidad de La Serena, La Serena, Chile; ^(d)Universidad Andres Bello, Department of Physics, Santiago, Chile; ^(e)Instituto de Alta Investigación, Universidad de Tarapacá, Arica, Chile ; ^(f)Departamento de Física, Universidad Técnica Federico Santa María, Valparaíso, Chile
- ¹³⁸ Department of Physics, University of Washington, Seattle, WA, USA
- ¹³⁹ Department of Physics and Astronomy, University of Sheffield, Sheffield, UK
- ¹⁴⁰ Department of Physics, Shinshu University, Nagano, Japan
- ¹⁴¹ Department Physik, Universität Siegen, Siegen, Germany
- ¹⁴² Department of Physics, Simon Fraser University, Burnaby, BC, Canada
- ¹⁴³ SLAC National Accelerator Laboratory, Stanford, CA, USA
- ¹⁴⁴ Department of Physics, Royal Institute of Technology, Stockholm, Sweden
- ¹⁴⁵ Departments of Physics and Astronomy, Stony Brook University, Stony Brook, NY, USA
- ¹⁴⁶ Department of Physics and Astronomy, University of Sussex, Brighton, UK
- ¹⁴⁷ School of Physics, University of Sydney, Sydney, Australia
- ¹⁴⁸ Institute of Physics, Academia Sinica, Taipei, Taiwan
- ¹⁴⁹ ^(a)E. Andronikashvili Institute of Physics, Iv. Javakhishvili Tbilisi State University, Tbilisi, Georgia; ^(b)High Energy Physics Institute, Tbilisi State University, Tbilisi, Georgia; ^(c)University of Georgia, Tbilisi, Georgia
- ¹⁵⁰ Department of Physics, Technion, Israel Institute of Technology, Haifa, Israel
- ¹⁵¹ Raymond and Beverly Sackler School of Physics and Astronomy, Tel Aviv University, Tel Aviv, Israel
- ¹⁵² Department of Physics, Aristotle University of Thessaloniki, Thessaloniki, Greece
- ¹⁵³ International Center for Elementary Particle Physics and Department of Physics, University of Tokyo, Tokyo, Japan
- ¹⁵⁴ Department of Physics, Tokyo Institute of Technology, Tokyo, Japan
- ¹⁵⁵ Department of Physics, University of Toronto, Toronto, ON, Canada
- ¹⁵⁶ ^(a)TRIUMF, Vancouver, BC, Canada; ^(b)Department of Physics and Astronomy, York University, Toronto, ON, Canada
- ¹⁵⁷ Division of Physics and Tomonaga Center for the History of the Universe, Faculty of Pure and Applied Sciences, University of Tsukuba, Tsukuba, Japan
- ¹⁵⁸ Department of Physics and Astronomy, Tufts University, Medford, MA, USA
- ¹⁵⁹ United Arab Emirates University, Al Ain, United Arab Emirates
- ¹⁶⁰ Department of Physics and Astronomy, University of California Irvine, Irvine, CA, USA
- ¹⁶¹ Department of Physics and Astronomy, University of Uppsala, Uppsala, Sweden
- ¹⁶² Department of Physics, University of Illinois, Urbana, IL, USA
- ¹⁶³ Instituto de Física Corpuscular (IFIC), Centro Mixto Universidad de Valencia-CSIC, Valencia, Spain
- ¹⁶⁴ Department of Physics, University of British Columbia, Vancouver, BC, Canada
- ¹⁶⁵ Department of Physics and Astronomy, University of Victoria, Victoria, BC, Canada
- ¹⁶⁶ Fakultät für Physik und Astronomie, Julius-Maximilians-Universität Würzburg, Würzburg, Germany
- ¹⁶⁷ Department of Physics, University of Warwick, Coventry, UK
- ¹⁶⁸ Waseda University, Tokyo, Japan
- ¹⁶⁹ Department of Particle Physics and Astrophysics, Weizmann Institute of Science, Rehovot, Israel
- ¹⁷⁰ Department of Physics, University of Wisconsin, Madison, WI, USA

¹⁷¹ Fakultät für Mathematik und Naturwissenschaften, Fachgruppe Physik, Bergische Universität Wuppertal, Wuppertal, Germany

¹⁷² Department of Physics, Yale University, New Haven, CT, USA

^a Also Affiliated with an Institute Covered by a Cooperation Agreement with CERN, Geneva, Switzerland

^b Also at An-Najah National University, Nablus, Palestine

^c Also at Borough of Manhattan Community College, City University of New York, New York, NY, USA

^d Also at Bruno Kessler Foundation, Trento, Italy

^e Also at Center for High Energy Physics, Peking University, Beijing, China

^f Also at Also at Center for Interdisciplinary Research and Innovation (CIRI-AUTH), Thessaloniki, Greece

^g Also at Centro Studi e Ricerche Enrico Fermi, Rome, Italy

^h Also at CERN, Geneva, Switzerland

ⁱ Also at Département de Physique Nucléaire et Corpusculaire, Université de Genève, Geneva, Switzerland

^j Also at Departament de Fisica de la Universitat Autònoma de Barcelona, Barcelona, Spain

^k Also at Department of Financial and Management Engineering, University of the Aegean, Chios, Greece

^l Also at Department of Physics and Astronomy, Michigan State University, East Lansing, MI, USA

^m Also at Department of Physics, Ben Gurion University of the Negev, Beer Sheva, Israel

ⁿ Also at Department of Physics, California State University, East Bay, USA

^o Also at Department of Physics, California State University, Sacramento, USA

^p Also at Department of Physics, King's College London, London, UK

^q Also at Department of Physics, Stanford University, Stanford, CA, USA

^r Also at Department of Physics, University of Fribourg, Fribourg, Switzerland

^s Also at Department of Physics, University of Thessaly, Volos, Greece

^t Also at Department of Physics, Westmont College, Santa Barbara, USA

^u Also at Hellenic Open University, Patras, Greece

^v Also at Institutio Catalana de Recerca i Estudis Avancats, ICREA, Barcelona, Spain

^w Also at Institut für Experimentalphysik, Universität Hamburg, Hamburg, Germany

^x Also at Institute for Nuclear Research and Nuclear Energy (INRNE) of the Bulgarian Academy of Sciences, Sofia, Bulgaria

^y Also at Institute of Applied Physics, Mohammed VI Polytechnic University, Ben Guerir, Morocco

^z Also at Institute of Particle Physics (IPP), Victoria, Canada

^{aa} Also at Institute of Physics and Technology, Ulaanbaatar, Mongolia

^{ab} Also at Institute of Physics, Azerbaijan Academy of Sciences, Baku, Azerbaijan

^{ac} Also at Institute of Theoretical Physics, Ilia State University, Tbilisi, Georgia

^{ad} Also at L2IT, CNRS/IN2P3, UPS, Université de Toulouse, Toulouse, France

^{ae} Also at Lawrence Livermore National Laboratory, Livermore, USA

^{af} Also at National Institute of Physics, University of the Philippines Diliman (Philippines), Quezon City, Philippines

^{ag} Also at Technical University of Munich, Munich, Germany

^{ah} Also at The Collaborative Innovation Center of Quantum Matter (CICQM), Beijing, China

^{ai} Also at TRIUMF, Vancouver, BC, Canada

^{aj} Also at Università di Napoli Parthenope, Naples, Italy

^{ak} Also at University of Chinese Academy of Sciences (UCAS), Beijing, China

^{al} Also at University of Colorado Boulder, Department of Physics, Colorado, USA

^{am} Also at Washington College, Maryland, USA

^{an} Also at Yeditepe University, Physics Department, Istanbul, Türkiye

* Deceased